Turun yliopisto
University of Turku

EXPERIMENTAL STUDIES ON NON-METALLIC COMPOSITE BONE IMPLANTS

With a Special Reference to Staphylococcal Biofilm Infections

Julia Kulkova

TURUN YLIOPISTON JULKAISUJA – ANNALES UNIVERSITATIS TURKUENSIS
Sarja - ser. D osa - tom. 1157 | Medica - Odontologica | Turku 2015

University of Turku

Faculty of Medicine

Department of Orthopaedic Surgery and Traumatology

Institute of Clinical Medicine

Doctoral Program of Clinical Investigation

National Doctoral Programme of Musculoskeletal Disorders and Biomaterials

Supervised by

Hannu T Aro, MD, PhD, Professor
Department of Orthopaedic Surgery
and Traumatology
University of Turku and Turku University Hospital

Reviewed by

Minna Kellomäki, PhD, FBSE, Professor
Institute of Biosciences and Medical
Technology BioMediTech and
Department of Electronics and
Communications Engineering
Tampere University of Technology

Juha Tuukkanen, DDS, PhD, Professor
Department of Anatomy and Cell Biology
Institute of Biomedicine
University of Oulu

Opponent

Heimo Ylänen, PhD, FBSE, Professor
Institute of Biosciences and Medical
Technology BioMediTech
Department of Electronics and
Communications Engineering
Tampere University of Technology

The originality of this thesis has been checked in accordance with the University of Turku quality assurance system using the Turnitin OriginalityCheck service.

ISBN 978-951-29-6000-2 (PRINT)
ISBN 978-951-29-6001-9 (PDF)
ISSN 0355-9483
Painosalama Oy - Turku, Finland 2015

To Ignat, Mervi
and Niko

ABSTRACT

Julia Kulkova

Experimental Studies on Non-metallic Composite Bone Implants with a Special Reference to Staphylococcal Biofilm Infections

From the Department of Orthopedics and Traumatology, Institute of Clinical Medicine, Faculty of Medicine, Doctoral Program of Clinical Investigation, University of Turku and Turku University Hospital, Turku, Finland

Annales Universitatis Turkuensis
Painosalama Oy, Turku, Finland 2015

Non-metallic implants made of bioresorbable or biostable synthetic polymers are attractive options in many surgical procedures, ranging from bioresorbable suture anchors of arthroscopic surgery to reconstructive skull implants made of biostable fiber-reinforced composites. Among other benefits, non-metallic implants produce less interference in imaging. Bioresorbable polymer implants may be true multifunctional, serving as osteoconductive scaffolds and as matrices for simultaneous delivery of bone enhancement agents. As a major advantage for loading conditions, mechanical properties of biostable fiber-reinforced composites can be matched with those of the bone. Unsolved problems of these biomaterials are related to the risk of staphylococcal biofilm infections and to the low osteoconductivity of contemporary bioresorbable composite implants.

This thesis was focused on the research and development of a multifunctional implant model with enhanced osteoconductivity and low susceptibility to infection. In addition, the experimental models for assessment, diagnostics and prophylaxis of biomaterial-related infections were established.

The first experiment (**Study I**) established an *in vitro* method for simultaneous evaluation of calcium phosphate and biofilm formation on bisphenol-A-glycidyldimethacrylate and triethylenglycoldimethacrylate (BisGMA-TEGDMA) thermosets with different content of bioactive glass 45S5. The second experiment (**Study II**) showed no significant difference in osteointegration of nanostructured and microsized polylactide-co-glycolide/β-tricalcium phosphate (PLGA /β-TCP) composites in a minipig model. The third experiment (**Study III**) demonstrated that positron emission tomography (PET) imaging with the novel ^{68}Ga labelled 1,4,7,10-tetraazacyclododecane-1,4,7,10-tetraacetic acid (DOTA) CD33 related sialic-acid immunoglobulin like lectins (Siglec-9) tracer was able to detect inflammatory response to *S. epidermidis* and *S. aureus* peri-implant infections in an intraosseous polytetrafluoroethylene catheter model. In the fourth experiment (**Study IV**), BisGMA-TEGDMA thermosets coated with lactose-modified chitosan (Chitlac) and silver nanoparticles exhibited antibacterial activity against *S. aureus* and *P. aeruginosa* strains in an *in vitro* biofilm model and showed *in vivo* biocompatibility in a minipig model. In the last experiment (**Study V**), a selective androgen modulator (SARM) released from a poly(lactide)-co-ε-caprolactone (PLCL) polymer matrix failed to produce a dose-dependent enhancement of peri-implant osteogenesis in a bone marrow ablation model.

Keywords: bioresorbable implants, bioactive glass, BisGMA-TEGDMA thermosets PLGA, β-TCP, PET, ^{68}Ga-DOTA-Siglec-9 PET tracer, Chitlac-nAg, bone infections, PLCL, SARM, osteogenesis

TIIVISTELMÄ

Julia Kulkova

Polymeereistä valmistettuihin ei-metallisiin komposiittiluuimplantteihin liittyvä kokeellinen tutkimus erityisesti liittyen biofilmiä muodostavaan stafylokokki -infektioon

Ortopedian ja traumatologian klinikka, Kliinisen lääketieteen laitos, Lääketieteellinen tiedekunta, Turun yliopiston kliinisen lääketieteen tohtoriohjelma, Turun yliopisto ja Turun yliopistollinen keskussairaala, Turku, Suomi

Annales Universitatis Turkuensis
Painosalama Oy, Turku, Finland 2015

Synteettisistä polymeereistä valmistetut biohajoavat ja biostabiilit implantit ovat vaihtoehtoja metallisille implanteille useissa kirurgisissa toimenpiteissä. Biohajoavia implantteja voidaan käyttää tähystyskirurgiassa ommelankkureina tai biostabiileita kuitulujitteisia implantteja kalloluun korjauksessa. Polymeereistä valmistetut implantit häiritsevät kuvantamistutkimuksia vähemmän kuin tavanomaiset metalliset implantit. Biohajoavat polymeerit voivat myös toimia luun kasvua ohjaavana rakenteena ja samalla vapauttaa paikallisesti luun kasvua edistävää lääkettä. Myös biostabiileista kuitulujitteisista polymeereistä voidaan valmistaa kuormaa kantavia implantteja, joiden mekaanisia ominaisuuksia on säädelty luun kanssa samankaltaisiksi. Biomateriaalien kliiniseen käyttöön liittyy aina jonkinasteinen infektioriski. Vaikeimmin hoidettavat infektiot liittyvät bakteerikantojen kykyyn kiinnittyä implanttien pinnalle (biofilmin muodostuminen). Myös biohajoavien implanttien käytössä riittämätön uudisluun muodostuminen on todettu yhdeksi ongelmaksi.

Tässä väitöskirjatutkimuksessa keskityttiin multifunktionaalisen implanttimallin tutkimukseen, jossa pyrkimyksenä oli saada parannettua implantin osteokonduktiivisuutta ja alentaa infektioalttiutta.

Ensimmäisessä osatyössä kehitettiin menetelmä, jolla voidaan seurata biofilmin ja hydroksiapatiitin muodostumista bioaktiivisen lasin 45S5 sekä bisfenoli-A-glysidyylidimetakrylaatin ja trietyleeniglykolidimetakrylaatin (BisGMA-TEGDMA) seoksesta valmistetun yhdistelmämateriaalin pinnalla. Toisessa osatyössä todettiin, että luun muodostusta edistävän β-trikalsiumfosfaatin (β-TCP) partikkelikoolla (nano versus mikro) ei ollut merkittävää vaikutusta biohajoavan yhdistelmämateriaalin (valmistettu polylaktidiglysidyylin seospolymeeristä ja β-TCP:sta) kiinnittymiseen luuhun. Kolmannessa osatyössä todettiin, että positroniemissiotomografian (PET) uusi Siglec-9 -niminen kuvausmerkkiaine pystyy tunnistamaan stafylokokkien (*S. epidermidis* ja *S. aureus* kannat) aiheuttamat implantti-infektiot. Siglec-9 valmistettiin 68Ga-isotoopilla leimattuun 1,4,7,10-tetra-atsasyklododekaani-1,4,7,10-tetraetikkahappoon (DOTA). Implantti oli luun sisäinen katetrityyppinen ratkaisu, ja se oli valmistettu polytetrafluorietyleenistä (PTFE). Neljännessä osatyössä osoitettiin, että nanokoon hopeapartikkeleita sisältävä laktoosi-modifioitu kitosaani (Chitlac) -pinnoite estää bakteerien kasvua (*S. aureus* ja *P. aeruginosa* kannat) biostabiilin BisGMA-TEGDMA:sta valmistetun implantin pinnalla. Pinnoitteella ei ollut haitallisia vaikutuksia implantin kiinnittymiseen luuhun. Viimeisessä osatyössä todettiin, että biohajoavista polylaktidikaprolaktonin (PLCL) seospolymeerimatriisista valmistetusta implantista vapautuva anabolinen lääkeaine (selektiivinen androgeenimodulaattori, SARM) ei edistänyt uudisluun muodostumista paikallisesti luuydinablaatiomallissa.

Hakusanat: biohajoavat implantit, bioaktiivinen lasi, BisGMA-TEGDMA kertamuovi, PLGA, β-TCP, PET, ^{68}Ga-DOTA-Siglec-9 PET -merkkiaine, luuinfektiot, PLCL, SARM, luunmuodostumis

TABLE OF CONTENTS

ABSTRACT 4
TIIVISTELMÄ 5
ABBREVIATIONS 7
LIST OF ORIGINAL PUBLICATIONS 9
1 INTRODUCTION 10
2 REVIEW OF THE LITERATURE 11
2.1 Bone 11
2.1.1 Composition and structure 11
2.1.2 Healing patterns of bone 13
2.2 Biomaterial-related infections 14
2.2.1 Aetiology 14
2.2.2 Pathogenesis 16
2.2.3 *Prophylaxis and treatment* 17
2.3 Skeletal reconstructive biomaterials 18
2.3.1 Classification 18
2.3.2 Bioresorbable polymers 20
2.3.3 Bioresorbable polymers as drug delivery systems 23
2.3.4 Osteoconductive calcium phosphate-based ceramics 24
2.3.5 Bioactive glass 25
2.3.6 Osteoconductive bioresorbable composites 26
2.3.7 Silver nanoparticles as an antimicrobial implant coating with a short-term release pattern 28
2.3.8 Therapeutic androgen receptor ligands 30
2.4 Animal models 33
2.4.1 Bone healing models 33
2.4.2 Implant infection models 34
2.5 Experimental methods for evaluation of implant related infections and biomaterial incorporations 35
2.5.1 Conventional microbiological techniques 35
2.5.2 Fluorescent techniques 36
2.5.3 Micro-computed tomography 36
2.5.4 Histomorphometry 37
2.5.5 Scanning electron microscopy 37
2.5.6 Positron emission tomography 38
3 AIMS OF THE STUDY 40
4 MATERIALS AND METHODS 41
4.1 Study I 41
4.2 Study II 42
4.3 Study III 43
4.4 Study IV 46
4.5 Study V 48
5 RESULTS 51
5.1 Study I 51
5.2 Study II 52
5.3 Study III 57
5.4 Study IV 62
5.5 Study V 67
6 DISCUSSION 72
7 CONCLUSIONS 81
8 ACKNOWLEDGEMENTS 82
9 REFERENCES 84
ORIGINAL PUBLICATIONS 103

ABBREVIATIONS

[^{18}F]-FDG	2-^{18}F-fluoro-2-deoxy-D-glucose
ACL	Anterior cruciate ligament
ADI	Arginine deiminase operon
AR	Androgen receptor
BAG	Bioactive glass
BCP	Biphasic calcium phosphates
BIC	Bone–implant contact
BisGMA-TEGDMA	Bisphenol-A-glycidyldimethacrylate and triethylenglycoldimethacrylate
BM	Bacterial-biofilm growing medium
BMD	Bone mineral density
rhBMP-2	Bone morphogenetic protein 2
BSA	Bovine serum albumin
Ca-P	Calcium phosphate
CFU	Colony forming units
Chitlac	1-deoxylactit-1-yl chitosan
Chitlac–nAg	Chitlac containing silver nanoparticles
CSLM	Confocal scanning laser microscopy
CT	Computed tomography
DHT	Dihydrotestosterone
DNA	Deoxyribonucleic acid
DOTA	1,4,7,10-tetraazacyclododecane-1,4,7,10-tetraacetic acid
EPS	Extracellular polymeric slime
FRC	Fiber-reinforced composite (glass fiber reinforced BisGMA-TEGDMA thermoset)
HA	Hydroxyapatite
HCA	Hydroxycarbonate apatite
HSP	Heat shock proteins
IL-6	Interleukin-6
M-CSF	Macrophage colony-stimulating factor
micro-CT	Micro computed tomography
MRI	Magnetic resonance imaging
OPG	Osteoprotegrin receptor
PCL	Poly(ε-caprolactone)
PCR	Polymerase chain reaction
PE	Polyethylene
PEEK	Polyaryletherketone
PET	Positron emission tomography
PIA	Polysaccharide intercellular adhesin
PGA	Poly(glycolide)
PLA	Poly(lactide)
PLCL	Poly(lactide)-co-ε-caprolactone
PLGA	Poly(lactide)-co-poly(glycolide)

OD	Optical density
RANKL	Receptor activator of NF_B Ligand
ROS	Reactive oxygen species
SARM	Selective androgen receptor modulator
SBF	Simulated body fluid
SCV	Small-colony variants
SERM	Selective estrogen receptor modulator
SEM	Scanning electron microscopy
Siglec	CD33 related sialic-acid immunoglobulin like lectins
SR	Self-reinforced (polymer)
SUV	Standardized uptake value
T	Testosterone
T_g	Glass transition temperature
T_m	Melting temperature
TMD	Tissue mineral density
TCP	Tricalcium phosphate
Ti6Al4V	Titanium alloy
VAP-1	Vascular adhesion protein-1
XRD	X-ray diffraction analysis

LIST OF ORIGINAL PUBLICATIONS

This thesis is based on the following original publications, which are referred to in the text by the Roman numerals I-V.

I. **Kulkova J**, Abdulmajeed AA, Könönen E, Närhi TO. Biofilm medium leads to apatite formation on bioactive surfaces. J Appl Biomater Funct Mater. 2013;11(2):95-98.

II. **Kulkova J**, Moritz N, Suokas E, Strandberg N, Leino K, Laitio T, Aro HT. Osteointegration of PLGA implants with nanostructured or microsized β-TCP particles in a minipig model. J Mech Behav Biomed Mater. 2014;6(40C):190-200.

III. Ahtinen A*, **Kulkova J***, Lindholm L, Eerola E, Hakanen A, Moritz N, Söderström M, Saanijoki T, Roivainen A, Aro HT. ^{68}Ga-DOTA-Siglec-9 PET/CT imaging of peri-implant tissue responses and staphylococcal infections. EJNMMI Res. 2014;4(45):2-11.
*Equal contribution

IV. Marsich E, Travan A, Donati I, Turco G, **Kulkova J**, Moritz N, Aro HT, Crosera M, Paoletti S. Biological responses of silver-coated thermosets: An *in vitro* and *in vivo* study. Acta Biomater. 2013;9(2):5088-5099.

V. Aro HT, **Kulkova J**, Moritz N, Kähkönen E, Mattila RA. Local delivery of a selective androgen receptor modulator fails to act as an anabolic agent in a rat bone ablation model. *Manuscript*.

1 INTRODUCTION

Typical short-term applications for bioresorbable implants include orthopaedic bone fixation devices, soft tissue anchorage implants of arthroscopic surgery drug delivery devices, as well as tissue engineering scaffolds. There is a trend toward the development of multifunctional bioresorbable devices. For example, bioresorbable bone fillers or fixation devices can be loaded with anti-bacterial agents to provide both bone healing and the prophylaxis or treatment of osteomyelitis.

Osteoconductive ceramics, *e.g.* calcium phosphates and bioactive glasses, have a unique ability to establish favoribale conditions for a direct and mechanically strong bond between the material and bone. Osteoconductive materials elicit extracellular response, providing a suitable surface for the attachment of bone cells.

Medical devices based on bioresorbable composites form another growing field of research. In composites, a polymer matrix is loaded with bioactive particles to alter the mechanical properties and to stimulate peri-implant bone formation. In addition, osteoconductive calcium phosphate ceramic particles neutralize the normally acidic environment around the dissolving implant, thus lowering the rate of clinical complications.

Drug delivery is a growing field for bioresorbable implants loaded with active compounds. Selective androgen modulators (SARMs) are among the novel molecules under investigation for induction of local osteogenesis in trauma patients with large bone defects as well as in osteoporotic patients with comminuted fractures. Experimental studies have shown that SARMs are able to protect the skeleton from the adverse effects of orchiectomy and ovariectomy.

The number of implantations is constantly increasing due to the aging of world populations. However, biofilm formation on the implant surface and the subsequent host response may challenge the success of implantation. *Staphylococcus aureus* (*S. aureus*) and *Staphylococcus epidermidis* (*S. epidermidis*) are prevalent micro-organisms associated with orthopaedic implant infection. There are a number of strategies for the prophylaxis of orthopaedic infections. Procedure, device, and patient characteristic dependent factors are significant and, if taken under control, may reduce infection rate. Biofilm bacteria are more resistant to antimicrobial agents than their planktonic counterparts and are difficult to detect by routine microbiological techniques. The approach of counting colony-forming units (CFU) is the gold standard for indicating bacterial viability. However, this technique is laborious and not always applicable. Positron emission tomography (PET) is a noninvasive metabolic imaging technique which is promising in terms of the detection of inflammatory tissue response induced by implant-related infections.

2 REVIEW OF THE LITERATURE

2.1 Bone

2.1.1 Composition and structure

Bone is a natural composite which has a hierarchical structure. The organic part of bone, about 30 wt-%, is represented by Type I collagen fibers, non-collagenous proteins and lipids [Fratzl and Weinkamer 2007]. The inorganic part of the bone, about 70 wt-% is prevalent and represented by hydroxy-carbonate-apatite (HCA), which is organized in plate-shaped crystallites. Collagen is a protein composed of triple-helix molecules and responsible for bone toughness. The apatite crystallites, which are embedded between the collagen molecules, reinforce the collagen fibers [Vigued-Carrin et al. 2006, Fratzl and Weinkamer 2007]. The crystallites are aligned in parallel with each other; however, their distribution is not uniform within bone.

Mineralized collagen molecules form fibrils, and in turn, fibrils self-assemble into fibers. These fibers can either arrange into well-organized parallel sheets of lamellar bone or form randomly-organized structures of woven bone [Rho et al. 1998]. The mechanical properties of lamellar bone are superior to those of woven bone. Woven bone appears during physiological and pathological states, when rapid bone formation is needed, *e.g*. fracture healing, tumors and Paget disease [Kalfas 2001]. Cortical and trabecular bone are normally formed in lamellar pattern and composed of osteons [Clarke 2008].

Cortical bone prevalence in adult human skeleton IS 80%, while trabecular bone comprises the remaining 20% [Clarke 2008]. Cortical bone is a dense and solid structure, which has a low metabolic activity compared with trabecular bone. Anatomically, the outer periosteum surface and the inner endosteal surface are outlined in cortical bone. The osteons of cortical bone, which form a wide branching network, are known as the Haversian system [Clarke 2008]. The remodeling activity of the Haversian system affects cortical bone porosity and cortical bone mass.

Trabecular bone is a porous and spongy structure, which consists of semilunar osteons known as packets [Clarke 2008]. Although the morphological structure of trabecular bone has similarity with cortical bone, the substantial heterogeneity of trabecular bone is distinguished [Choi and Goldstein 1992, Keaveny et al. 2001].

In addition, bone is composed of water and cells. Water in bone is particularly found inside the blood vessels and accounts for 25 % of the fresh bone weight % [Weiner and Wagner 1998]. The cellular part of bone accounts for 2 %. There are mesenchymal and hematopoietic stem cell lineages, which give rise to bone cells.

Mesenchymal stem cells are located in bone marrow, endosteum, periosteum and bone canals [Buckwalter et al. 1996a]. These cells proliferate and differentiate into the osteoblasts line. Osteoblasts are large cuboidal cells with one nuclei, enlarged Golgi apparatus, and abundant endoplasmic reticulum [Buckwalter et al. 1996a]. Osteoblasts undergo one of the three scenarios. In the first scenario, osteoblasts maturate and become involved in the synthesis and secretion of the organic matrix of

bone, which is the most recognized function of these cells [Buckwalter et al. 1996a]. In addition, mature osteoblasts influence the mineralization of the bone organic matrix via production of extracellular matrix vesicles and non-collagenous proteins. The nucleation core of extracellular matrix vesicles contains components that allow precipitating of hydroxyapatite crystals [Clarke 2008]. In turn, non-collagenous proteins are known to regulate the amount and size of hydroxyapatite crystals in the matrix [Clarke 2008]. In the second scenario, mature osteoblasts can differentiate into osteocytes, which are the most numerous bone cells in the adult skeleton [Buckwalter et al. 1996a]. Immature osteocytes have inherent similarities in structure with osteoblasts and are surrounded by the bone organic matrix [Downey and Siegel 2006]. Once osteocytes become mature, they shift to the deeper layers of the bone organic matrix and diminish in size due to the loss of cytoplasm [Downey and Siegel 2006]. Osteocytes form broad cell communication networks via long cytoplasmic processes that occupy canaliculi in bone organic matrix. These communication networks are thought to be important in the transportation of nutrients, minerals, and metabolic products, and thus facilitate the coordination of bone cells activity [Downey and Siegel 2006]. In the third scenario, osteoblasts may become quiescent and proceed into bone-lining cells [Downey and Siegel 2006]. Flattened bone-lining cells are metabolically inactive and have cytoplasmic processes that permeate the bone organic matrix [Buckwalter et al. 1996a]. The function of these cells is still unclear [Downey and Siegel 2006]. However, it has been shown that the presence of parathyroid hormone stimulates bone-lining cells to secrete enzymes that prepare the bone surface for osteoclastic activity [Buckwalter et al. 1996a].

For a long time osteoclast precursors remained unidentified. At present, there is no doubt of the hematopoietic origin of these cells. It is believed that monocytes, macrophages and osteoclasts are similar in nature and combined into a unified phagocyte system. However, the initial precursors of these cells are different. Originally, preosteoclasts circulate in the blood as mononuclear cells. Once preosteoclasts reach the resorption area, they merge with each other and give rise to the osteoclast. The osteoclast is a large, motile, multinucleated cell with numerous mitochondria [Buckwalter et al. 1996a, Downey and Siegel 2006]. The main function of this cell is bone resorption. Osteoclasts become polarized, when tightly bound to the bone organic matrix. Thereafter, the ruffled border of the osteoclast, which is a key feature in high lytic and phagocytic activity, secretes H^+ and cathepsin K into resorption domain [Buckwalter et al. 1996a]. Osteoclasts activity creates erosive Howship's lacunas. When the resorption process is complete, bone-turnover products are removed by transcytosis, and osteoclasts undergo apoptosis or return to the dormant state [Buckwalter et al. 1996a].

Bone tissue has metabolic and mechanical function [Buckwalter et al. 1996b]. Metabolic function of bone is expressed in the ability to accumulate and balance the mineral composition of body fluids. The mechanical function of bone is expressed in load bearing capacity. Strength is the main mechanical property of bone, which characterized by the ability of bone to resist external forces. When external forces applied to bone exceed its strength, deformation may occur [Buckwalter et al. 1996b].

Overall, bone is a viscoelastic and anisotropic material [An 2000, Downey and Siegel 2006]. The amount of deformation depends on the type of external forces, rate of applied force and individual bone characteristics. If the amount of external force is low, bone has a lower elasticity and behaves as a viscous material. However, when the amount of external force is high, bone becomes brittle. In contrast with trabecular bone, which has a greater porosity and lower elasticity, cortical bone is able to resist compression better than tensile. In turn, trabecular bone demonstrates a greater resistance to compression when applied parallel to the bone. Hence, bone naturally resists higher external forces in the longitudinal direction [An et al. 2000, An 2000].

External loads applied to bone are known to be a mechanical signal for bone-lining cells and osteocytes. These mechanical signals transform to a chemical one and, thereafter, regulate bone modeling and remodeling [Downey and Siegel 2006]. Modeling and remodeling are physiological adaptation processes, which bone undergoes during its lifespan. While modeling affects overall bone size and shape in response to physiologic changes or external forces, remodeling is a renewing process, which maintains bone strength [Buckwalter et al. 1996b, Clarke 2008]. Modeling is a less frequent process than remodeling in the adult skeleton [Kobayashi et al. 2003]. However, modeling may be increased under certain pathological conditions *e.g*. treatment with anabolic agents, renal osteodystrophy and hypoparathyroidism [Ubara et al. 2003, Ubara et al. 2005, Lindsay et al. 2006].

The remodeling process is dependent on the bone cellular component. In conjunction with osteocytes and lining cells, osteoblasts and osteoclasts constitute the bone reconstruction multicellular unit, which is well balanced and capable of detecting damage in bone and, subsequently, repairing it with new bone [Seeman and Delmas 2006]. The central issue in bone remodeling is that the new bone structure must comply with the upcoming external forces. The natural process of bone formation is absolutely irreproachable. However, without proper arrangement, unbalanced activity of the multicellular unit might lead to increased bone remodeling or provoke extensive bone loss [Seeman and Delmas 2006]. In both cases, bone strength is compromised and the rate of fracture risk is extremely high.

2.1.2 Healing patterns of bone

Bone has a unique capability to regenerate. Fracture healing is a four-phase process, where the inflammation, soft and hard callus formation phases precede the phase of bone remodeling. However, in natural conditions all phases overlap [Schindeler et al. 2008]. During the inflammation phase, the developed hematoma is rapidly infiltrated by inflammatory cells, which produce cytokines and growth factors; subsequently the clotting proceeds into a fibrinous thrombus [Gerstenfeld et al. 2003, Schindeler et al. 2008]. Thereafter, granulation tissue forms as a result of sprouting capillaries in the clot. Phagocytic cells act as sweepers; they remove dead cells and other fragments. Cytokines and growth factors guide this cellular response [Gerstenfeld et al. 2003, Schindeler et al. 2008]. During the soft callus formation phase, growth factors stimulate and coordinate the proliferation of chondrocytes and

fibroblasts, which are the dominant cells at this milestone. These cells create a soft callus, which functions as a mechanical support, as well as a pattern for the hard callus. Chondrocytes attempt to replace the granulation tissue with the cartilage. However, when cartilage production is insufficient, fibroblasts cover these regions with fiberous tissue. Thereafter, the central fibrocartilaginous plug immobilizes the fracture fragments and undergoes mineralization [Barnes et al. 1999].

Soft callus vascularization is accompanied by pro-angiogenic factors stimuli [Gerstenfeld et al. 2003, Kalfas 2001, Deckers et al. 2002]. In addition, the morphogenesis of larger blood vessels and collateral branches is coordinated by angiopoietin I and II. The hard callus formation phase is characterized by the high activity of mature osteoblasts, which leads to bone organic matrix development. This process starts directly in the stable marginal parts of the soft callus. The newly formed bone is irregular woven bone. Interestingly, a hard callus may develop without cartilaginous pattern, either in the state of great mechanical stability or in appositional bone growth [Schindeler et al. 2008]. The differentiation of osteoblasts requires a high local level of oxygen. Therefore, proper vascularization of the fracture healing region is critical for adequate hard callus formation [Peng et al. 2005, Tarkka et al. 2003]. The fourth phase of fracture healing is bone remodeling.

Physiological bone remodeling is characterized by osteoclastic elimination of calcified bone tissue. In terms of bone fracture healing, remodeling is a two-phased process, which consists of the removal of soft callus which is accompanied by the ultimate remodeling of the hard callus [Schindeler et al. 2008]. Soft callus remodeling, which occurs between phases two and three of fracture healing, is mostly osteoclast-independent process. Resent evidence suggests that the remodeling of the soft callus is a non-specific catabolic process which involves various cell types [Schindeler et al. 2008]. This process includes the ongoing elimination of the soft callus fibrocartilage and subsequent woven bone formation. In turn, hard callus remodeling is restricted by osteoclastic activity. M-CSF and Receptor Activator of NFκB Ligand (RANKL) produced by osteoblasts are essential for osteoclastogenesis from their hematopoietic stem cells. In addition, M-CSF is responsible for the initial stimulation of the differentiation of haemopoietic stem cells [Fan et al. 1997]. RANKL, synthesized by mature osteoblasts, plays an important role in bone remodeling being activator of osteoclastogenesis and stimulator of mature osteoclasts. The RANKL activity is tightly regulated by the osteoprotegrin (OPG) receptor, which is an antagonist of osteoclasts differentiation [Blair et al. 2006]. In addition, numerous cytokines and growth factors are known to mediate osteoclastogenesis [Quinn and Gillespie 2005, Lee and Lorenzo 2006, Kaneko et al. 2000].

2.2 Biomaterial-related infections

2.2.1 Aetiology

It is highly important to note, that all implants are to some extend inclined to bacterial colonization. Clinical observations and experiments with animal models have

shown that the presence of skeletal implants promotes immediate and delayed infections [Gristina and Costerton 1985]. The surface of the implant material dictates the propensity for bacterial colonization [Hickok and Shapiro 2012]. As an example, enhanced protein absorption to the implant surface may enhance osteointegration; however, this material property may also predispose the surface to bacterial colonization.

Recently, it has been shown that after primary hip and shoulder replacements, the intra-operative infection rates are 1% and 2% respectively. However, after secondary total hip and knee replacements, the infection rates increase to 3.2% and 5.6 % respectively [Stoodley et al. 2005, Zimmerli et al. 2004]. Although, the occurrences of infection seem to be low, total hip replacements are common orthopaedic procedures. Therefore, complications due to infection dramatically increase the hospital costs and morbidity of the patients.

American Association of Orthopaedic Surgeons has identified four classes of prosthetic infections:

Class 1 is characterized by two positive intraoperative cultures.

Class 2 is characterized by first month postoperative infection.

Class 3 is characterized by chronic infection which is present for more than 1 month [Montenaro et al. 2011].

Consequently, the infection may occur peri-operatively or hematogenously at a later phase of the implant's lifespan. In the peri-operative scenario, the patient's skin and the airborne particles *e.g.* originating from surgical personnel are the main sources of infection [Pittet and Ducel 1994]. In the hematogenous scenario, the infection often result from microorganisms originating from contaminated focus in the body, such as a urinary tract infections, or a transient bacteremia related to a dental surgical procedure. Even 100 CFU are able to induce the biofilm formation on the implant surface [Montenaro et al. 2011]. Normally, the host immune system is able to identify and prevent infection. However, in some cases, the host itself enhances the infection rate by creating the conditions favorable for pathogen colonization [Ahmed et al. 2001, Hauck and Ohlsen 2006, Piroth et al. 2008, Bos et al. 1999].

Coagulase-positive or-negative species, belonging to the *Staphylococcus* genus, are the dominant isolates in biomaterial-related infections of joint replacement [Tsukayama et al. 2003, Montenaro et al. 2011].

It was reported [Montenaro et al. 2011] that *Staphylococcus aureus* (S. aureus) is the most prevalent (35.5% overall) among the staphylococcal species causing orthopaedic infections. In the presence of medical devices, the frequency of orthopaedic infections caused by *S. aureus* was reported as 31.7 % compared to 40.2 % without medical devices. In contrast, *Staphylococcus epidermidis* (S. epidermidis) causes 39.0 % medical-device associated infections compared to 15.9% without medical devices. The overall frequency of orthopaedic infections caused by *S. epidermidis* was reported as 29.9%.

2.2.2 Pathogenesis

The pathogenesis of biomaterial-related infections depends on biofilm formation. Biofilm is a multilayer structure, where communities of microorganisms are imbedded in extracellular polymeric slime (EPS) and attached to the surface. The exact mechanism of mature *Staphylococcal* biofilm formation is poorly known [Fey and Olson 2010]. However, it has been suggested to be a four/step process including the initial interaction with the surface, accumulation, maturation and detachment [Montanaro et al. 2011].

The initial interaction, the first step of biofilm formation, is a non-specific process dependent on, hydrophobicity, the charge and the chemical composition of the implant surface [Bos et al. 1999]. The cell wall autolysins/adhesins AtlE in *S. epidermidis* and AtlA in *S. aureus* are specific proteins which mediate the initial interaction with hydrophobic surfaces and possibly take part in subsequent biofilm accumulation [Heilmann et al. 1997]. In addition, these autolysins are able to release extracellular deoxyribonucleic acid (DNA), which is an essential adherence factor in both species. Thereafter, the host rapidly coats foreign body, such as an implant, with plasma proteins, including vitronectin, fibronectin and fibrinogen. These host proteins give microorganisms an advantage in regard to attachment and subsequent biofilm formation [Bos et al. 1999]. In both *S. epidermidis* and *S. aureus,* several adherence factors, reported as microbial surface components recognizing adhesive matrix molecules (MSCRAMMs) have been identified to mediate binding to serum proteins [Pei and Flock 2001a, Pei and Flock 2001b, Sellman et al. 2008].

In the second step of biofilm formation, known as accumulation, the intercellular adhesion locus (ica ADBC) mediates the synthesis of polysaccharide intercellular adhesin (PIA) in both *S. epidermidis* and *S. aureus*. PIA is a cell surface glycan composed of β-1,6-linked 2-acetamido-2-deoxy-D-glucopyranosyl residues (GlcNAc) [Mack et al. 1996, Heilmann et al. 1996, Gerke et al. 1998, Cramton et al. 1999]. The synthesis of PIA is dependent on environmental stress conditions and tightly regulated by numerous factors affecting ica expression [Knobloch et al. 2001, Baldassarri et al. 2001, Cue et al. 2012]. The main role of PIA is to enhance biofilm formation in parallel with inhibition of neutrophil-dependent killing and antibiotic activity [Vuong et al. 2004a, Vuong et al. 2004b, Begun et al. 2007, Lewis 2008, Ganeshnarayan et al. 2009]. In addition, it has been shown in *S. epidermidis* that PIA has a stimulating effect on the maturation of biofilm [Fey and Olson 2010].

During the third step of biofilm formation, known as biofilm maturation, micro-organisms exist in four metabolic states: aerobic, anaerobic, dormant and dead [Rani et al. 2007]. These metabolic states permit bacteria to change cell wall properties, DNA-synthesis, and, therefore, increase their survival rate and virulence [Stewart and Franklin 2008]. Bacteria living within the biofilm are more tolerant to environmental stress that their planktonic counterparts [Beenken et al. 2004, Yao et al. 2005, Resh et al. 2005]. In contrast to the planktonic form, *S. epidermidis* and *S. aureus* living in biofilm carry a specific arginine deiminase operon (ADI). This ADI pathway serves as a survival mechanism under microaerobic and anaerobic conditions when arginine is

catabolized and ammonia and adenosine triphosphate are generated [Beenken et al. 2004, Yao et al. 2005, Fuchs et al. 2007, Kohler et al. 2008, Zhu et al. 2007]. Overall, the energy derived through arginine catabolism is significant in biofilm maturation.

The fourth step of biofilm formation is detachment, which involves dispersal of planktonic cells from the biofilm and their subsequent accumulation in other organs and systems. The exact mechanism of this stage remains unclear [Fey and Olson 2010]. However, it has been shown previously that changes in pH level and cell starvation are initial factors for detachment. Thereafter, phenol-soluble modulins act as surfactants and disturb bacterial interaction [Otto 2008, Boles and Horswill 2011].

Overall, bacterial biofilm serves as a shelter and protects bacteria from immune system surveillance and antibiotics. Therefore, deep understanding of the biofilm formation scenario is essential for hospital personnel, who are involved in diagnostics and treatment of surgical infections.

2.2.3 Prophylaxis and treatment

Challenges in biomaterial-related infections are associated with complicated diagnostics and microbial antibiotic resistance. Antibiotic resistance is based on two mechanisms. The first mechanism is related to the thickness of EPS, which may predict or lower the antibiotic diffusion. The second mechanism is related to the low metabolic activity of bacteria embedded in the deeper layers of EPS. This dormant bacterial metabolic state, also known as small-colony variants (SCVs), has been reported for a broad range of bacterial genera, including *S. epidermidis* and *S. aureus* [Jensen 1957, Baddour et al. 1990]. The clinical presentation of SCV varies from 1% to 30% in different studies [Proctor 2006]. SCV are characterized by a low growth rate, increased PIA production [Al Laham et al. 2007] and the ability to survive in nutrient and oxygen depletion [Neut et al. 2007, Costerton et al. 1987, Montenaro et al. 2011].

SCV metabolic stage is denoted by reduced production of toxins which prevents mammalian cell lysis [von Eif et al. 2000] and which subsequently allow bacteria to persist inside non-professional phagocytes, *e.g.* endothelial cells, fibroblasts, and osteoblasts [Hudson et al. 1995, Vaudaux et al. 2002]. Once antimicrobial therapy is completed and immune response to the infection has subsided, SCVs return to the virulent form and lyse the host cell [Proctor et al. 1998]. The immune response and antibiotic efficiency are limited, when SCV are shielded inside the host cells. In addition, the slow growth rate and reduction in electron transport of SCVs lead to diminished effectiveness of cell-wall active antibiotics and a decline in the uptake of antimicrobial agents. These mechanisms are crucial in understanding antibiotic resistance.

Moreover, detection of SCVs by routine microbiological techniques is limited due to their very slow growth rate on standard agar plates. It has been shown previously that culture period for SCVs is at least 6 days in contrast to the 48 h needed for culturing of metabolically normal *S. aureus* [Proctor et al. 1995, Neut et al. 2007]. Therefore, a longer culture period may increase the detection rate for infections.

Generally, treatment of biomaterial-related infections is difficult and requires adequate surgical revision in addition to prolonged antibiotic eradication [McDonald et al. 1989, Tauffevin et al. 1999]. The combination of rifampin with other antibiotics, *e.g.* fluoroquinolone, is the most effective therapy against slowly growing bacteria [Vaudaux et al. 2006, Widmer et al. 1990, Sendi et al. 2006]. However, the vascularization of the infected site is frequently compromised; therefore systemic antibiotic administration alone is not sufficient [Gristina 1987, Arciola et al. 2012, Busscher et al. 2013]. Prior to re-implantation, local antibiotic administration is obligatory. Gentamicin-loaded bone cement beads have been used as an effective drug delivery system for the local treatment of bone and soft-tissue infections [Jiranek et al. 2006]. Nevertheless, although a high local concentration of gentamicin is effective against staphylococci [von Eiff et al. 1997], the surface of the beads can provoke bacterial attachment and antibiotic resistance [Neut et al. 2001]. In addition, this treatment strategy causes tremendous harm to the patient, since it requires at least two surgical interventions. Antimicrobial implant coatings may prevent the relapse of the infection in the case of revision surgery and serve as a prophylactic in the case of the placement of a primary prosthesis [Hickok et al. 2012].

2.3 Skeletal reconstructive biomaterials

2.3.1 Classification

Traditionally, biomaterials are defined as non-toxic natural or synthetic biomedical materials, which have been engineered to intimately interact with living systems and are intended to replace, treat or improve the function of the tissues and organs of living beings [Williams 1999, Williams 2009]. The biomaterials in clinical use are chemically different and can be divided into four categories; metals, ceramics, polymers and composites.

Every implanted material evokes a tissue reaction, but the response of the host depends on the type of material. In this regard, biomaterials can be subdivided into nearly bioinert, bioresorbable, bioactive and porous [Cao and Hench 1996], see Table I. Nearly bioinert materials are always surrounded with a non-adherent fibrous capsule. These materials allow bone formation on their surface although this bone is structurally weak and there is no bone bonding interaction. Bioresorbable materials are progressively decomposed and replaced with host tissues. These types of temporary materials are optimum for short-term applications, when load bearing capacity is not required. Bioactive materials are characterized by bone bonding capacity [Cao and Hench 1996]. In particular, bioactive ceramics form a biologically active hydroxycarbonate apatite layer (HCA). HCA has the same chemical structure, as the mineral phase of bone and is formed due to ion exchange between the material surface and the host. Bioactive materials are divided according to their biological behavior into osteopromotive and osteoconductive [Cao and Hench 1996]. Osteopromotive bioactive materials induce the extra- and intracellular response at the interface and endorse *de novo* bone formation. In contrast, osteoconductive

materials allow bone growth only on the implant surface or inside material pores, channels etc [Albrektsson and Johansson 2001].

Bone growth on the implant surface is restricted by the differentiation of bone cells. Trauma, which occurs during the implantation, is a major boost for the recruitment of undifferentiated cells. Therefore, the assertion that certain biomaterials perform as osteoinductors has been questioned [Albrektsson and Johansson 2001]. Nevertheless, it should be noted that the amount of newly formed bone is dependent not only on the healing patterns of bone, but also on the individual biomaterial properties.

Table I. Examples of biomaterials [Williams 1992, Hench and Wilson 1993, Cao and Hench 1996, Middleton and Tipton 2000, Aunoble et al. 2006, Kurtz and Devine 2007, D'Amelio et al. 2013, Moritz et al. 2014]

Chemical composition	Biomaterial	Bone-bonding	Reactivity
Metals	• Stainless steel	Bioinert	Biostable
	• CrCo-alloys	Bioinert	Biostable
	• Tantalum	Bioinert	Biostable
	• Titanium and alloys	Bioinert	Biostable
Ceramics	• Al oxide	Bioinert	Biostable
	• Zr oxide	Bioinert	Biostable
	• Hydroxyapatite (HA)	Bioactive	Bioresorbable
	• Calcium phosphates (Ca-P)	Bioactive	Bioresorbable
	• Bioactive glasses (and glass-ceramics)	Bioactive	Bioresorbable
Polymers	• Polymethylmetacrylate	Bioinert	Biostable
	• Polyaryletherketone (PEEK)	Bioinert	Biostable
	• Polyethylene (PE)	Bioinert	Biostable
	• Bisphenol-A-dimethacrylate and triethyleneglycoldimethacrylate (BisGMA-TEGDMA)	Bioinert	Biostable
	• Silicones	Bioinert	Biostable
	• Aliphatic polyesters (PLA, PGA, PLGA *etc.*)	Bioinert	Bioresorbable
	• Polysaccharides (*e.g.* Chitosan, Chitlac)	Bioinert	Bioresorbable
Composites	• PEEK / carbon fibers	Bioinert	Biostable
	• PE / carbon fibers	Bioinert	Biostable
	• PE / HA (Hapex ^{TM})	Bioactive	Partially bioresorbable
	• Aliphatic polyesters / HA or Ca-P	Bioactive	Bioresorbable
	• BisGMA-TEGDMA / glass fibers	Bioinert	Biostable

In addition, porous biomaterials allow fluid exchange, cell migration, vascularization and bone ingrowth into the pores and incorporation of the implant into the host tissue [Jones et al. 2009]. This is also called “biological fixation”. The optimal pore size needed for bone ingrowth is generally considered to be in the range of 100 – 400 μm.

2.3.2 Bioresorbable polymers

Bioresorbable polymers are used in various medical applications. In contact with physiological environment, the bioresorbable polymers start to degrade but preserve their mechanical properties for a certain period of time, thereafter being absorbed and excreted [Middleton and Tipton 2000]. The degradation is a heterogeneous process, which proceeds by a chemical hydrolysis of the hydrolytically unstable backbone [Middleton and Tipton 2000]. Initial degradation occurs rapidly on the implant surface due to abundant water access; however, surface degradation products are easily washed away. When the water penetrates the bulk of the implant and attacks the chemical bonds, an increased concentration of carboxylic end groups creates an acidic environment. In turn, the hyperacidity catalyzes the process of hydrolytic scission of ester bonds; therefore, degradation occurs faster in the middle of the bulk. The acidic degradation products in the chain ends and the presence of additives may result in a subsequent adverse cellular response [Ignatius and Claes 1996, Böstman and Pihlajamäki 2000, Meyer et al. 2012]. Consequently, the degradation is denoted by gradual decrease of molecular weight, followed by the decline of mechanical strength and, eventually, mass loss [Athanasiou et al. 1998, Middleton and Tipton 2000]. In addition, enzymatic activity of phagocytizing cells may influence the process of degradation [Bergsma et al. 1995, Ignatius and Claes 1996, Middleton and Tipton 2000].

The most commonly used and well-studied synthetic bioresorbable polymers are high molecular weight aliphatic polyesters such as poly(lactide) (PLA) and poly(glycolide) (PGA). These polymers are composed of homopolymers or copolymers of lactide or glycolide and are synthesized by ring-opening polymerization. Originally, lactide and glycolide are intermediate cyclic dimers of lactic and glycolic acid respectively. Lactic acid is asymmetrical in structure; hence, PLA exists in two stereo forms, which are dexorotary D PLA and levorotary L PLA, in addition, DL PLA is a mixture of both forms [Athanasiou et al. 1998, Middleton and Tipton 2000]. PGA exists in one form and is known to be the simplest linear aliphatic polyester. Co-polymers of PLA and PGA (PLGA) are commonly used in combinations represented in different ratios. The ratio variations are essential for altering the material mechanical properties and degradation rate [Athanasiou et al. 1998, Middleton and Tipton 2000]. PLA degrades to lactic acid, which enters the tricarboxylic acid cycle and is decomposed into water and dioxide [Athanasiou et al. 1998]. The end degradation product of PGA is glycolide, which is either removed by urine or form glycine. After further transformations, glycine enters the tricarboxylic acid cycle and is converted to water and carbon dioxide [Athanasiou et al. 1998].

Molecular weight, intrinsic viscosity, crystallinity, glass transition temperature (T_g) and melting temperature (T_m) are important physical properties of polymers [Athanasiou et al. 1998, Middleton and Tipton 2000]. Molecular weight and intrinsic viscosity are correlated with each other and both have a strong influence on mechanical properties and the degradation rate of the polymer. Intrinsic viscosity is

the measure which determines the average size of the molecules in the polymer chain and polymer flow resistance [Athanasiou et al. 1998].

Table II. Physical and degradation properties of selected bioresorbable polymers (Adapted from Middleton and Tipton 2000)

Polymer	Crystallinity (%)	Hydrophilicity	T_m (°C)	T_g (°C)	Modulus (GPa)	Degradation time (months)
PGA	45 - 55	Hydrophilic	220 - 225	35 - 40	7.0	6 – 12
L PLA	~ 37	More hydrophobic than PGA	173 - 178	60 - 65	2.7	> 24 (3 - 5 yrs.)
DL PLA	Amorphous	More hydrophobic than PGA	Amorphous	55 - 60	1.9	12 -16
PLGA 50DL:50G	Amorphous*	related to PGA content**	Amorphous	45 - 50	2.0	1 – 2
PLGA 85DL:15G	Amorphous*	related to PGA content**	Amorphous	50 - 55	2.0	5 – 6
PCL	~ 40	More hydrophobic that PGA and PLA	58 - 63	-65 - -60	0.4	> 24 (2 - 3 yrs.)

*Semicrystalline, contains amorphous and crystalline regions [Athanasiou et al. 1998].
**Makadia and Siegel 2011

Crystallinity denotes the ordered spatial arrangement of polymer chains and has a profound effect on the mechanical [Nielsen 1974] and degradation [Athanasiou et al. 1998, Middleton and Tipton 2000] properties of polymers. Regarding the degree of crystallinity, polymers are classified as semicrystalline or amorphous. There is no fully organized crystalline polymer; therefore semicrystalline polymers contain both crystalline and amorphous regions [Middleton and Tipton 2000]. PGA, D PLA and L PLA are mostly crystalline, while DL PLA is mostly amorphous. During the synthesis process of L PLA and PGA copolymers, glycolic units disrupt the crystallinity of L PLA which then accelerates the degradation process. The higher hydrophilicity of glycolic units results in rapid degradation compared to aliphatic polyesters composed of enantiomeric lactic units [Li 1999]. As seen in Table II, there is frequently no linear relationship between copolymer composition and degradation rate [Middleton and Tipton 2000]. The molecular weight of the polymers is directly related to the melting point and degree of crystallinity [Makadia and Siegel 2011].

The T_g and T_m influence both mechanical properties as well as the degradation rate [Middleton and Tipton 2000]. Semicrystalline polymer may be prepared in a rod shape or molded parts, when raised above T_m. The amorphous regions of semicrystalline polymers and amorphous polymers exhibit T_g. When temperature is above T_g, a polymer possesses elastic rubber properties; however, when the temperature is below T_g, a polymer resembles a glass [Middleton and Tipton 2000]. Polymers with a T_g near the body temperature are more ductile, which can be taken advantage of in some clinical applications.

To serve as implant materials, bioresorbable polymers should have an adequate degradation rate to allow for the gradual load transfer from implant to bone as the implant is resorbed and replaced by host tissues [Athanasiou et al. 1998]. In addition, bioresorbable polymers should be readily metabolized, without provocation of a toxic or inflammatory reaction [Middleton and Tipton 2000]. A simple manufacturing process and acceptable shelf-life are of extra importance [Middleton and Tipton 2000]. During the manufacturing process, the choice of monomers and initiators, process conditions and the presence of additives are noted to affect the final properties of the polymers [Middleton and Tipton 2000]. In turn, these properties which include molecular weight, crystallinity, hydrophilicity, melt and glass transition temperatures, etc., determine the mechanical strength [Nielsen 1974] and *in vivo* performance of the bioresorbable polymers [Athanasiou et al. 1998, Middleton and Tipton 2000] (Table II).

In knee surgery, interference screws made of bioresorbable polymers have conclusively shown to be comparable to ordinary titanium interference screws in the fixation of anterior cruciate ligament (ACL) grafts [Andersson et al. 2009, Shen et al. 2010]. The major advantage of bioresorbable interference screws is the absence of artifacts in magnetic resonance imaging (MRI) of the knee; in addition, due to complete resorption, there are fewer complications with knee surgery in the future [Andersson et al. 2009]. Similarly, the use of bioresorbable suture anchors and tacks is a distinguished method in shoulder surgery [Park et al. 2006] which played a critical role in the transition from open to arthroscopic techniques [Dhawan et al. 2012].

Despite these promising findings, in terms of patients' functional recovery after surgery, bioresorbable implants bear a certain risk of complications. The reported complications of bioresorbable interference screws in ACL reconstructions include breakage on insertion and slower healing of the surgical approach [Andersson et al. 2009]. Based on a recent study, when bioresorbable interference screw fixation is used for ACL reconstruction, knee joint effusion is more frequent than with metallic interference screw fixation [Shen et al. 2010]. The reported complications of bioresorbable anchors implanted in the shoulder include implant fracture, secondary migration due to poor fixation, aseptic loosening, osteolysis and chondrolysis [Park et al. 2006, Dhawan et al. 2012]. High local acidity due to fast degradation may lead to the adverse tissue reactions [Böstman and Pihlajamäki 2000], or at least negatively interfere with the normal healing processes during degradation. *In vitro* studies have shown that high concentrations of lactic and glycolic acids have negative effects on osteoblasts [Meyer et al. 2012]. This finding was proven *in vivo* during long-term clinical studies on ACL-reconstruction patients. It has been shown that the ACL screws made of pure L PLA degrade completely; however, L PLA was never replaced by bone tissue [Barber and Dockery et al. 2006].

Complications related to the incomplete degradation of crystalline PLA were also reported [Bergsma et al. 1995, Nho et al. 2009]. Even over 5 years postoperatively, residues of the material were found internalized by various types of cells causing swelling at the site of implantation [Bergsma et al. 1995]. In addition, incomplete ossification may lead to replacement of bone by fibrous tissue [Nho et al.

2009]. All these complications emphasize the need for further investigations in the area of bioresorbable polymers for orthopedic implant materials.

2.3.3 Bioresorbable polymers as drug delivery systems

Controlled drug delivery is an essential clinical application of bioresorbable polymers. In general, drug delivery systems are subdivided into two categories: temporal and local [Nair and Laurecin 2005]. Temporal delivery systems maintain the therapeutic drug level in the body for a prolonged period of time to avoid recurrent administration as well as over- and under dosages. In turn, local delivery systems release drugs and other biologically active compounds targeting a specific tissue or organ for a predefined period of time [Nair and Laurecin 2005].

In drug delivery systems, bioresorbable polymers either serve as matrices for the incorporation of drugs, or form conjugates with the drugs. When conjugates are formed, drug molecules are attached to the side chains of the polymers [Leong and Langer 1987]. The release of the drug is achieved by chemically controlled mechanisms and occurs simultaneously with the degradation of the polymer matrix. However, it should be taken into consideration that the diffusion of the drug molecules might influence the rate of release [Leong and Langer 1987]. The properties and geometry of the polymer matrix, the characteristics and the amount of the drug, and the nature of matrix-drug interaction were reported to influence the efficacy of a drug delivery system [Nair and Laurecin 2005, Makadia and Siegel 2011]. In an ideal case, the degradation rate of the polymer matrix should match the release of the drug in order to avoid the accumulation of the undegraded polymer in the body [Leong and Langer 1987].

Initially, PLA matrices were widely used. Later on, drug delivery systems based on PLGA became common, since the degradation properties of these matrices, and consequently the drug release rate, can be controlled by altering the properties and the ratio of the copolymers [Nair and Laurecin 2005, Makadia and Siegel 2011]. For example, the increase in release rate was reported to be related to the decrease in the PLA/PGA ratio, crystallinity and hydrophilicity [Makadia and Siegel 2011].

Poly(ε-caprolactone) (PCL) is a biocompatible polyester which exhibits exceptionally low T_g and T_m and a low degradation rate (Table II). In addition, unlike PGA and PLA, the degradation products of PCL do not create an acidic environment which could provoke adverse tissue reaction and affect the structural integrity of the drugs [Park et al. 1995]. The degradation properties of PCL can be controlled by copolymerization with PLA in different ratios [Malin et al. 1996]. Consequently, blends of PCL and copolymers are recommended for long-term drug delivery applications [Ueda and Tabata 2003, Nair and Laurecin 2005].

Chitosan is a natural polymer, which is produced by the deacetylation of chitin. Chitosan is widely acknowledged in literature for its excellent biocompatibility [Di Martino et al. 2005, Suh and Matthew 2000]. However, chitosan is characterized by pH-dependent solubility and low specifity of molecular signaling. Therefore, to overcome these limitations lactose-modified chitosan, termed Chitlac, was

developed. Chitlac is a highly branched biocompatible and bioactive polymer due to the presence of terminal galactose units on the side chains [Donati et al. 2005]. In addition, Chitlac was proposed as a biological slow-release drug delivery system, which serves as a matrix for the incorporation of silver ions [Travan et al. 2009]. This system is capable of promoting bone cells proliferation and simultaneously possesses antibacterial properties [Marsich et al. 2013, Travan et al. 2009].

2.3.4 Osteoconductive calcium phosphate-based ceramics

Osteoconductive calcium phosphate-based (Ca-P) ceramics have received considerable attention owing to their similarity to the bone mineral phase, HCA, in terms of chemical composition and structure. Upon exposure to physiological fluids, osteoconductive Ca-P ceramics degrade into phosphate and calcium ions and form a direct bond with bone via a HCA layer which forms on their surface. In long term of implantation, osteoconductive Ca-P ceramics elicit extracellular response, providing a suitable surface for cellular attachment [Cao and Hench 1996, Välimäki and Aro 2006] and are gradually replaced by bone.

These biomaterials are commonly used as bone graft substitutes or as coatings on implants in medical and dental applications [LeGeros 1993]. Implantable forms include particulate, blocks and injectable materials, *e.g.* some bone cements. Osteoconductive Ca-P ceramics can be of natural origin, *e.g.* xenogenic bone mineral, or synthetic. Synthetic osteoconductive ceramics include HA, tricalcium phosphates (TCP) and biphasic calcium phosphates (BCP) which consist of mixed HA and TCP phases in different ratios [LeGeros 2003]. In addition, there are osteoconductive silica-based bioactive glass and glass-ceramics [Cao and Hench 1996, Ducheyne and Qiu 1999].

The processing conditions, *e.g.* temperature, pressure and duration of the sintering process, influence physico-chemical properties of osteoconductive Ca-P ceramics. Density increases and microporosity decreases with the increase in sintering temperature time and pressure [LeGeros 1993]. In turn, dissolution properties are dependent on morphology, composition, crystallographic structure and crystallinity, i.e. crystal size and perfection. In addition, the dissolution rate is influenced by the properties of the solution, *e.g.* pH [Christoffersen et al. 1978]. The dissolution rate of HA is relatively low [LeGeros 1993], which can be a clinical disadvantage. BCPs provide a way to improve the dissolution and bioreactivity by manipulation of the HA/TCP ratio [LeGeros 2003]. Osteoconductive Ca-P ceramics of different physical morphologies, *e.g.* bulk, granules or powder dissolve with a different rate. Moreover, denser materials dissolve slower than materials with high porosity [LeGeros 1993]. The dissolution rate of osteoconductive Ca-P ceramics of equal composition but different crystallographic structure varies. For example, TCP exists in two crystallographic structures, α-TCP and β-TCP. The dissolution rate of α-TCP is higher than that of β-TCP. The crystallinity of osteoconductive Ca-P ceramics is influenced by the sintering temperature. For example, for HA sintered at lower temperature, the lattice defects are more abundant than at high temperature [LeGeros 1993].

In general, ceramics are brittle materials *e.g.* for HA the reported Young's modulus and bending strength were 81.4 GPa and 113 MPa, respectively [Akao et al. 1981]. When ceramics are subjected to loads they fail without plastic deformation. In addition, the mechanical properties of these materials are difficult to assess, as surface cracks and voids act as stress-concentration centers and influence the results of measurements.

2.3.5 Bioactive glasses

Bioglass® 45S5 is a silica-based bioactive glasse (BAG) introduced by Larry Hench in the early 1970s [Hench et al. 1971]. Bioglass® 45S5 is a biodegradable glass, which is composed of 45 % SiO_2, 24.5 % Na_2O, 24.5 % CaO and 6 % P_2O_5 by weight and possesses a bone-bonding ability. Bioglass® 45S5 was approved by the US Food and Drug Administration and has been used as a bone graft substitute in more than a million patients [Jones 2012]. The invention of Bioglass® 45S5 launched the field of biomaterials and gave rise to various novel biomaterials based on BAGs. S53P4 (BonAlive™, BonAlive Biomaterials Ltd., Finland) contains 53 % SiO_2 by weight. It is a moderately reactive BAG developed in Åbo Akademi University.

Bone-bonding, a distinctive feature of BAG, is achieved via the formation of a bone-like HA layer on the material surface when in contact with aqueous solutions [Kaur et al. 2014]. HA resembles bone mineral and interacts with the collagen fibrils of the host´s bone. The mechanism of bone-bonding relies on the initial BAG dissolution and subsequent HA layer formation. HA layer formation is comparable with a glass corrosion process. In particular, rapid cation exchange of Na^+ and Ca^{2+} is accompanied by a dramatic increase in pH level. In turn, the high local pH attacks the Si-O-Si chemical bonds; thereafter, the increased concentration of Si-OH groups creates a silica-rich layer. The silica-rich layer is permeable and allows the migration of Ca^{2+} and PO^{3-}_4 groups. This leads to the formation of a surface film rich in amorphous $CaO\text{-}P_2O_5$. Subsequently, hydroxyls and carbonates from aqueous solution are incorporated within the surface film. The amorphous $CaO\text{-}P_2O_5$ film is crystallized and the formation of the HA layer is completed [Jones 2012]. The formation of the HA layer on a biomaterial surface *e.g.* BAG when immersed in a simulated body fluid (SBF) is an *in vitro* golden standard to assess the potential of a biomaterial *in vivo* [Kokubo et al. 1990].

BAG has been shown to possess antibacterial properties *in vitro* [Mortazavi et al. 2010, Leppäranta et al. 2008, Hu et al. 2009]. The antibacterial properties of BAG are mainly attributed to the increase of pH level caused by the leaching of the ions. In addition, high ionic concentration creates a hyperosmotic environment which in turn can challenge the bacterial growth [Stoor et al. 1998]. S53P4 was approved in Europe for the treatment of osteomyelitis. Since then, S53P4 attracts a considerable attention in terms of local application for the treatment of bone infections *per se* [Lindfors et al. 2010, McAndrew 2013, Romanò et al. 2014].

2.3.6 Osteoconductive bioresorbable composites

Composites are defined as materials which contain at least two components and two phases [Nielsen 1974]. This thesis reviews bioresorbable particulate composites only. Bioresorbable composites typically contain a continuous polymer matrix phase and discontinuous osteoconductive ceramic phase. The properties of the composites are different compared to those of plain polymers or ceramics.

Composite materials comprised of osteoconductive Ca-P ceramic particles incorporated into a bioresorbable polymer matrix are theoretically anticipated to have improved mechanical and osteoconductive properties [Mohn et al. 2010, Zhou et al. 2012]. In general, the size and the morphology of the particulate phase as well as the strength of the interfacial bond between the phases determine the mechanical properties of the composite materials [Nielsen 1974, Wang 2003]. In practice, in the case of osteoconductive bioresorbable composites, the addition of osteoconductive Ca-P ceramic particles into the polymer matrix leads to an increase in stiffness, *i.e.* Young's modulus. However, the strength of these composites was reported to be marginal or even decreased compared to pure polymers. Weak interfacial bond between polymer matrix and ceramic fillers are suggested to be the reason for the low mechanical strength [Kikuchi et al. 1997, Kunze et al. 2003]. A number of studies were performed to assess the mechanical properties of the composites [Verheyen et al. 1992, Kikuchi et al. 1997, Shikinami and Okuno 1999, Shikinami and Okuno 2001, Ignatius et al. 2001, Hasegawa et al. 2006, Ehrenfried et al. 2008, Yamadi and Kobayashi 2009]. A summary of the results is given in Table III.

An ideal implant material should exhibit Young's modulus similar to that of cortical bone. Thus, the effect of "stress-shielding", adverse peri-implant bone remodeling due to non-physiological loading conditions, could be avoided. For adequate load-bearing, the strength of the implant should be superior to that of cortical bone. For comparison, the Young's modulus and bending strength of human cortical bone are 9.1 – 15.7 GPa and 103 - 238 MPa respectively [An 2000], for Ti-alloy (Ti6Al4V), the values are 116 GPa and 897 – 1034 MPa for stainless steel, the values are 190 GPa and 792 MPa [Hallab et al. 2004]. For Cr-Co-alloys the values are even higher. As seen in Table III, the mechanical properties of osteoconductive bioresorbable composites are inferior to those of cortical bone and typical implant materials; therefore, these composites are not suitable for load-bearing applications [Verheyen et al. 1992]. It should also be taken into consideration that the mechanical properties of osteoconductive bioresorbable composites decrease as a function of implantation time. Therefore, improved initial mechanical properties may be of little clinical relevance if the implants have a high degradation rate [Ignatius et al. 2001]. Moreover, it is expected that the addition of osteoconductive Ca-P ceramic particles neutralizes the normally acidic environment in the vicinity of the dissolving implants, increasing the onset time of degradation [Ehrenfried et al. 2008] and thus, possibly lowering the risk of adverse tissue reactions. Osteoconductive Ca-P ceramic fillers have been shown to improve the surface wettability of bioresorbable polymers and

therefore, enhance the attachment and proliferation of osteogenic cells [Kim et al. 2007]. Alternatively, the acidic products of the degradation of the polymer matrix were shown to increase the degradation rate of osteoconductive Ca-P ceramics [Yamamuro et al. 1988]. To summarize, implants made of bioresorbable composites should have a balance between the implant composition, mechanical properties and degradation rate.

Table III. Initial mechanical properties of selected bioresorbable micro- and nanocomposites

Study	Polymer matrix	Filler material	Amount of filler (wt %)	Filler granule size (µm)	Modulus (GPa)	Strength in bending (MPa)
Verheyen et al. 1992	L PLA	-	0	-	5.2 ± 0.7*	131.7 ± 11.0
	L PLA	HA	30	<45	6.8 ± 0.3*	93.0 ± 2.8
	L PLA	HA	50	<45	8.0 ± 2.1*	52.8 ± 12.4
	L PLA	HA	30	< 5	4.8 ± 0.3*	59.6 ± 1.9
Kikuchi et al. 1997	PLA	-	0	-	2.0 ± 0.3	51.0 ± 6.1
	PLA	HA	60	nd	2.3 ± 0.1	22.0 ± 1.3
	PLA	HA	72	nd	2.3 ± 0.3	15.0 ± 1.1
Shikinami and Okuno 1999	L PLA	-	0	-	6.5 ± 0.3	258.5 ± 2.8
	L PLA	HA	20	3	7.0 ± 0.2	252.2 ± 3.1
	L PLA	HA	30	3	7.6 ± 0.1	269.2 ± 2.5
	L PLA	HA	40	3	9.1 ± 0.4	270.0 ± 4.1
	L PLA	HA	50	3	12.3 ± 0.2	267.5 ± 2.3
Rakovsky et al. 2013	PLA	HA	20	0.015 x 0.15	~ 9.5	~ 59
	PLA	HA	30	0.015 x 0.15	~ 7.1	~ 60
	PLA	HA	40	0.015 x 0.15	~ 4.1	~ 88
Kikuchi et al. 1997	PLA	β-TCP	60	nd	2.1 ± 0.3	42.0 ± 2.2
	PLA	β-TCP	75	nd	4.2 ± 1.1	51.0 ± 6.3
	PLA	β-TCP	80	nd	8.2 ± 3.1	46.0 ± 5.5
Ignatius et al. 2001	L,DL PLA	-	0	-	nd	152.0 ± 9.0
	L,DL PLA	β-TCP	10	<200	nd	128.0 ± 9.0
	L,DL PLA	β-TCP	30	<200	nd	112.0 ± 6.0
Niemelä 2005	SR PLA (3.5-4)**	-	0	-	4.7 ± 0.08	185 ± 2.2
	SR PLA (3.5-4)**	β-TCP	20	50 - 125	3.3 ± 0.14	130 ± 0.8
Rakovsky et al. 2013	PLA	β-TCP	20	0.05 – 0.15	~ 7.2	~ 71
	PLA	β-TCP	30	0.05 – 0.15	~ 4.2	~ 62
	PLA	β-TCP	40	0.05 – 0.15	~ 3.4	~ 54
Niemelä et al. 2005	PLA	-	0	-	2.9 ± 0.2	44.6 ± 5.7
	PLA	BAG	20	50-125	3.3 ± 0.1	38.8 ± 0.7
	PLA	BAG	30	50-125	2.9 ± 0.6	36.5 ± 1.8
	PLA	BAG	40	50-125	3.2 ± 0.4	34.5 ± 2.2
	PLA	BAG	50	50-125	4.0 ± 0.3	35.5 ± 1.4
Niemelä et al. 2005	SR PLA (3.5)**	-	0	-	3.6 ± 0.3	105.5 ± 3.3
	SR PLA (3.5)**	BAG	20	50-125	2.7 ± 0.3	81.0 ± 6.2
	SR PLA (3.5)**	BAG	30	50-125	2.2 ± 0.2	68.6 ± 3.5
	SR PLA (3.5)**	BAG	40	50-125	2.0 ± 0.3	54.5 ± 4.1
	SR PLA (2.0)**	BAG	50	50-125	1.8 ± 0.4	39.3 ± 7.2

* Compression

** Draw ratio

nd = not disclosed

In clinical use, complete osseous replacement of bioresorbable implants is supposed to occur within two or three years [Weiler et al. 2000]. The benefit of composites containing β-TCP has been demonstrated in a long-term implantation study. In contrast to implants prepared from pure polymer, the composite implants showed continuous contact osteogenesis [Daculsi et al. 2011]. Clinical data for ACL interference screws made of polymer/β-TCP verified this finding [Barber and Dockery 2006, Barber et al. 2011]. However, after implant degradation the ossification of the screw tract was complete in only 19% of the cases [Barber et al. 2011]. In addition, a dose-dependent effect of TCP content on osteogenic response has been demonstrated in a rabbit implantation model [Aunoble et al. 2006].

Bioresorbable composites can be manufactured by a thermo-chemical route (e.g. melt-mixing and injection molding) and a physico-chemical route (e.g. solution-casting) [Wang 2003]. In addition, self-reinforcement (SR) is a recognized method to reorganize the microstructure of bioresorbable composites into oriented reinforcement elements. This allows significant improvement of the mechanical strength, Young's modulus and toughness of implant materials [Törmälä 1992, Majola et al. 1992, Törmälä 1993, Niemelä et al. 2005]. Examples are shown in Table III. In addition, novel bioactive bioresorbable hybrid composites were developed to tackle the issue related to the weak mechanical properties [Huttunen et al. 2008].

In the fabrication of composites containing ceramic particles, agglomeration is a typical problem [Wang M 2003, Zhou et al. 2012] resulting in an inhomogeneous distribution of the filler and unexpected material properties. High energy ball-milling [Takamatsu et al. 2006, Roveri and Iafisco 2010] and attrition milling [Yang et al. 2009, Rakovsky et al. 2013] were reported to reduce agglomeration, and increase the density and the mechanical properties of the composites. High energy ball-milling allows the fabrication of molecular level nanocomposites. The possible advantages of nanostructures have been widely discussed [Gerber et al. 2006, Tran and Webster 2009, Yang et al. 2011, Zhou et al. 2012, Rakovsky et al. 2013]. Some of the benefits have been described in *in vitro s*tudies [Webster et al. 2000, Liu et al. 2008, Cui et al. 2009, Jayabalan et al. 2010, Kim et al. 2011, Zhou et al. 2012].

However, as seen in Table III, the mechanical properties of nano-structured composites are similar to those of conventional composites. Moreover, there is a lack of convincing scientific evidence of the benefit of nano-structured osteoconductive bioresorbable composites; therefore, systematic *in vivo* studies designed to compare micro- and nano-structured composite implants should be performed.

2.3.7 Silver nanoparticles as an antimicrobial implant coating with a short-term release pattern

Antibacterial coatings are subdivided in releasing (*e.g.* antibiotics, soluble silver (Ag) ions) and non-releasing (*e.g.* HA-Ag coatings [Chen et al. 2006]) coatings. Releasing coatings are applied onto the implant surface by spray or dip coating methods while non-releasing coatings are produced by thermal-processes. At present,

silver-based coatings are clinically used for various medical devices (*e.g.* central venous catheters, sutures) [Odekerken et al. 2013]. However, the use of these coatings in orthopaedic applications remains at an experimental level. Typical forms of silver for medical applications include silver chloride particles, polymer-silver nanoparticle composites, metallic silver nanoparticles and silver-titanium dioxide composite nanopowders [Choi et al. 2008, Damm C and Münstedt 2008, Hlidek et al. 2008, Arora et al. 2008, Yeo and Kang 2008]. The preparation of monodisperse silver colloids is preferable and traditionally referred to as a two-step process. The first step includes a chemical reduction of a silver salt in water in the presence of strong reducing compounds *e.g*. borohydride. Thereafter, these "seed" particles are enlarged by weaker reducing compounds *e.g.* ascorbate ions. [Shirtcliffe et al. 1999]. However, the reducing compounds are frequently considered toxic. Hence, there is a need to develop alternative green synthesis methods of silver nanoparticles. The proposed methods involve the use of polysaccharides and polyphenols as coating and reduction compounds [Panacek et al. 2006, Sharma et al. 2009].

Silver is known to have antibacterial properties; however, the exact mechanisms remain unexplored [Jung et al. 2008, Asharani et al. 2009]. Three key mechanisms behind the antibacterial activity of silver have been suggested: free silver ion uptake, the generation of reactive oxygen species (ROS) and direct bacteria membrane damage [Marambio-Jones and Hoek 2010]. *In vivo,* the interaction between silver nanoparticles and H_2O_2 results in the oxidative dissolution of nanoparticles and generation of silver ions [Asharani et al. 2009]. It has been suggested that this chemical reaction may occur in the bacterial mitochondria or cell membrane [Asharani et al. 2009, Marambio-Jones and Hoek 2010]. During oxidative phosphorylation, the antioxidant defenses in mitochondria are intended to preserve a constant level of ROS, the natural metabolic products of respiring organisms [Nel et al. 2006]. However, ROS production may be altered by toxic agents such as silver. Deposition of ionic silver in bacterial mitochondria and interaction with the enzymes of the respiratory chain reaction leads to an increase in ROS production and lower adenosine-5'-triphosphate yield. This mechanism is due to the exceptional resemblance of Ag^+ ions with thiol groups in the cysteine residues of respiratory chain enzymes [Marambio-Jones and Hoek 2010]. In turn, highly reactive ROS causes oxidative damage to DNA which disturbs the cell cycle. Thereafter, if the DNA is irreversibly damaged, the cell will undergo apoptosis. In addition, abundant morphological changes of silver-treated cells can be observed. These changes are related to cytoplasm reduction, detachment and degradation of cell wall membranes causing leakage of intracellular content [Jung et al. 2008].There are no precise explanations of the mechanisms of direct bacteria membrane damage [Marambio-Jones and Hoek 2010]. However, silver nanoparticles are presumably able to interact with sulfur containing proteins and increase the permeability of the cell wall membrane and respiratory function [Marambio-Jones and Hoek 2010].

In summary, literature reports present evidence of cytotoxic, genotoxic and antiproliferative effects of silver nanoparticles on bacterial cells [Asharani et al. 2009, Marambio-Jones and Hoek 2010]. If these effects of silver nanoparticles are

extrapolated to human cells, the use of silver nanoparticles could be a risk factor in carcinogenesis [Asharani et al. 2009, Marambio-Jones and Hoek 2010]. Therefore, further investigation is needed to discover whether silver nanoparticles are to be used as coatings in orthopaedic applications.

2.3.8 Therapeutic androgen receptor ligands

Due to the extensive aging of human population during the past decades, the attention of the scientific community was focused on aging-associated deteriorations and their influence on socioeconomic matters. The evidence published to date suggests that age and hormone status in both male and female are key factors in progressive bone and muscle loss [Bhasin et al. 2006, Clarke and Khosla 2009, Manolagas et al. 2002]. Aged or hypogonadial males as well as post-menopausal females undergo increased bone turnover and decrease in bone mineral density (BMD). Therefore, a greater risk of fracture does exist in this population group [Huber et al. 2001]. Animal studies simulating androgen deficiency in rodent models, demonstrated that surgical/chemical castration led to enhanced bone and muscle loss; however, therapeutic intervention with androgens had a reversal effect on the bone and muscle loss [Tobias et al. 1994, Prakasam et al. 1999, Vanderschueren et al. 2000].

Androgens have been known since 1889; they play an essential role in the induction of male and female physiology and reproduction [Mohler et al. 2009, Wu et al, 2006]. Testosterone (T), the most vigorous endogenous androgen, is synthesized and further secreted by the Leydig cells in testes in males and by the ovaries in females. In addition, in females and castrated males, T is also produced by the adrenal cortex [Mohler et al. 2009].

Dihydrotestosterone (DHT) is a potent natural metabolite of T, which is produced by 5-α-reduction and accounts for approximately 6 to 8% of all converted T. Nearly 0.3% of all converted T, is estradiol, which is synthesized via accomplishment of aromatase and expressed in adipose tissue, liver and brain [Chen et al. 2005].

T and DHT are the crucial intracellular mediators of most androgen actions including the protective effects on human skeleton [Clarke and Khosla 2009, Pederson et al. 1999]. The overall physiological action of T and DHT is executed by targeting the intracellular androgen receptor (AR) [Tsai and O'Malley 1994, Manolagas et al. 2002].

The AR is a DNA binding transcription factor which belongs to the extended class of nuclear receptors [Tsai and O'Malley 1994]. Prior to ligand binding, inactive AR is in a conjunction with heat shock proteins 70 (HSP) and HSP 90 located in the cytoplasm. Upon ligand binding, HSPs detach from AR. Thereafter, the receptor undergoes homo-dimerization and is transported to the nucleus. The following sequence of conformational changes of AR leads to binding to androgen responsive elements and activation of the receptor resulting gene transcription [Narayanan et al. 2008]. Regarding bone tissue, it is evident that ARs are localized in osteoblasts, osteoclasts as well as in osteocytes and chondrocytes [Abu et al. 1997, Pederson et al. 1999, Huber et al. 2001, Manolagas et al. 2002]. The AR ligand affects BMD by altering

an individual bone cell´s activity and the total amount of each cell type [Chen et al. 2005]. Interestingly, the amount and distribution of AR in bone tissue does not dependent on gender [Manolagas et al. 2002]. Hence, this finding indicates that the therapeutic effect of androgens on bone is comparable in the female and male.

Interleukin-6 (IL-6) is a cytokine that is known to play a pivotal role in osteoclast differentiation and activation during abnormal physiological states; therefore, this cytokine is of a great importance in the pathogenesis of conditions associated with progressive bone loss *e.g.* osteoporosis, Paget`s disease, rheumatoid arthritis [Edwards and Williams 2010, Manolagas et al. 2002]. It has been shown previously that androgens are able to suppress the production of IL-6 and prevent the bone loss [Manolagas et al. 2002]. This mechanism is based on the interaction of androgens with the IL-6 receptor and the subsequent partial downregulation of receptor expression [Manolagas et al. 2002]. However, although the effects of androgen replacement therapy are well established, the severe side effects overlap the benefits [Bhasin et al. 2006 Chen et al. 2005].

Recently, the androgen replacement therapy was subjected to substantial changes. There are two main influential factors that contribute to these changes. First factor is a breakthrough in hormone replacement therapy in postmenopausal females which enables the prevention and treatment of major disorders *e.g.* osteoporosis, breast cancer, etc. This breakthrough raised the prospect of developing innovative approaches in solving health disorders in male. The second factor is the selective estrogen receptor modulator (SERM) paradigm discovery. The great tissue selectivity of SERMs with the diminished side effects has provided evidence that a new generation of design-like molecules could be created [Negro-Vilar 1999, Cosman and Lindsay 1999].

The first report on SARM in 1998 originated from James T. Dalton and coworkers [Dalton et al. 1998]. They were able to synthesize the non-steroidal ligand with agonist activity. However, the term SARM was proposed by A. Negro-Vilar in 1999 and was based on an already known SERM molecule [Negro-Vilar 1999]. In addition, A. Negro-Vilar proposed the criteria for the novel class of non-steroidal androgens, which include high oral bioavailability, high tissue selectivity and absence of undesired effects. Since then, the research field of SARMs has been tremendously broadened. SARM pharmacophores are currently represented by four categories: analogs of tetrahydroquinoline, bicyclic hydantoin, aryl-propionamide and quinoline [Chen et al. 2005]. In muscle and bone, which are anabolic tissues, these AR ligands act as full agonists; however, in androgenic tissues such as seminal vesicles or prostate, they possess partial agonistic activity [Chen et al. 2005]. Most of the SARMs are orally available drugs with considerably reduced side effects, and which are eliminated through hepatic metabolism [Bhasin et al. 2006, Thevis et al. 2008, Mohler et al. 2009, Gao and Dalton 2007]. The molecular mechanisms of tissue selectivity of SARMs are still under investigation. Nevertheless, the evidence suggests that these mechanisms are mainly based on the resistance of SARMs to 5α-reduction, ligand-dependent conformational changes in AR, and tissue specific differences in the recruitment of coregulators [Narayanan et al. 2008, Chen et al. 2005].

Numerous studies have demonstrated that SARMs may represent a therapeutic approach of choice in management of osteoporosis [Kearbey et al. 2007, Kearbey et al. 2009, Gao et al. 2005, Hanada et al. 2003]. Current interventions of osteoporosis are listed in Table IV.

SARMs were able to improve bone strength and BMD in ovariectomized and orchidectomized rats. SARMs stand out in comparison to clinically available bisphosphonates, SERMs, calcitonin etc., which are not sufficient to maintain the already lost bone mass [Chen et al. 2005]. In addition, as a benefit in the treatment of osteoporosis, SARMs are able to improve muscle strength and mass, which in turn possesses a stimulatory effect on mechanical bone stress [Mohler et al. 2009].

To conclude, SARMs are still in the primary phase of development and various mechanisms at the molecular level remain unclear; however, there are several clinical trials ongoing [Mohler et al. 2009, Gao and Dalton 2007]. Notably, since January 2008, according to the anti-doping regulations of the World Anti-Doping Agency, SARMs has been prohibited in sports [Gao et al. 2006].

Table IV. Managment of osteoporosis

Drug Class	Principe of action	Side Effects
Bisphosphonates (Alendronate, Risedronate, Ibandronate, Zoledronic acid)	Reduce bone turnover by decreasing the recruitment of osteoclast precursors. Weaken osteoclast working capacity or increase apoptosis [Riggs and Parfitt 2005]	Gastrointestinal side effects, ocular inflammation, severe musculoskeletal pain, hypocalcemia, osteonecrosis of the jaw [Kennel and Drake 2009]
SERMs (Triphenylethylenes, Benzothiophenes)	Estrogen agonist in bone with antiresorptive effect [Muchmore 2000]	Venous thromboembolic events, leg cramps, hot flashes, increased risk of endometrial carcinoma in women over age 50 [Muchmore 2000]
Calcitonin	Inhibits osteoclast activity, thus reduces bone resorption [Siminoski and Josse 1996]	Gastrointestinal side effects, vascular phenomena, local and generalized rash, headache and diuresis [Siminoski and Josse 1996]
Parathyroid Hormone	Anabolic or bone-forming drug which increases the bone turnover by influencing the number and activity of osteoblasts and osteoclasts [Jodar-Gimeno 2007]	No evidence of severe side effects. Occasional nausea and headache [Neer et al. 2001], hypercalciuria, hypercalcemia, dizziness [Jodar-Gimeno 2007]
Denosumab (Fully human monoclonal antibody IgG_2 immunoglobulin isotype)	Binds to the RANKL receptor and prevents the interaction of RANKL and RANK. Therefore, this inhibits osteoclast formation [Lewiecki 2008]	No evidence of severe side effects. Minor transient dose-dependent decreases in albumin-adjusted serum calcium and corresponding increases in serum intact parathyroid (iPTH) levels [Lewiecki 2008]
Strontium Ranelate	Increases osteoblastogenesis and osteoblast activity and reducing osteoclast differentiation and function [Brandi et al. 2013]	In short term: gastrointestinal side effects, dermatitis, and headache, Drug Rash with Eosinophilia and Systemic Symptoms [Brandi et al. 2013]

2.4 Animal models

2.4.1 Bone healing models

For the creation of an optimal bone-implant interface, an ideal bone implant material should possess high biocompatibility and mechanical stability. Prior to clinical trials, implant materials should undergo *in vitro* and *in vivo* characterization. *In vitro* characterization is usually a precisely standardized process, which allows screening of a large number of specimens simultaneously with subsequent rejection of inappropriate ones [Pearce et al. 2007]. Hence, primary *in vitro* characterization is required to avoid unnecessary animal experiments [Pearce et al. 2007]. However, the lack of adequate information regarding *e.g.* tissue response and biomechanical properties of implant materials is the major limitation of *in vitro* characterization.

In turn, the use of animal models for the *in vivo* characterization of implant materials enables the simulation of physiological and pathological conditions, which are comparable to human. An adequate animal model is essential for the creation of a standardized bone defect, which mimics bone loss in human. The instability influence should be eliminated by sufficient fixation of the bone defect. Quantitative analysis of bone healing should be performed as a final stage of *in vivo* characterization [den Boer et al. 1999]. It is important to take into consideration, that each animal model has certain limitations. For instance, the size of the animal may serve as a limitation and impose restrictions regarding implant design. In order to avoid pathological fracture, the ratio between implant dimensions and animal size should be set according to the guidelines of the International Organization for Standardization (ISO) [Pearce et al. 2007, Huffer 2006]. International standards consider dogs, goats, sheep, rabbits and pigs as appropriate animal species for biomaterials research [Pearce et al. 2007].

Based on scientific knowledge, it has been assumed that the dog animal model is the most accurate simulator of human *in vivo* conditions [An and Friedman 1999]. This model has been successfully used in a large number of studies focused on healing patterns of bone and bone infections [An and Friedman 1999, Lindsey et al. 2006, Keränen et al. 2007, Johnson et al. 1996, Petty et al. 1985, Petty et al. 1988]. However, dogs are considered companion animals; therefore, the use of dog models in research is frequently regarded unethical.

In contrast, the use of goats and sheep for research is subjected to less pronounced criticism. The body size of these animals is optimal for the implantation of multiple implants. In addition, their bone healing capacity is rather similar to that of humans [Pearce et al. 2007, den Boer et al. 1999, Dai et al. 2005]. It has been shown that during bone graft integration, the chain of events in bone tissue is also similar in humans and in goats [Lamerigts et al. 2000].

The rabbit model has been used in numerous screening studies due to ease of handling [Neyt et al. 1998, Itälä et al. 2003, Zhao et al. 2009]. Although there are clear differences between the rabbit and human bone anatomy and bone loading, a

similarity in BMD and the fracture toughness of mid-diaphyseal bone has been reported [Neyt et al. 1998].

The use of pigs is challenging due to their aggressive behavior and extensive growth rate. In this respect, the use of a minipig model is preferable. Despite these limitations, the similarities in the anatomy and healing patterns of porcine and human bone can be traced. In addition, the mineralization rate of porcine cortical bone is similar to that in humans [Thorwarth et al. 2005, Kragstrup et al. 1989].

Although rats are frequently used for *in vivo* characterizations in biomaterials science; there are considerable dissimilarities between the rat and human bone structure. In addition, the rat is a rather small animal, which complicates the simultaneous testing of multiple implants. However, rats are reported as the animals of choice for the creation of bone infection models [An et al. 2006].

2.4.2 Implant infection models

The orthopaedic implant infection model is effective scientific tool, which is based on the foreign body infection model and used to determine bacterial behavior on biomaterial surface, as well as the influence of implant surface modifications on infection rate. At present, the most widely used implant infection models are skeletal implant, total joint replacement and soft tissue models [An and Friedman 1998].

Research objectives dictate the shape, size, and implant material properties. In certain cases due to the nature of the implant shape, poorly vascularized or avascular per-implant zones, known as dead spaces, may be created. These dead spaces are lined with necrotic tissue and detritus, which provide an ideal environment for bacterial proliferation and biofilm formation [Melcher et al. 1994]. In addition, the size of the implant is critically important for the tissue integration; however, the impact of this parameter on bacterial attachment is frequently underestimated. Nevertheless, among all implant characteristics, the individual properties of the implant material are of primary importance. Due to these properties, a material can possess an antibacterial effect, or *vice versa* promote bacterial growth [Melcher et al. 1994]. In order to mimic infection, in the majority cases investigators use laboratory or clinical strains of *S. aureus*, *S. epidermidis*, *Pseudomonas aeruginosa* (*P. aeruginosa*) or *Escherichia coli*, which are common pathogens of human prosthetic infection [An and Friedman 1998]. During animal surgery, bacteria can be disseminated on the implant surface and surrounding tissues by three different routes. In the first route, a bacterial biofilm is created on the implant surface prior to the implantation [Buret et al. 1991, Chang and Merritt 1994, An et al. 1996, Sheehan et al. 2004]. In the second route, bacterial suspension is inoculated directly into the implant site through the surgical access [Horn et al. 2004, Melcher et al. 1994, Melcher et al. 1995, Arens et al. 1996]. The third route is the injection of bacterial suspension into the bloodstream [Blomgren et al. 1981, Southwood et al. 1985, An and Friedman 1999]. Most investigators use only one bacterial strain; nevertheless multispecies bacterial biofilm is also known to occur on the implant surface [Lambe et al. 1991, Philipov et al. 1995]. The number of bacteria needed to create an

experimental infection varies and depends on the virulence of the selected strain and the biofilm formation ability. However, based on scientific evidence, one can conclude that regardless of bacterial strain, an average of 10^5 CFU to 10^8 CFU would be sufficient to induce an implant related infection [Melcher et al. 1994, Melcher et al. 1995, Arens et al. 1996, Horn et al. 2005].

In order to increase the infection rate, sclerosing agents, such as sodium morrhuate, are commonly used [An et al. 2006]. Norden was one of the first to establish the chronic osteomyelities rabbit tibial model wherein the use of a sclerotic agent to increase the probability of infection was the main concept [Norden 1970]. Sclerosing agents trigger vascular sclerosis in the medullary canal and subsequent tissue necrosis. Thereafter, the host´s local immune response is suppressed; this chain of events leads to enhanced bacterial proliferation and osteomyelitis. Interestingly, a surgical trauma itself is considered as an impetus and sometimes even a gateway for infection [An et al. 2006]. Clinical symptoms of infection are extremely important. However, additional methods should be applied for accurate diagnosis.

2.5 Experimental methods for evaluation of implant related infections and biomaterial incorporations

2.5.1 Conventional microbiological techniques

Biomaterial-related infections occur less frequently than aseptic loosening of implants. However, infection-associated implant failure is a devastating complication, which is often difficult to diagnose. In practice, there is lack of diagnostic tools with ideal sensitivity and accuracy. Therefore, the combination of different techniques was appropriately pointed out to be the most efficient [Trampuz and Zimmerli 2005].

One of the primary diagnostic actions includes a division of operated patients according to the probability of infection into the following categories: 1. definitive; 2. probable; 3. possible; 4. rejected [Dora et al. 2007]. Thereafter, tissue specimens and implants should be collected for further laboratory analysis. It should be noted that cultures of periprosthetic tissue provide most reliable results. In contrast, cultures of a superficial wound or sinus tract might give a false positive due to contamination by microbial inhabitants from surrounding skin and therefore should be avoided [Zimmerli et al. 2004]. For maximum diagnostic yield, at least three deep periprosthetic tissue specimens should be obtained from different sites around the implant and processed under aerobic and anaerobic conditions [Lew and Waldvogel 2004, Zimmerli et al. 2004, Tunney et al. 1999]. It has been shown, that prolonged culture period can double the detection rate of slow-growing or “dormant” bacteria [Neut et al. 2007]. In the case when the operated patient is categorized with a definitive and probable infection, periprosthetic tissue specimens and explanted implant are subjected to cultural investigations [Dora et al. 2007]. Collective evidence suggests that although ultrasonication of the explanted implant is related to a risk of contamination, this method is able to significantly improve the sensitivity of conventional periprosthetic tissue culture without affecting microbial viability

[Tunney et al. 1999, Trampuz et al. 2007]. In the case when the operated patient is categorized with a possible or rejected infection, periprosthetic tissue specimens are also subjected to culture investigations. In the case of positive culture, postsonication polymerase chain reaction (PCR) has been suggested for improving the sensitivity of culture microbiologic investigations [Dora et al. 2007, Kobayashi et al. 2006, McDowell and Patrick 2005] However, the use of highly sensitive techniques such as PCR may result in false positive cultures, since biomaterial-related infections are frequently associated with commensal species, which might be mistaken for contaminants [Smeltzer et al. 2009]. In addition, conventional PCR cannot differentiate between viable and nonviable bacteria [Smeltzer et al. 2009]. Therefore, the infection commenced by nonviable bacteria and their products might be diagnosed as an ongoing infection and lead to a loss of reference points in the strategy of treatment. The use of fluorescence microscopy as an alternative or additional diagnostic approach was designed to overcome this limitation.

2.5.2 Fluorescent techniques

Fluorescence is a process in which molecules in electronically excited states emit light. The excited states are created by physical, mechanical or chemical stimuli. Florescence and confocal scanning laser microscopy (CSLM) in conjunction with fluorescent probes are special instruments in scientific toolbox which enable to image and analyze events in a cell under native conditions [Cook et al. 1999, Suzuki et al. 2007, Gitai 2009].

It has been shown previously that fluorescent techniques offer the great advantage in diagnosis of biomaterial-related infections. Stoodley and co-workers [Stoodley et al. 2008] have demonstrated in a case study, that fluorescent techniques successfully assist the diagnosis of chronic recurring infection, which persisted for five years and previously yielded in serial of negative bacterial cultures [Stoodley et al. 2008].

*Bac*Light (Molecular Probes, Eugene, OR, USA) is a fluorescent bacterial viability probe that is becoming more ubiquitous. It consists of propidium iodide and SYTO 9 nucleic acid stains which are used together. The SYTO 9 stain penetrates and labels all bacteria with an intact and damaged membrane, while propidium iodide penetrates only bacteria with a damaged membrane, i.e., those being dead or dying. As an additional benefit, this fluorescent bacterial viability probe can be applied rapidly due to short incubation period.

2.5.3 Micro-computed tomography

Computed tomography (CT) was developed by Hounsfield in 1972 [Hounsfield 1973]. Subsequently, CT became a routine method in medical practice. It allows non-destructive visualization of biological tissues in cross-section. Later, based on CT principles, high spatial resolution micro-computed tomography (micro-CT) was developed for the imaging of small objects [Feldkamp et al. 1989]. Micro-CT has been

widely used for the creation of high-resolution three-dimensional images of calcified tissues [Feldkamp et al. 1989, Bouxsein et al. 2010]. This imaging technique enables the assessment of biological response in the peri-implant zone; therefore, the obtained image data may reinforce the knowledge about the behaviour features of particular implant materials [De Smet et al. 2006]. However, it should be taken into consideration that imaging artefacts and inadequate resolution of current micro-CT scanners may challenge direct quantification of the interfacial contact area between the implant and bone [Stoppie et al. 2007, Schouten et al. 2009]. Therefore, histological sectioning is required and should be performed in addition to micro-CT analysis.

2.5.4 Histomorphometry

Histomorphometry is a standard technique for the evaluation of bone modelling and remodelling processes. In addition, histomorphometry is widely used to assess the infection rate in bone tissue. Microscopic examination of plastic-embedded undemineralized bone sections was established in the 1950s. Previously, prior to bone histological analysis, the mineral content of bone tissue had to be removed [Recker et al. 2011]. From that time onwards, decalcified and undecalcified tissues are used depending on the research aim. Different staining methods are available for the identification of different tissues and their components [Donath 1995]. Standardized grading scales are used for the analysis of histological sections. Petty and co-workers suggested a grading scale for the quantification of implant-associated inflammatory reactions in bone (Table V) [Petty et al 1985]. A histological grading scale for the assessment of peri-implant tissue reactions was suggested by Jansen and co-workers in 1994 (Table VI) [Jansen et al 1994].

2.5.5 Scanning electron microscopy

Scanning electron microscopy (SEM) is a routine high-resolution imaging techniques used in biomedical research to study the morphology and chemical composition of materials. The principle of operation is based on scanning the specimens under investigation with a focused electron beam. When electrons interact with the atoms of the specimen, secondary electrons are emitted and primary electrons are backscattered. The electrons are collected by respective detectors to generate images of the surface. Conventional SEM is a typical method for the visualization of bacterial biofilms [Walker et al. 2001]. Since imaging is performed in a high vacuum, bacterial biofilm should be pre-treated before imaging. Pre-treatment includes the following procedures: fixation, staining, drying. In addition, to create a conductive surface the specimens are coated with carbon, gold or other metals. However, the pre-treatment procedures may affect the EPS. Environmental SEM, which does not require high vacuum and conductive coatings, is alternative method to overcome biofilm dehydration [Walker et al. 2001, Priester et al. 2006].

Table V. Implant associated inflammatory reactions in bone (Adapted from Petty et al. 1985)

Grade	Periosteum	Cortex	Medullary Canal
0	No reaction or laminated reaction which is limited to 1-2 thin eccentric layers and related to a defect.	Haversian canals are small. Slow repair rate. Polymorphonuclear leukocytes are not in granulation tissue: occasional subperiosteal resorptive pockets.	Repair with woven bone; inflammatory cells range from none to foci of many intact polymorphonuclear leukocytes.
1	Laminated reaction limited to 1-2 eccentric layers, not related to a defect.	Occasional polymorphonuclear leukocytes are present in Haversian canals.	Increased amount of polymorphonuclear leukocytes. In addition, micro-abscesses are present.
2	Sunburst type, nearly circumferential reaction.	Haversian canals are focally enlarged and filled with granulation tissue and fragmented polymorphonuclear leukocytes. Occasional micro-abscesses are present.	Increased amount of polymorphonuclear leukocytes with fragmented forms: several definite micro-abscesses are present.
3	Florid, always circumferential sunburst type reaction.	Subperiosteal, endosteal and intracortical resorption associated with fragmented polymorphonuclear leukocytes. Numerous micro-abscesses.	Increased amount of polymorphonuclear leukocytes. Numerous micro-abscesses.
4			As above, but with sinus-tract formation and soft-tissue micro-abscesses

Table VI. Histologic grading scale for bone implants (Adapted from Jansen et al. 1994)

Grade	Bone reaction semi-quantitavely (Thickness rating)	Bone reaction qualitatively	Interface qualitatively
0	Not applicable	Inflammation	Inflammation
1	> 501 µm	Other tissue than bone	Fibrous tissue capsule
2	251 – 500 µm	Lamellar or woven bone with bone formation and resorption	Localized fibrous tissue with no encapsulation
3	51 – 250 µm	Lamellar or woven bone with bone forming activity	Remodelling lacuna with osteoblasts and/or osteoclasts
4	0 – 50 µm	Similar to original cortical bone	Direct bone contact

2.5.6 Positron emission tomography

Positron emission tomography (PET) is a non-invasive quantitative imaging technique, which enables the evaluation of biochemical and physiological processes *in vivo*. PET allows monitoring the distribution of biologically active compounds labeled

with positron-emitting radioisotopes (*e.g.* ^{13}N, ^{15}O, ^{11}C, ^{18}F) which are intravenously administrated to the patient [Surti et al. 2004]. After the emission of the isotop from the nucleus, positrons travel a short distance in the tissue prior to annihilation with electrons. The energy of the annihilation of the positron and electron is released in the form of two gamma photons which diverge in the opposite directions (almost 180°). The PET scanner's ring-shaped radiation detectors register the two gamma photons which arrive simultaneously [DeGrado et al. 1994]. The origins of the annihilations are then calculated by special computer software to create three-dimensional PET images. PET scanners are often combined with CT to specify the anatomic origin of the annihilation signal.

The most common biologically active compound labeled with radioisotope chosen for PET imaging is 2-^{18}F-fluoro-2-deoxy-D-glucose, [^{18}F]-FDG [Love et al. 2005, Vos et al. 2006]. [^{18}F]-FDG is an analogue of glucose that accumulates in cells with high metabolic activity such as cancer and inflammatory cells. After intravenous administration, [^{18}F]-FDG initially repeats the metabolic pathway of glucose. At the final step of reaction cascade, the glucose transporters deliver [^{18}F]-FDG to the targeted cell, where it is phosphorylated by hexokinase. Unlike glucose phosphate, the reaction product of [^{18}F]-FDG is not further utilized and remains in the targeted cell during the study. The number of glucose transporters and the metabolic activity of the targeted cell are the main factors in the uptake of [^{18}F]-FDG. Recently, it has been shown that [^{18}F]-FDG PET imaging is capable of diagnosis of numerous orthopaedic infections [Kälicke et al. 2000, Schmitz et al. 2001, Gratz et al. 2002, De Winter et al. 2003, Mahfouz et al. 2005].

Vascular adhesion protein-1 (VAP-1) is induced during the inflammatory process and has a crucial input during the rolling, adhesion and transmigration of leukocytes [Salmi et al. 2001, Salmi and Jalkanen 2001]. One remarkable feature of VAP-1 is that this protein is still constantly present on the cell surface after the first phase of inflammation. Hence, VAP-1 is a highly potential target for *in vivo* imaging of inflammation [Autio et al. 2010, Autio et al. 2011]. Originally, ^{68}Ga labelled 1,4,7,10-tetraazacyclododecane-1,4,7,10-tetraacetic acid (DOTA) organic compound was suggested for PET imaging by Ujula and co-workers [Ujula et al. 2009]. In turn, CD33 related sialic-acid immunoglobulin like lectins (siglecs) are known to be involved during inflammatory and immune responses in a subset of leukocytes [Crocker et al. 2012]. Recent findings demonstrated that Siglec-9 is a granulocyte ligand for VAP-1 and a ^{68}Ga-labeled Siglec-9 motif peptide specifically detects VAP-1 in vasculature at sites of inflammation and cancer by PET [Aalto et al. 2011].

3 AIMS OF THE STUDY

Study I

To establish a new method for simultaneous evaluation of Ca-P and biofilm formation on BisGMA-TEGDMA thermosets with different content of BAG.

Study II

To evaluate the biological response of bone tissue to two PLA-PGA/β-tricalcium phosphate composites in a minipig model.

Study III

To study the feasibility of novel ^{68}Ga-DOTA-Siglec-9 PET tracer to detect the inflammatory response caused by S. epidermidis peri-implant infection.

Study IV

To evaluate the antibacterial properties of the Chitlac-nAg coated material in vitro and to evaluate the physiological response of bone tissue at the interface with the Chitlac-nAg coated material in a minipig model.

Study V

To evaluate the effect of SARM (ORM-11984) in a local drug delivery system in a rat bone healing model.

4 MATERIALS AND METHODS

4.1 Study I

In vitro experiment

Two groups of BisGMA-TEGDMA thermosets with different content of Bioglass® 45S5 (50% and 75% by weight) were investigated. BisGMA-TEGDMA thermosets without BAG served as a negative control. The BisGMA-TEGDMA thermosets (diameter 12mm; thickness 2mm) were prepared by mixing the light-polymerizable acrylate resin with BAG particulate (fraction <50 μm). Then, the BisGMA-TEGDMA thermosets were photopolymerized and postcured. Subsequently, one side of the BisGMA-TEGDMA thermoset was ground to expose the BAG surface.

Bacterial-biofilm growing medium (BM) was prepared as described by Lemos et al. [Lemos et al. 2010]. SBF was prepared as described by Kokubo et al [Kokubo et al. 1990]. The comparison between BM and SBF in terms of ion concentration is presented in Table VII.

Table VII. Nominal ion concentration of SBF, BM and human blood plasma. (Adapted from Study I).

Ions	Ion concentration (mM)		
	SBF	**BM**	**Human blood plasma**
Na^+	142.0	34.2	142.0
K^+	5.0	129.5	5.0
Mg^{2+}	1.5	2.0	1.5
Ca^{2+}	2.5	1.0	2.5
Cl^-	147.8	38.8	103.0
HCO^{3-}	4.2	n/a	27.0
HPO_4^{2-}	1.0	72.1	1.0
SO_4^{2-}	0.5	11.8	0.5
pH	**7.4**	**7.2**	**7.2–7.4**

n/a = not available

The total volumes of SBF and BM were calculated according to the surface area of BisGMA-TEGDMA thermosets. The BisGMA-TEGDMA thermosets were placed individually into the flat-bottom test tubes filled with 11.3 ml of sterile SBF and BM, respectively with the grinded surface upwards. The tubes were placed in a water bath (Heto Lab Equipment SBD-50 type BIO, 160 strokes per minute, amplitude 36 mm) at a constant temperature (37 °C) for 3 days. After incubation, the BisGMA-TEGDMA thermosets were dried in a desiccator for 2 days.

Thereafter, the top surfaces of the BisGMA-TEGDMA thermosets were examined with SEM (Model JSM 5500, Jeol Ltd, Tokyo, Japan) and x-ray energy dispersive spectroscopy (Spirit, Princeton Gamma-Tech Inc., Princeton, NJ, USA) for HA formation. Then the BisGMA-TEGDMA thermosets were cut in cross-section and the thickness of the HA layer was measured.

4.2 Study II

In vitro experiment

Four groups of implant materials were prepared and characterized *in vitro* prior to implantation. Micro-composite was an equivalent of a contemporary ACL screw and composed of PLGA 95L:5G/β-TCP with micro-sized particulate. Micro-composite was prepared by melt compounding with further self-reinforcement. Nano-composite was an experimental self-reinforced PLGA 85L:15G/β-TCP material prepared by high-energy ball milling with further self-reinforcement. The high-energy ball milling technique was used to reduce the size of the filler particles to nano-scale. Micro-roughened Ti6Al4V implants served as positive control and pure PLGA implants served as negative control. All implants were prepared in the shape of truncated cone (Ø 3.6 and Ø 5.0 mm, height 8 mm).

Gas chromatography was used to measure the residual monomer content in the initial PLGA 85L:15G and PLGA 95L:5G polymer matrices and in the ready composite implants. Inherent viscosity of the initial polymer matrices and the ready composite implants was measured with Ubbelohde viscometer. Particle size distributions of the initial β-TCP particle and β-TCP particles in the composite implants were studied with the laser diffractometer. Likewise, the crystal sizes of the β-TCP particulates were evaluated by X-ray diffraction analysis (XRD). The mechanical properties of the composites were assessed by shear and bending tests in accordance with standards ASTM B 769-94 and D 790-84, respectively. The morphologies of Micro-composite and Nano-composite were investigated with SEM. The *in vitro* degradation study was performed according to ISO 15814 standard. The duration of the hydrolysis was 78 weeks. At regular intervals, 0, 6, 12, 18, 24, and 36 weeks, the implant materials were withdrawn and the inherent viscosity, thermal properties and crystallinity of the composites were assessed. Modulated differential scanning calorimetry was used to assess the crystallinity of the polymers.

In vivo experiment

In Study II and Study IV the identical animal model was used (Figure 2). Study II included 21 implants inserted into the femurs of seven adult male Göttingen minipigs (Ellegaard Göttingen Minipigs A/S, Denmark). The animals were euthanized 8 weeks after the surgery. The mechanical strength of the bone-implant interface was measured in a push-out test. Thereafter, the volume of peri-implant bone was assessed in micro-CT analysis. Histological analysis involved the qualitative and

quantitative characterization of the bone tissue reaction by a standardized histologic grading scale [Jansen et al. 1994]. Non-parametric ANOVA (Kruskall-Wallis test) and t-test (Mann-Whitney) was applied to analyze the significance of differences between the implant materials.

4.3 Study III

In vitro experiment

S. epidermidis clinical isolate T-54580 was provided by Dr. Kaisu Rantakokko-Jalava. *S. aureus* clinical isolate 52/52A/80 was provided by Dr. Jon T. Mader. These two strains were used in *in vitro* and *in vivo* experiments.

S. epidermidis T-54580 and *S. aureus* 52/52A/80 were grown overnight on blood agar plates. Thereafter, bacterial suspensions were adjusted to the known optical density (OD), which corresponded to Mc Farland 1. One mL of *S. epidermidis* and one mL of *S. aureus* suspension were found to be equal to 3×10^8 CFU and 3×10^5 CFU respectively. Bacterial suspensions were stored at 4°C and further used for *in vitro* and *in vivo* experiments at the day of preparation.

S. epidermidis T-54580 and *S. aureus* 52/52A/80 were tested for their *in vitro* biofilm formation capability. The overnight cultures were prepared in Brain Heart Infusion broth (BHI) (Sigma-Aldrich, co, St. Louis, MO, USA). Thereafter, the bacterial suspensions were adjusted to the known O.D. which corresponded to Mc Farland 1. Then static biofilms were constructed according to Merrit et al [Merrit et al. 2005]. The total biofilm mass was analyzed by the crystal -violet technique [Merrit et al. 2005]. Pure BHI surved as a control. The biofilm production capability of *S. aureus* and *S. epidermidis* was compared using a Student's t test.

In vivo experiment

The animal study protocol was approved by the Finnish National animal Experiment Board, ELLA (Permit #ESAVI/3485/04.10.03/2012). The animal experiments were performed in the Central Animal Laboratory of the University of Turku. The institutional guidelines and the protocols for the analgesia, anaesthesia and housing of the rats were followed.

Thirty adult male Sprague Dawley rats (Harlan, the Netherlands) were used in the *in vivo* experiment. Three experimental animal groups were selected: 1. Rats challenged with *S. epidermidis* 2. Rats challenged with *S. aureus*, positive control 3. Negative control group without infection. Each group included 10 rats. The left tibia of each rat was operated and the right tibia served as an inta-animal control. The intravenous catheter (BD Venflon™, Becton Dickinson Infusion Therapy, Helsingborg, Sweden) made of polytetrafluoroethylene was used for implantation. Under standard aseptic conditions, the surgical access was created in the proximal tibia using the cannula needle. The cannula was implanted into the medullary cavity and the needle was removed. Thereafter, the bacterial suspension was inoculated into the medullary

cavity through catheter of the cannula. The rats from the first experimental group were challenged with 0.05 mL suspension of 3×10^8 CFU/ mL of *S. epidermidis*. The rats from the second experimental group, a positive control, were challenged with 0.05 mL suspension of 3×10^5 CFU/ mL of *S. aureus*. In addition, aqueous sodium morrhuate (Scleromate, Glenwood, Englewood, N.J. 07631, USA) was injected into the medullary cavity of each rat form the first and second groups. The rats from the third group, a negative control, were not challenged with bacteria or sclerosing agent. Consequently, the catheter was cut at the bone level and the soft tissues were closed in layers.

Two weeks after operation, rats were anesthetized and CT imaging was performed. Thereafter, 19 ± 2.0 MBq of ^{68}Ga-DOTA-Siglec-9 was injected via tail vein of each rat and PET imaging was accomplished. PET data was reconstructed and the quantitative analysis was performed. Two regions of interest were determined in the proximal and distal part of the operated tibia, contralateral tibia and muscle using Inveon Research Workplace software (Siemens Medical Solutions) as shown in Figure 1. The ^{68}Ga-DOTA-Siglec-9 accumulation was expressed as standardized uptake value (SUV). The SUV ratios between the operated tibia and contralateral tibia, as well as between operated tibia and contralateral muscle were calculated and used for intra- and inter-group comparisons.

Subsequently, rats were euthanized and tissue samples (operated tibia, contralateral tibia and muscle, blood, plasma, heart, lung, liver, kidney and urine) were harvested, weighed and measured for total radioactivity.

Operated tibia was divided into five sections. Each section was prepared for certain type of analysis: histological analysis, histomorphometrical analysis, microbiological analysis, PET *ex vivo* radioactivity measurements and fluorescence microscopy (Figure 1).

The first and the second sections of the harvested tibia were taken for the histological and histomorphometric analysis. The undecalcified and decalcified histological sections were prepared. The grading scale described by Petty et al. [Petty et al. 1985] was used to quantify the inflammatory stage. Undecalcified sections were used to evaluate the periosteal reaction and cortex appearance. In turn, decalcified sections were used to evaluate the cellular response.

The third section of the harvested tibia was prepared for microbiological analysis. The catheter and the bone specimens were placed in the separate tubes containing the Fastidious Anaerobe Broth (LabM, Lancashire, UK). The catheters were incubated under aerobic conditions for 7 days. In the case of visual bacterial growth, the bacterial suspension was cultured on the blood agar plate and the Staphaurex latex agglutination test (Remel Europe Ltd, UK) was performed. In the case of negative agglutination test, the Analytical Profile Index (API; API®/ID 32, BioMérieux SA, Marcy l'Etoile, France) was used to identify the Staphylococcal colonies. If no visual bacterial growth was noticed during the incubation of the catheter, the bone specimens were grounded. Consequently, the resulting material was cultured on a blood agar plate. In the case of negative culture, the polymerase chain reaction with universal 16S ribosomal DNA primers was performed.

The forth section of the harvested tibia was prepared for PET *ex vivo* radioactivity measurements.

The fifth section of the harvested tibia was prepared for imaging with fluorescence microscope. Prior to imaging, the catheters were separated from bone and stained with live/dead staining (*Bac*Light kit™; Invitrogen, Barcelona, Spain) according to the manufacturer's instructions.

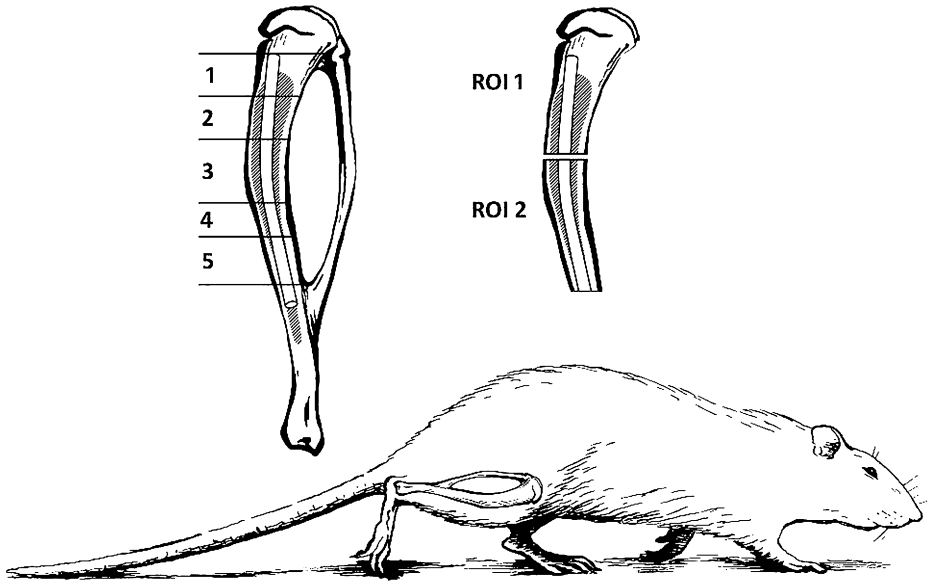

Figure 1. Rat model used in Study III. The tibia with implant was sliced into five sections for further characterization: 1) histological analysis (decalcified sections); 2) histological analysis (undecalcified sections); 3) microbiological analysis; 4) *ex vivo* radioactivity measurement; 5) fluorescent microscopy analysis. The PET data was analyzed in two ROIs.

Kolmogorov-Smirnov test was used to study the normality of the distribution of the data. Levene test was used to validate the homogeneity of variances. The biofilm production capability of *S. aureus* and *S. epidermidis* was compared using a *t*-test.

A paired *t*-test was used to compare the intra-animal differences in PET-data between the operated and the contralateral intact sites. In addition, the data from the three experimental groups were compared using one-way ANOVA with Tukey's post-hoc test. The PET parameters studied were SUV mean of the proximal part of the operated tibia; SUV mean ratio between the proximal part of the operated tibia and the proximal part of the contralateral intact tibia; SUV mean of the distal part of the operated tibia; SUV mean ratio between the distal part of the operated tibia and the distal part of the contralateral intact tibia; SUV mean of the operated *ex vivo* bone sample and SUV mean ratio between the operated *ex vivo* bone sample and the contralateral bone sample.

The histological data were analyzed by non-parametric Kruskal-Wallis test. Further, Mann-Whitney tests were performed to find differences between the groups. In addition, correlations between histological and PET data were studied using non-parametric Spearman rank-order correlation analysis (two-tailed).

4.4 Study IV

In vitro experiment

For *in vitro* experiment, BisGMA-TEGDMA thermosets were coated with polysaccharide 1-deoxylactit-1-yl chitosan (Chitlac) and with Chitlac containing silver nanoparticles (Chitlac–nAg). In addition, uncoated BisGMA-TEGDMA thermosets were prepared as a control. Thereafter, the electro-thermal atomic absorption spectroscopy was used to quantify the total amount of the silver content on the surface of Chitlac–nAg thermosets. Furthermore, the treatment with analytical grade nitric acid was performed during 1, 2 and 3 weeks to define the silver concentration in Chitlac–nAg solution.

In order to ensure the antibacterial properties of Chitlac–nAg solution, the bacterial killing assay was accomplished. Two bacterial strains, *S. aureus* ATCC 25923 and *P. aeruginosa* ATCC 27853, were used in current and in further *in vitro* microbiological experiments.

Subsequently, a modified protocol of the Japanese Industrial Standard method (JIS Z 2801: 2000) was applied to test the antimicrobial efficacy of Chitlac–nAg thermosets and serum-treated Chitlac–nAg thermosets. Serum-treated Chitlac–nAg thermosets were included in the experiment in order to test the possible influence of serum proteins on the antimicrobial potential of Chitlac–nAg thermosets. The uncoated thermosets were used as a control group.

The biofilm model was constructed to assess the biofilm production capability of *S. aureus* ATCC 25923 and *P. aeruginosa* ATCC 27853 on the surface of Chitlac–nAg thermosets, serum-treated Chitlac–nAg thermosets and uncoated BisGMA-TEGDMA thermosets. The crystal-violet technique proposed by Christensen [Christensen et al. 1985] was used to measure the total biofilm mass. In addition, the biofilm was fixed and prepared for SEM analysis to allow the visualization of the morphology and distribution of the biofilm.

The biofilm model was constructed on the surface of Chitlac–nAg thermosets and uncoated BisGMA-TEGDMA thermosets. Subsequently, Chitlac–nAg thermosets and uncoated BisGMA-TEGDMA thermosets were stained with the fluorescence dye (Film Tracer™ FM® 1-43 green biofilm cell stain) according to the manufacturer's instructions. In addition, to investigate the effect of protein coating on antibacterial properties of Chitlac–nAg, the thermosets were stained with the fluorescein-labeled ion-bovine serum albumin. Thereafter, all thermosets were examined with CLSM.

The simulated physiological conditions were created for 21 days to test the durability of antimicrobial effect of Chitlac–nAg thermosets and the release of silver

ions. A modified protocol of the Japanese Industrial Standard method (JIS Z 2801: 2000) was applied to test the antimicrobial efficacy against *S. aureus* ATCC 25923.

In vitro stem cell response was evaluated to indicate the biocompatibility of tested materials. Human adipose-derived stem cells were seeded and grown on the surface of Chitlac–nAg thermosets and uncoated BisGMA-TEGDMA thermosets in an osteogenesis medium. Cells which were able to differentiate into osteoblasts in 4 weeks were subsequently stained with Alizarin Red S to outline the mineralized extracellular matrix.

In the *in vitro* experiment, the differences between groups were studied using Student's t test. The level of statistical significance was selected either 0.05 or 0.01, as specified for each examination separately.

In vivo experiment

For the *in vivo* experiment, the unidirectional E-glass fibers were used to reinforce the BisGMA-TEGDMA thermosets (FRC) and the truncated cone implants were prepared (Ø 3.6 and Ø 5.0 mm, height 8 mm). Consequently, the implants were coated with Chitlac and Chitlac–nAg. A micro-roughened Ti6Al4V implant served as the control material.

The animal study protocol was approved by the Finnish National Animal Experiment Board, ELLA (permit #ESLH-2007-06829/Ym-23) and the institutional guidelines and the protocol for the analgesia and anesthesia for the minipigs were followed. The animal experiments were performed in the Central Animal Laboratory of the University of Turku. The *in vivo* experiment was planned according to the 3R's principles (Refining, Reducing, and Replacing). Therefore, to reduce the number of animals, Study II and Study IV were subsets of the same animal experiment.

Three adult male Göttingen minipigs (Ellegaard Göttingen Minipigs A/S, Denmark) were used in this subset of the *in vivo* experiment. The animal model included the unicortical placement of Chitlac and Chitlac–nAg-FRC implants in the minipig femur. In addition, a control Ti6Al4V implant was inserted in each minipig femur to allow intra-animal comparisons of the implants (Figure 2). The standard sterile surgical conditions were followed during the surgery. The femur was exposed using an anteromedial intermuscular approach. The high-speed dental drill was used to create the unicortical conical-shaped surgical access; thereafter, the implants were firmly press-fitted and the soft tissues were closed in layers. The animals were euthanized 8 weeks after the surgery and the femurs were harvested for histological and histomorphometrical analysis. During the histological analysis, the qualitative and quantitative characterizations of the bone reaction were performed using a standardized histological grading scale [Jansen et al. 1994]. The quantitative assessment of bone–implant contact (BIC) in the cortical area was performed in the histomorphometric analysis.

In the *in vivo* experiment, no statistical analysis was performed, due to the low number of implants.

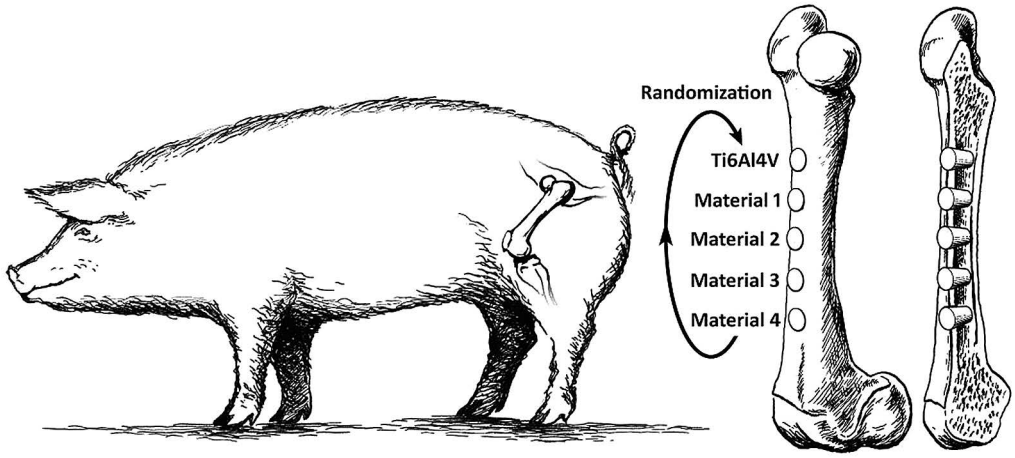

Figure 2. Minipig model used in Studies II and IV. Schematic illustration of the femur with five conical implants; positions of the implants were randomized for each animal.

4.5 Study V

In vitro experiment

Four groups of implant materials were prepared and characterized *in vitro* prior to implantation. The implants were composed of copolymers of L-lactide and ε-caprolactone (PLCL) (PURASORB PLC 7015, Purac Biomaterials, Gorinchem, The Netherlands) loaded with the SARM (ORM-11984) compound in different ratios (10%, 30%, 50% by weight). Placebo control group contained pure polymer implants without the active compound. All implants were prepared in the shape of a cylinder (Ø1mm, height 10mm) from the extruded mixture of polymer and ORM-11984.

In order to assess the release of ORM-11984 from the implants containing 10%, 30% and 50% of this compound, an *in vitro* dissolution test was performed during 14 days. Six implants of group 10%, two implants of group 30% and one implant of group 50% were used in this experiment. Current set-up was dictated by the sensitivity of the experiment i.e. the release of the compound from a particular implant of group 10% was relatively low. The release of ORM-11984 from the composites was measured every day by spectrophotometry.

In vivo experiment

The animal study protocol was approved by the Finish National Animal Experiment Board (permit #ESAVI/1184/04.10.03/2011). The animal experiments were performed in the Central Animal Laboratory of the University of Turku in accordance with the institutional guidelines for the analgesia and anesthesia.

A total of 47 female Sprague-Dawley rats (Harlan, the Netherlands) were used in this study. Two time-points were selected: 6 and 12 weeks. The animals were divided into five experimental groups listed in Table VIII.

Two implants were placed in each experimental animal. In the negative control group, the medullary cavity was left unfilled. In the placebo control group, implants prepared from pure PLCL were inserted into the medullary cavity. During the surgery, standard aseptic conditions were followed. The tibia was operated using an intramedullary ablation model as described by Itälä et al [Itälä et al. 2003]. A round cortical window was was drilled. In addition, a smaller cortical defect (vent was) drilled 5mm distally. In order to allow the insertion of the implant through the cortical window, the implants (10 mm) were divided into two parts (5 mm each) and placed between the cortical defects in the medullary cavity (Figure 3). Subsequently, the cortical window was placed back and the surgical access was closed in layers.

The animals were euthanized 6 and 12 weeks after the surgery and the tibia were harvested for micro-CT imaging and histomorphometry.

In micro-CT analysis included the measurements of the volume of newly formed bone, tissue mineral density (TMD), cortical thickness, periosteal radius and endosteal radius (Figure 3).

In histomorphometric analysis, the area of newly formed bone was assessed in the whole medullary cavity and in a peri-implant ring of 50 µm. In addition, bone-implant contact (BIC) was quantified (Figure 3).

In statistical analysis of the data, Kolmogorov-Smirnov test was used to verify the normal distribution of the data. Consequently, one-way ANOVA with Tukey's post-hoc test was performed. In order to investigate the dose response to the concentrations of ORM-11984, non-parametric Spearman rank-order correlation analysis (two-tailed) was used.

Table VIII. Experimental groups in Study V. (Adapted from Study V).

Group	Experimental group	6 weeks	12 weeks
Placebo control group	PLCL 100%	n=5	n=5
10%	PLCL loaded with 10% of ORM-11984	n=4	n=4
30%	PLCL loaded with 30% of ORM-11984	n=4	n=4
50%	PLCL loaded with 50% of ORM-11984	n=4	n=4
Negative control group	empty	n=4	n=4

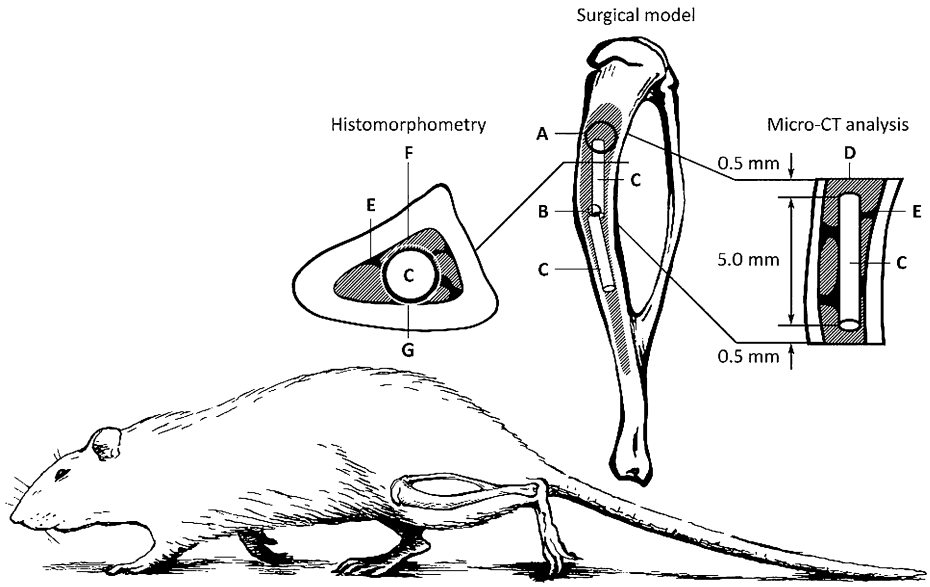

Figure 3. Rat model used in Study V. Schematic illustration of rat tibia with cortical window (A), cortical vent (B) drilled 5mm distally and intramedullary implants (C). In μCT analysis, VOI (D) was selected within the intramedullary space, 0.5 mm proximally and 0.5 mm distally from ends of the implant (C). The volume of new bone (E) was measured inside the VOI. In histomorphometric analysis, ROI 1 (F) was selected by outlining the endosteal border of the cortex. ROI 2 (G) was constructed by offsetting the outer border of the implant by 50 μm. The area of new bone (E) was evaluated inside ROI 1 and ROI 2.

5 RESULTS

5.1 Study I

In vitro experiment

In SBF, a uniform Ca-P-layer formation was seen on the surface of BisGMA-TEGDMA thermosets with 75 wt% and 50 wt% of BAG. There was no Ca-P formation on control BisGMA-TEGDMA thermosets without BAG. In BM, there was a thick layer of Ca-P on the surface of the BisGMA-TEGDMA thermosets with 75 wt% of BAG. However, only scattered islands of Ca-P on BisGMA-TEGDMA thermosets with 50 wt% of BAG were seen; no Ca-P formation was detected on control BisGMA-TEGDMA thermosets without BAG. Unexpectedly, in both SBF and BM, Ca-P-layer formed on the surface of the BAG granules and on the resin. The thicknesses of the Ca-P layers are shown in Table IX. SEM micrographs of the top surfaces and cross-sectional views of BisGMA-TEGDMA thermosets with BAG particulate are shown in Figure 4.

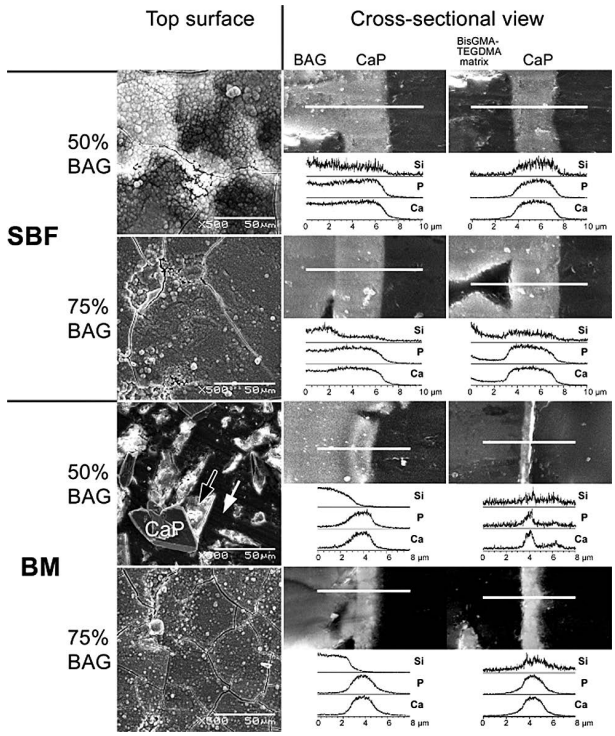

Figure 4. Top surfaces and cross-sectional views of BisGMA-TEGDMA thermosets with BAG particles. On top views, black arrow indicates BAG granule, white arrow indicates BisGMA-TEGDMA matrix. On cross-sectional images, the tickness of Ca-P-layer is measured on top of BAG granule (left) and on top of the polymer (right). (Adapted from Study I).

Table IX. The thickness of Ca-P-layer (μm) on the BisGMA-TEGDMA thermosets. The data is presented as mean ± standard deviation. (Adapted from Study I).

Solution	BisGMA-TEGDMA thermosets without BAG		BisGMA-TEGDMA thermosets with 50 wt.% BAG		BisGMA-TEGDMA thermosets with 75 wt.% BAG	
	BAG phase	Polymer phase	BAG phase	Polymer phase	BAG phase	Polymer phase
SBF	n/a	n/a	3.1 ± 0.9	2.9 ± 0.8	4.7 ± 1.0	4.8 ± 1.1
BM	n/a	n/a	2.1 ± 0.3	1.8 ± 0.7	3.2 ± 0.4	2.7 ± 0.1

n/a = not available

5.2 Study II

In vitro experiment

The residual monomer content was measured by gas chromatography. In Micro-composite and Nano-composite, the residual monomer content was below the detection limit of 0.02 and 0.05 % for L-lactide and glycolide respectively.

Ubbelohde viscometer was used to measure the inherent viscosity. In Micro-composite, the inherent viscosity remained at a level close to 3.13 dl/g of the initial PLGA 95L:5G polymer matrix (Table X). In contrast, the inherent viscosity in Nano-composite dropped to 2.23 dl/g from 3.01 dl/g of the initial PLGA 85L:15G polymer matrix (Table X).

Laser diffractometer was used to study particle size distributions of β-TCP particulates. Compared to the initial β-TCP particulate, the size of the β-TCP particles increased in Micro-composite and in Nano-composite due to agglomeration. The particle size in Micro-composite increased to 22.7 μm from 3.67 μm of the initial β-TCP particulate. In Nano-composite, nano-structuring and cryo-alloying fused β-TCP particles together and agglomerates of 70.4 μm were formed (Table X). In addition, agglomeration decreased the surface area of the β-TCP particles in both composites (Table X).

XRD analysis was used to study the crystal size of the β-TCP particulate. Nano-structuring decreased the crystal size of β-TCP in Nano-composite to 10-20 nm from 35 nm of the initial β-TCP particulate as indicated by the XRD analysis.

Mechanical tests were performed to study the mechanical properties of the composites. The bending and shear strength of Micro-composite was comparable with that of pure PLGA 95L:5G. The bending strength of Micro-composite was 21% higher than that of Nano-composite. The shear strength of Micro-composite was 58% higher than that of Nano-composite. The bending modulus was comparable in the case of both composites and pure PLGA 95L:5G. Mechanical properties are shown in Table X.

In order to investigate the morphologies of Micro-composite and Nano-composite, SEM analysis was performed. As seen in SEM micrograph (Figure 5A), the distribution of the particles in the initial β-TCP particulate was homogenous. In Micro-composite, β-TCP particles were partially agglomerated after melt-compounding, as manifested by the two-phased microstructure of the surface of the composite (Figure 5B). The particles were, however, entrapped in the polymer matrix indicating good wetting. In Nano-composite, the agglomeration was substantial. Scattered β-TCP particles were not surrounded by the polymer matrix (Figure 5C) indicating poor wetting. Moreover, fibrillar polymer fractions resulting from the cryo-alloying step were observed (Figure 5C).

The *in vitro* degradation properties of the composites were studied in hydrolysis for 78 weeks. The degradation was faster for Nano-composite compared with Micro-composite. The crystallinity of the PLGA 95L:5G matrix in Micro-composite increased from 42.3 % to 50.4 % after 36-weeks of hydrolysis. The initial crystallinity of the PLGA 85L:15G matrix Nano-composite was 32.9 % and it turned amorphous already after 24 weeks of hydrolysis. This change was reflected in the mass loss. By 78 weeks of hydrolysis, the mass loss in Micro-composite was 4% while the mass loss in Nano-composite was 40%.

Table X. Results of *in vitro* characterization of implant materials. (Adapted from Study II).

Property	**Raw materials**			**Composite implants**	
	PLGA 95L/5G	PLGA 85L/15G	β-TCP	Micro-composite 84 wt% PLGA 95L:5G 16 wt% β-TCP	Nano-composite 84 wt% PLGA 85L:15G 16 wt% β-TCP
Inherent viscosity [dl/g]	3.13 ± 0.03	3.01 ± 0.08	-	3.15 ± 0.05	2.23 ± 0.05
Crystallinity of matrix [%]	-	-	-	42.3 ± 2.2	32.9 ± 1.0
β-TCP, median particle size [μm]	-	-	3.67	22.7	161
β-TCP, specific surface area [m^2/kg]	-	-	1835	961	195
Shear strength [MPa]	-	-	-	87.9 ± 1.8	55.5 ± 2.3
Bending strength [MPa]	-	-	-	165.7 ± 5.1	136.5 ± 3.8
Bending modulus [GPa]	-	-	-	3.9 ± 0.1	3.8 ± 1.2

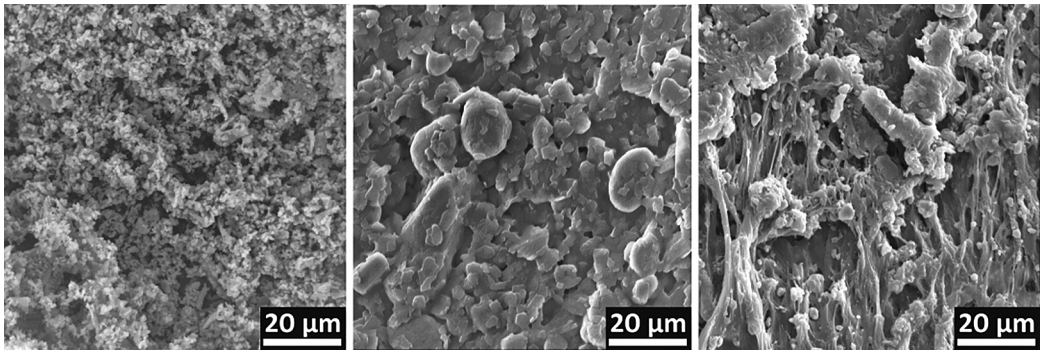

A B C

Figure 5. SEM micrographs of initial β-TCP particulate (A); Agglomeration of β-TCP particulate in Micro-composite (B) and in Nano-composite (C). (Adapted from Study II).

In vivo experiment

In the *in vivo* experiment, push-out test was the key characterization method. The differences between Micro-composite and Nano-composite were not statistically significant. The results of the push-out test are shown in Table XI. The intra-animal comparison with Ti6Al4V implants was challenged, as upon tissue retrieval one Ti6Al4V implant appeared loose. Moreover, one Ti6Al4V implant and one Nano-composite implant were excluded as outliners, since the measured push-out forces were negligible. Therefore, statistical analysis was not performed due to the small number of the remaining specimens. The results of the intra-animal comparison are shown in Table XII. The push-out force and stiffness of Micro-composite and Nano-composite were 35-72 % of the values of Ti6Al4V implants. The push-out force and stiffness of pure PLGA 95L/5G implants were low, 16-49 % of the values of Ti6Al4V implants.

Table XI. Results of the push-out test. The data is presented as mean (± standard deviation).

Parameter	**Implant group**			
	Micro-composite (N=6)	Nano-composite (N=5)	PLGA 95L:5G (N=3)	Ti6Al4V (N=6)
Force [N]	156.7 (± 128.5)	109.1 (± 82.6)	89.6 (± 25.8)	271.2 (± 213.1)
Stiffness [N/mm]	413.9 (± 218.6)	317.9 (± 94.4)	282.6 (± 95.2)	660.5 (± 378.0)
Absorbed energy [N*mm]	42.6 (± 45.5)	24.0 (± 19.5)	20.1 (± 11.0)	73.7 (± 67.8)

Table XII. Results biomechanical test (intra-animal comparison). Results are expressed as percentages of the values obtained for Ti6Al4V in the same animal. The data is presented as median (range). (Adapted from Study II).

Parameter	Implant group	
	Micro-composite	Nano-composite
Force	49.7 % (35.1 – 60.1)	48.1 % (35.8 – 60.4)
Stiffness	56.4 % (39.4 – 71.7)	53.1 % (48.7 – 57.4)
Absorbed energy	45.5 % (23.4 – 68.0)	38.1 % (26.2 – 49.9)

The micro-CT-based measurements and histological evaluation performed after the push-out test should be considered as approximations. The results of the volumetric analysis of the peri-implant bone are shown in Table XIII. In the statistical analysis, there were no significant intergroup differences: the peri-implant bone volume of Micro-composite and Nano-composite was similar to that of Ti6Al4V implants. Micro-CT images are shown in Figure 6.

The results of the histological analysis are shown in Table XIII. For all implant groups, the average thickness of the reaction zone was in the range of 136 - 197 µm µm (Table XIII), which corresponded to score 3 in the standardized grading scale. Hence, instead of the scores, the actual reaction zone thickness values were used to compare the implant groups. There were no statistical differences between the implant groups, when tested with ANOVA. For Micro-composite implants, the peri-implant reaction zone was generally comprised of newly formed woven bone with local areas of BIC (Figure 7A). For Nano-composite implants, the peri-implant tissue in the reaction zone was ranging from the spikes of woven new bone (lines in Figure 7B) attaching to the surface of the implant to the presence of a thin fibrous tissue layer. For the pure PLGA implants, there were narrow areas of woven newly formed bone in local contact with the implant surface (lines in Figure 7C) alternating with areas of peri-implant fibrous tissue. For the Ti6Al4V implants, the reaction zone mainly contained narrow areas of woven newly formed bone with the trabecular extensions, which were locally attached to the implant surface (Figure 7D); however, local areas of peri-implant fibrous tissue were also observed. The qualitative and quantitative assessment of histologic bone reaction revealed no distinct differences between the composite implants and the controls (Table XIII). There were no cases of encapsulation or inflammatory reaction at the bone-implant interface. Favorable biologic response was observed in all four implant groups.

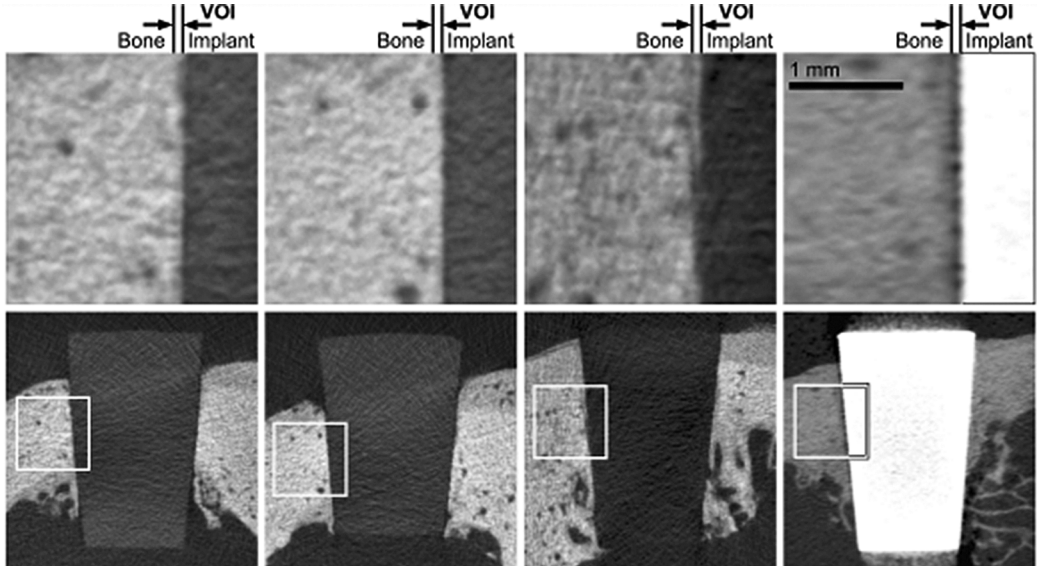

Figure 6. Micro-CT imaging and analysis of the peri-implant bone. Micro-composite implant (A), Nano-composite (B), control Ti6Al4V implant (C) and control pure PLGA implant (D). Upper row show details of the selection of the peri-implant VOI, the respective areas are marked with boxes on the images in the lower row. (Adapted from Study II).

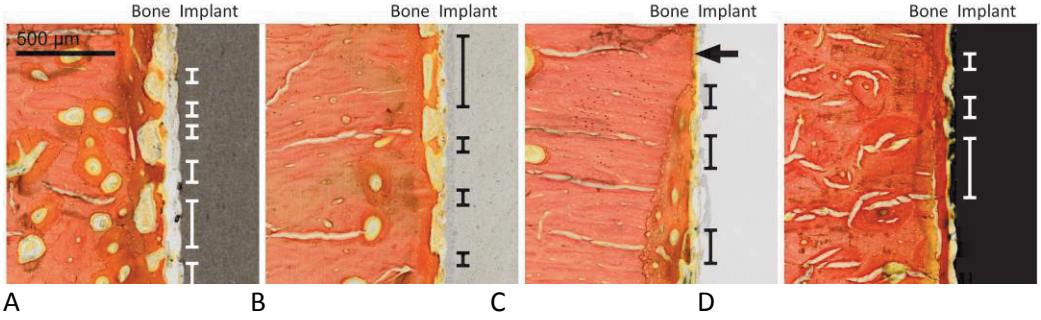

Figure 7. Light micrographs of bone-implant interfaces after 8 weeks of implantation in cortical bone stained by van Gieson method (red): Micro-composite implant (A), Nano-composite (B), control Ti6Al4V implant (C) and control pure PLGA implant (D). Areas of direct BIC with newly formed woven bone are shown with lines. Arrows indicate BIC with cortical lamellar bone. (Adapted from Study II).

Table XIII. Summary of peri-implant bone assessment by micro-CT and histology. The data is presented as median (range).

Parameter	Implant group			
	Micro-composite (N=6)	Nano-composite (N=5)	PLGA 95L:5G (N=3)	Ti6Al4V (N=6)
Peri-implant bone volume [%]	47.9 (33.3 – 70.0)	60.1 (18.7 - 79.1)	75.6 (64.6 - 81.6)	58.3 (50.5 - 83.8)
Reaction zone thickness [µm]	146.3 (88.1 – 348.5)	136.4 (38.0 - 222.4)	197.2 (145.6 - 728.9)	187.2 (117.2 – 218.51)
Bone reaction qualitatively [score]	3.2 (3.0 - 3.7)	3.0 (3.0 - 3.7)	3.0 (3.0 - 3.2)	3.0 (2.7 - 3.5)
Interface qualitatively [score]	3.2 (2.0 - 4.0)	2.5 (2.0 - 2.5)	3.0 (2.5 - 3.5)	3.0 (2.5 - 3.5)

5.3 Study III

In vitro experiment

Prior to the *in vivo* experiment, the bacterial strains were tested for their *in vitro* capability to form biofilm. After 24 hours of incubation, both strains were able to form the biofilm. Moreover, there were no significant differences in biofilm mass and, therefore, in biofilm production capability between *S. epidermidis* and *S. aureus* tested strains.

In vivo experiment

Distributions of radioactivity after intravenous injection of ^{68}Ga-DOTA-Siglec-9 in rats as determined by *in vivo* PET/CT imaging and *ex vivo* gamma counting are summarized in Table XIV. ^{68}Ga-radioactivity was accumulated especially in proximal part of the tibia (Figure 8). The highest difference (SUV ratio) between operated and contralateral tibia was observed in rats with implant infection caused by *S. epidermidis* (58.1%, $P = 0.009$) followed by *S. aureus* (41.7 %, NS) and negative control group (29.5%, $P < 0.001$). The SUV ratios of *S. epidermidis* group were significantly higher compared to those of negative control group (Table XIV). The excess of radioactivity excreted through kidneys to the urinary bladder and these organs were clearly visible in PET images (Figure 8).

Table XIV. Distribution of radioactivity in rat tibias after intravenous injection of ^{68}Ga-DOTA-Siglec-9 (SUV mean). Results are expressed as mean ± standard deviation. P values indicate differences between operated and contralateral tibia (Paired t-test).

Group	Operated	Contralateral	Ratio	*P* value
S. epidermidis n = 10				
Proximal tibia (ROI 1)	1.12 ± 0.36	0.71 ± 0.23	1.58 ± 0.20*	<0.001
Distal tibia (ROI 2)	0.83 ± 0.25	0.56 ± 0.17	1.48 ± 0.15**	<0.001
Tibia, *ex vivo*	0.14 ± 0.05	0.08 ± 0.02	1.82 ± 0.48†	0.043
S. aureus (positive control) *n* = 7				
Proximal tibia (ROI 1)	1.12 ± 0.39	0.75 ± 0.24	1.50 ± 0.31	0.035
Distal tibia (ROI 2)	0.75 ± 0.23	0.54 ± 0.15	1.38 ± 0.20	0.027
Tibia, *ex vivo*	0.15 ± 0.05	0.11 ± 0.03	1.34 ± 0.33	0.028
Negative control *n* = 10				
Proximal tibia (ROI 1)	1.02 ± 0.07	0.79 ± 0.10	1.30 ± 0.13*	<0.001
Distal tibia (ROI 2)	0.75 ± 0.06	0.61 ± 0.05	1.24 ± 0.11**	<0.001
Tibia, *ex vivo*	0.12 ± 0.04	0.10 ± 0.02	1.26 ± 0.45†	n.s.

* *S. epidermidis* and negative control, P = 0.011 (ANOVA with Tukey's post-hoc)

** *S. epidermidis* and negative control, P = 0.007 (ANOVA with Tukey's post-hoc)

† *S. epidermidis* and negative control, P = 0.018 (ANOVA with Tukey's post-hoc)

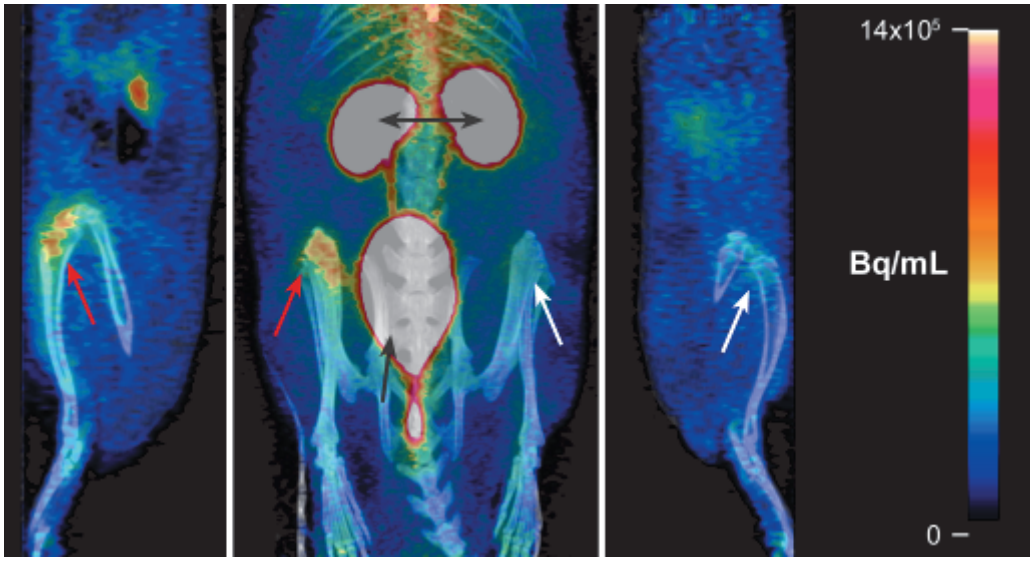

Figure 8. PET/CT images of ^{68}Ga-DOTA Siglec-9 peptide uptake in the rat with catheter-related *S. epidermidis* infection. High focal uptake of radioactivity in the operated right tibia is observed (red arrows) compared with the contralateral intact left tibia (white arrows). Excess of radioactivity is excreted through kidneys (two headed black arrow) to the urinary bladder (black arrow). (Adapted from Study III).

The histological analysis was performed to associate the infection with the signs of inflammatory response. Results are presented in Table XV. The most representative histological views are shown in Figure 9. In the *S. epidermidis* group the periosteal reaction was mainly sunburst type and circumferential. There was a moderate subperiosteal, endosteal and intracortical resorption of the cortex. Haversian canals were enlarged and filled with granulation tissue and fragmented polymorphonuclear leukocytes. Occasional microabscesses were also detected in the cortex. Increased amount of polymorphonuclear leucocytes were observed in the medullary canal in the proximity of the implant (Figure 9A). The median grade in the group was 3, range 1 – 3. In the *S. aureus* group, there was a high deviation in the histological views, ranging from low to severe inflammatory reaction. Significant periosteal reaction, extensive destruction of the cortex and increased number of the polymorphonuclear leucocytes in the medullary canal were seen in the severe cases of the inflammatory reaction (Figure 9B). The median grade in the group was 3, range 1 – 3. In the negative control group there were signs of uneventful healing and the inflammatory reaction was low. For the samples with grade 1, reactive bone formation was observed in the medullary canal, mainly around the implant. The medullary canal contained normal bone marrow hematopoietic cells (Figure 9C). The median grade in the group was 0, range 0 – 1. Statistical analysis of the histological data revealed significant differences between negative control group and *S. aureus* group ($P < 0.001$) as well as between negative control group and *S. epidermidis* group ($P < 0.001$). There were no statistically significant differences between *S. aureus* and *S. epidermidis* group. In the *S. epidermidis* group, Spearman rank-order correlation analysis showed statistically significant correlations with respect to histological data for SUV mean of the operated proximal tibia ($r_S = 0.719$, $P = 0.019$), SUV mean of the operated distal tibia ($r_S = 0.719$, $P = 0.019$) and SUV mean of the operated *ex vivo* bone sample ($r_S = 0.674$, $P = 0.033$). There were no other statistically significant correlations for the data analyzed within the groups. However, when the analysis was performed on ungrouped data, statistically significant correlations with respect to histological data were found for all PET parameters with the exception of the SUV mean ratio between the operated ex vivo bone sample and the contralateral bone sample.

The pathogens were cultured from the bone samples and from the catheters.

As shown in Table XV, in the *S. epidermidis* group, the visual bacterial growth was detected during the incubation period in the 91% of cultures (catheters and bone samples). Thereafter, the API test verified that the isolated pathogens matched with the inoculated ones (*S. epidermidis*). In *S. epidermidis* group, 9% of the cultures were negative; no visual bacterial growth was detected. Therefore, the bone samples were ground and subsequently cultured on blood agar plates for 48 hours. Since, the results obtained after the incubation period were negative, the 16s PCR was performed. However, the results of 16s PCR were also negative. In the *S. aureus* group, the visual bacterial growth was detected during the incubation period in 70% and 60% of tubes containing catheters and bone samples respectively (Table XV). In these positive cultures, *S. aureus* was differentiated by the Staphaurex latex

agglutination test. The isolated pathogens matched with the inoculated ones. In *S. aureus* group, there was no visual bacterial growth in 30-40%. Hence, the 16s PCR was performed, the results were negative. No bacteria could be cultured from catheters and bone samples retrieved from the control animals (Table XV). In addition, the 16s PCR results were negative.

The catheters were stained with live/dead staining to confirm the presence of bacterial biofilm in the case of *S. epidermidis* and *S. aureus* groups and verify the absence of the biofilm in the negative control group. The coccoid bacterial cells were observed on the surface of catheters in *S. epidermidis* (Figure 10A) and *S. aureus* groups (Figure 10B). As seen in Table XV, imaging with fluorescent microscope demonstrated the presence of biofilm in 82% in the *S. epidermidis* group and 70% of samples in the *S. aureus* group. In addition, no bacterial biofilm could be seen in the negative control group (Figure 10C), except for one sample with a probable contamination.

Table XV. Results of fluorescent microscopy, microbiological and histological analysis

Group	Rat number	Fluorescent microscopy	Microbiological analysis		Histological analysis
		Implant	Bone	Implant	
S. epidermidis	23	+	-	-	1
	24	+	+	+	3
	25	+	+	+	3
	26	+	+	+	3
	27	+	+	+	2
	28	-	+	+	3
	29	+	+	+	2
	30	+	+	+	3
	31	+	+	+	3
	32	n/a	+	+	3
	33	+	+	+	2
S. aureus	1	+	+	+	3
	2	+	+	+	2
	3	+	+	+	3
	4	+	+	+	3
	5	+	+	+	3
	6	+	+	-	2
	10	-	-	+	3
	11	-	-	-	1
	12	-	-	-	1
	13	+	+	-	3
Control	7	+	-	-	1
	8	-	-	-	1
	9	-	-	-	1
	14	-	-	-	0
	15	-	-	-	0
	16	-	-	-	0
	17	-	-	-	0
	18	-	-	-	0
	19	-	-	-	1
	20	-	-	-	1
	21	-	-	-	0
	22	-	-	-	0

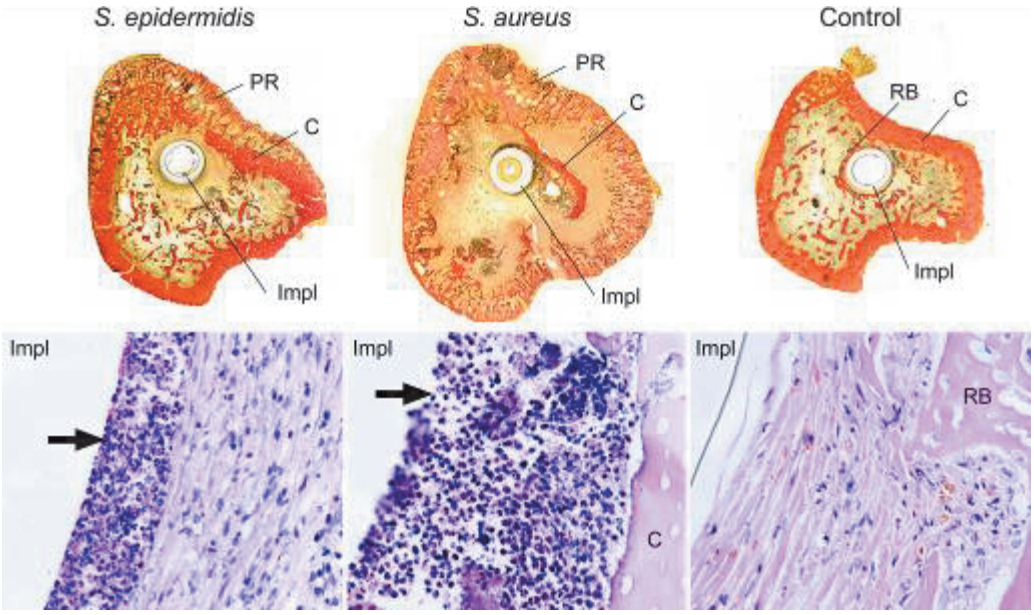

A B C

Figure 9. Histological analysis. Upper row: van Gieson stain, lower row: haematoxylin and eosin stain. Cortex is denoted as "C", implant as "Impl", periosteal reaction as "PR" and reactive bone formation as "RB". *Staphylococcus epidermidis* group. Van Gieson stain: inflammatory response is expressed as sunburst type periosteal reaction and partial resorption of the cortex. Haematoxylin and eosin stain: a layer of polymorphonuclear leucocytes is visible in the proximity of the implant (arrow). This layer is surrounded by granulation tissue (A). *Staphylococcus aureus* group. Van Gieson stain: Inflammatory response is expressed as circumferential sunburst type periosteal reaction and almost complete resorption of the cortex. Haematoxylin and eosin stain: polymorphonuclear leucocytes are seen in the proximity of the implant (arrow) (B). Negative control group. Van Gieson stain: periosteal and cortical reactions are absent. Reactive bone formation is seen around the implant. Haematoxylin and eosin stain. Implant is surrounded by fibrous capsule and reactive bone (C). (Adapted from Study III).

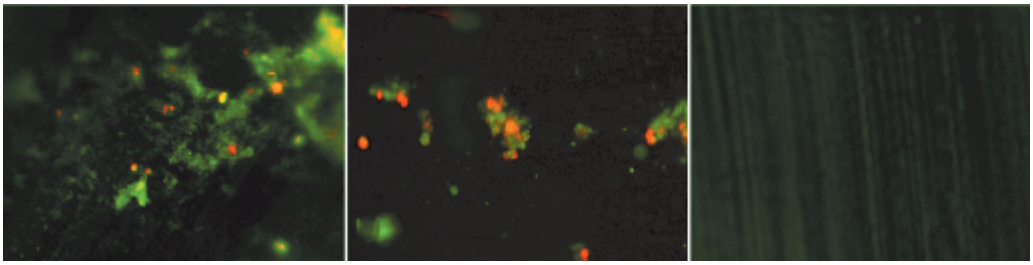

A B C

Figure 10. Fluorescence microscope images of the surface of the catheter. Biofilm clusters composed of aggregates of viable coccoid bacterial cells which were stained with SYTO® 9 (green color) and dead bacteria stained with PI (orange-red). *Staphylococcus epidermidis* clinical isolate T-54580(A); *Staphylococcus aureus* clinical isolate 52/52A/80(B); Control (C). (Adapted from Study III).

5.4 Study IV

In vitro experiment

The effect of serum proteins on the antibacterial properties of Chitlac-nAg colloidal solution and Chitlac–nAg-coated thermosets was evaluated. As shown in Figure 11, the antibacterial effect of Chitlac–nAg colloidal solution against *S. aureus* ATCC 25923 was not compromised by serum proteins. In turn, the inhibitory effect of the serum proteins on antibacterial properties of Chitlac–nAg colloidal solution against *P. aeruginosa* ATCC 27853 was evident (Figure 11). However, the serum protein layer significantly reduced the antibacterial properties of Chitlac–nAg-coated thermosets against both bacterial strains; although, Chitlac–nAg-coated thermosets were effective in comparison with the uncoated BisGMA-TEGDMA thermosets (Figure 12A).

The biofilm production capability of *S. aureus* ATCC 25923 and *P. aeruginosa* ATCC 27853 was assessed on the surface of uncoated BisGMA-TEGDMA thermosets, Chitlac–nAg-coated thermosets and serum-treated Chitlac–nAg-coated thermosets. Thermosets with silver content were significantly more effective for the inhibition of biofilm formation of *S. aureus* ATCC 25923 and *P. aeruginosa* ATCC 27853 in comparison with the uncoated BisGMA-TEGDMA thermosets (Figure 12B). However, the results of this experiment clearly indicated that antibacterial properties of silver containing thermosets were challenged by the addition of serum proteins which is in line with the previous observations (Figure 12B).

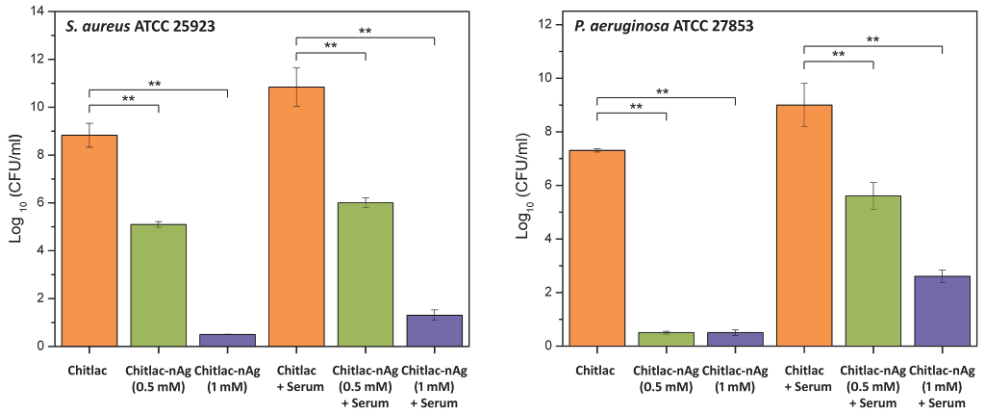

Figure 11. The effect of serum proteins on the antibacterial properties of Chitlac-nAg colloidal solution and Chitlac–nAg-coated thermosets. (Adapted from Study IV).

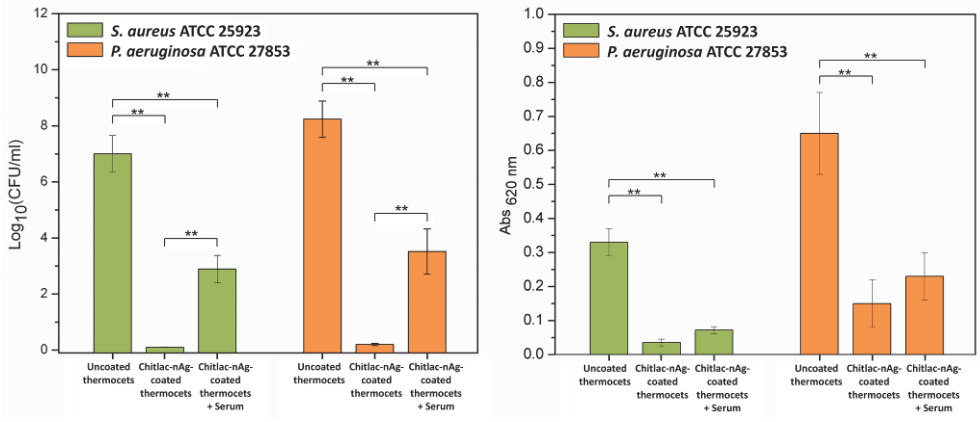

A B

Figure 12. The effect of serum proteins on antibacterial properties of Chitlac–nAg-coated thermosets. (A) and biofilm production capability (B) of *S. aureus* ATCC 25923 and *P. aeruginosa* ATCC 27853 on the surface of Chitlac–nAg-coated thermosets. (Adapted from Study IV).

SEM and CLSM analyses were performed to evaluate the distribution and morphological changes in the biofilm. SEM micrographs indicated a remarkable difference between the arrangement of the biofilm on the surface of uncoated BisGMA-TEGDMA thermosets, Chitlac-nAg-coated thermosets and serum-treated Chitlac–nAg-coated thermosets. On the surface of uncoated BisGMA-TEGDMA thermosets, *S. aureus* ATCC 25923 produced a thick biofilm, which was distributed across the entire surface with the prevalence in the center of the thermosets (Figure 13). In contrast, 90% of the surface of Chitlac–nAg-coated thermosets was free from *S. aureus* ATCC 25923 colonization (Figure 13). In compliance with the results obtained by crystal-violet assay, the surface of the serum-treated Chitlac-nAg-coated thermosets was slightly colonized by *S. aureus* ATCC 25923; however, bacterial cells

were present mostly in an isolated form (Figure 13). The same results were obtained in the SEM analysis of the thermosets pretreated with *P. aeruginosa* ATCC 27853. Uncoated BisGMA-TEGDMA thermosets were covered with multilayered and uniformly distributed *P. aeruginosa* ATCC 27853 biofilm (Figure 13). However, bacterial cells were barely found on the surface of Chitlac–nAg-coated thermosets (Figure 13). In turn, several scattered microcolonies embedded in extracellular matrix were found on the surface of the serum-treated Chitlac–nAg-coated thermosets (Figure 13).

CLSM analysis confirmed that Chitlac–nAg is potent against *S. aureus* ATCC 25923 and *P. aeruginosa* ATCC 27853; nevertheless, the antibacterial properties might be moderated by serum proteins (Figure 14).

In order to investigate the durability of antibacterial properties of Chitlac–nAg, the release of silver ions from Chitlac–nAg thermosets was measured during 21 days in simulated physiological conditions. Extensive and sustained release of silver ions was observed during the first 7 days. The content of silver ions dropped from 96 ± 3.1 ng cm^{-2} at day 0 to 1.5 ± 1 ng cm^{-2} at day 21, explicitly 90% of the total amount (Figure 15A). In addition, an extensive leakage of silver ions resulted in the decrease of antibacterial properties of Chitlac–nAg thermosets against *S. aureus* ATCC 25923. After 21 days of incubation, antibacterial activity was accounted for 30% of the initial level (Figure 15A).

In vitro mesenchymal stem cell response on the surface of uncoated BisGMA-TEGDMA thermosets and Chitlac–nAg-coated thermosets was evaluated. As seen in Figure 15B, calcium deposits were found on the surfaces of both thermosets suggesting differentiation of mesenchymal cells in osteoblasts.

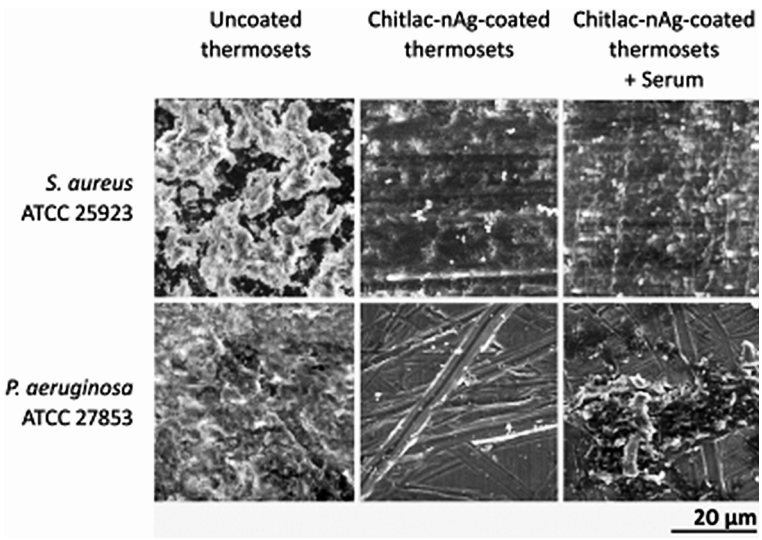

Figure 13. The effect of serum proteins on *S. aureus* ATCC 25923 and *P. aeruginosa* ATCC 27853 biofilm formation on the surface of Chitlac–nAg-coated thermosets. SEM examination. (Adapted from Study IV).

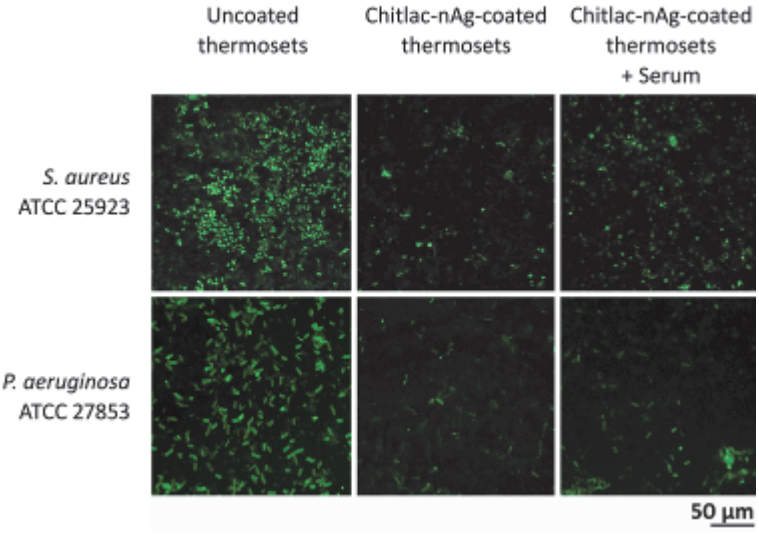

Figure 14. The effect of serum proteins on *S. aureus* ATCC 25923 and *P. aeruginosa* ATCC 27853 biofilm formation on the surface of Chitlac–nAg-coated thermosets. CLSM examination. (Adapted from Study IV).

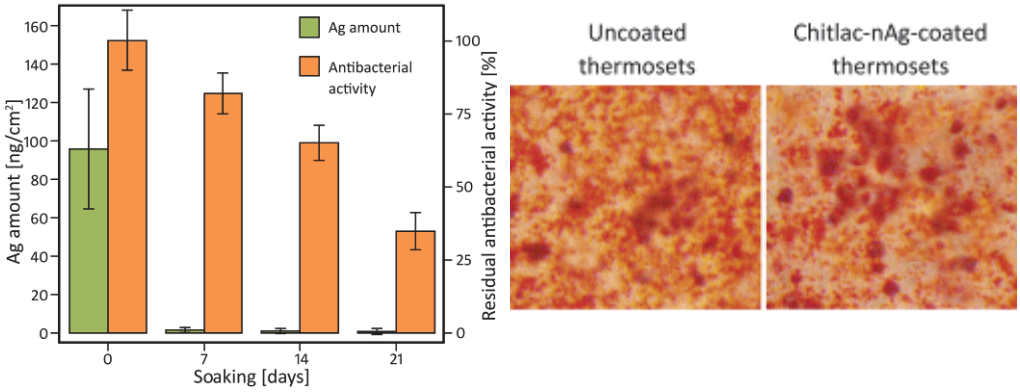

Figure 15. The durability of antibacterial properties of Chitlac–nAg (A). *In vitro* mesenchymal stem cell response on the surface of uncoated BisGMA-TEGDMA thermosets and Chitlac–nAg-coated thermosets (B). (Adapted from Study IV).

In vivo experiment

The minipig animal model was used in order to investigate bone tissue response induced by Chitlac-coated FRC, Chitlac–nAg-coated FRC and Ti6Al4V implants. The most representative histological images are shown in Figure 16. The results of the histomorphometrical and histological analysis are shown in Table XVI. The results on Chitlac-coated FRC implants were previously reported by Travan and co-workers [Travan et al. 2012] and are given for comparison. Histomorphometrical

analysis showed scant bone tissue remodeling in the case of Chitlac-coated FRC implants. The old cortical lamellar bone accounted for 44% (min. 18%, max. 68%) of the peri-implant bone interface and the newly formed woven bone comprised only 28% (min. 12%, max. 41%). Hence, the total BIC value was 72% (min. 59%, max. 80%). In contrast, both Chitlac–nAg-coated FRC and Ti6Al4V implants were surrounded by predominantly newly formed woven bone. The BIC values of the newly formed bone were 26% (min. 22%, max. 27%) for Chitlac–nAg-coated FRC and 46% (min. 30%, max. 60%) for Ti6Al4V implants. Although the statistical analysis was not performed due to the low number of implants, the BIC value of Chitlac–nAg-coated FRC implants was lower than that of Chitlac –coated FRC and Ti6Al4V implants.

The quality of the peri-implant bone was characterized using a standardized histological scale for hard-tissue implants. The results are shown in Table XVI. In Chitlac-nAg-coated FRC implants, the thickness of the reaction zone was higher than that in Chitlac -coated FRC implants, but lower than in Ti6Al4V implants. As shown in Table XVI, the analysis of bone reaction quality and bone interface quality indicated bone remodeling activity for all implant materials. Nevertheless, the grading scale used in this experiment prefers lamellar bone over woven bone, which leads to higher grades for Chitlac–coated FRC implants.

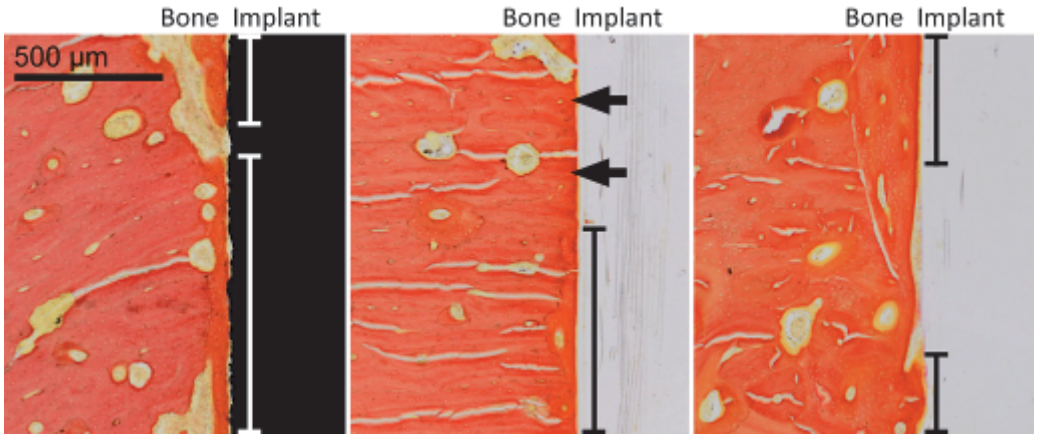

Figure 16. Light micrographs of bone-implant interfaces after 8 weeks of implantation in cortical bone stained by van Gieson method (red): micro-roughened control Ti6Al4V implant (A); Chitlac-coated FRC implant (B); Chitlac–nAg-coated FRC implant (C). Areas of direct BIC with newly formed woven bone are shown with lines. Arrows indicate BIC with cortical lamellar bone. (Adapted from Study IV).

Table XVI. Results of the histomorphometrical and histological analysis. (Adapted from Study IV).

Parameter		Implant material		
		Ti6Al4V (control)	Chitlac-coated FRC	Chitlac-nAg-coated FRC
Bone-implant contact average (min – max)	Newly-formed woven bone (%)	46 (30 - 60)	28 (12 - 41)	26 (22 - 27)
	Lamellar bone (%)	0	44 (18 - 68)	0
	Total bone (%)	46 (30 - 60)	72 (59 - 80)	26 (22 - 27)
Histologic grading scale average (min – max)	Reaction zone width (μm)	13.5 (11.0 – 15.1)	1.9 (0.0 – 3.0)	11.7 (10.2 – 13.5)
	Bone reaction qualitatively	3.2 (3.0 – 3.5)	3.8 (3.5 – 4.0)	3.0 (3.0 – 3.0)
	Interface reaction qualitatively	3.2 (3.0 – 3.5)	3.9 (3.8 – 4.0)	3.2 (2.5 – 3.8)

5.5 Study V

In vitro experiment

The release of ORM-11984 from the implants was assessed during the dissolution test. The most rapid dissolution rate of 6 mg of ORM-11984 was measured in group 10% (six implants) and the slowest in group 50% (one implant) (Figure 17A). In all experimental groups, the release of the compound followed the linear trend with the slope of 1.49 (R^2 =0.98) in group 10%, 1.47 (R^2 =0.99) in group 30% and 0.99 (R^2 >0.99) in group 50%. Nevertheless, due to the differences in the number of implants in each experimental group, the results are not directly comparable with the *in vivo* data. To allow the direct comparison of *in vitro* and *in vivo* results, the approximation of ORM-11984 release from a single implant was made (Figure 17B). Unsurprisingly, the highest release of ORM-11984 was seen in group 50% and the lowest in group 10%.

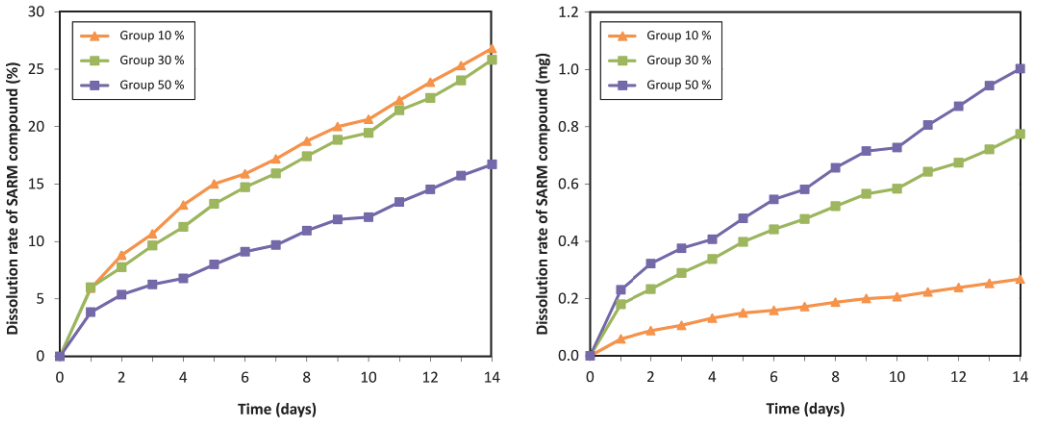

A B

Figure 17. Dissolution rate of 6 mg of ORM-11984: 6 implants in group 10%, 2 implants in group 30%, 1 implant in group 50% (A). Dissolution rate of ORM-11984 in groups 10%, 30% and 50% normalized to one implant (B). (Adapted from Study V).

In vivo experiment

New bone formation was seen in the intramedullary cavity in all groups. Qualitatively the new bone was mature. The most descriptive images of micro-CT data and histological sections are shown in Figure 18.

In micro-CT analysis, the highest volume of new bone was observed in group 10% in both time-points (Figure 19 A). Unexpectedly, there were no statistically significant correlations (Spearman rank-order correlation) between the dose of ORM-11984 compound and the volume of newly formed bone in micro-CT. In the analysis of TMD data, there were no statistically significant differences between the groups. ORM-11984 had no effect on the density of cortical and intramedullary newly formed bone. Statistically significant differences were detected in the measurements of cortical thickness. In group 10% (591 µm) the cortical thickness was lower than in group 50% (673 µm), P=0.05, and the negative control (656 µm), P=0.027. In the measurement of periosteal radius, no statistically differences were detected. However, in group 10% there was a notable increase in periosteal radius in both time-points, which is an important finding. Although, with a low number of animals (n=4) used in this screening study, statistically significant differences were unlikely. In the measurement of endosteal radius, no statistically significant differences were detected.

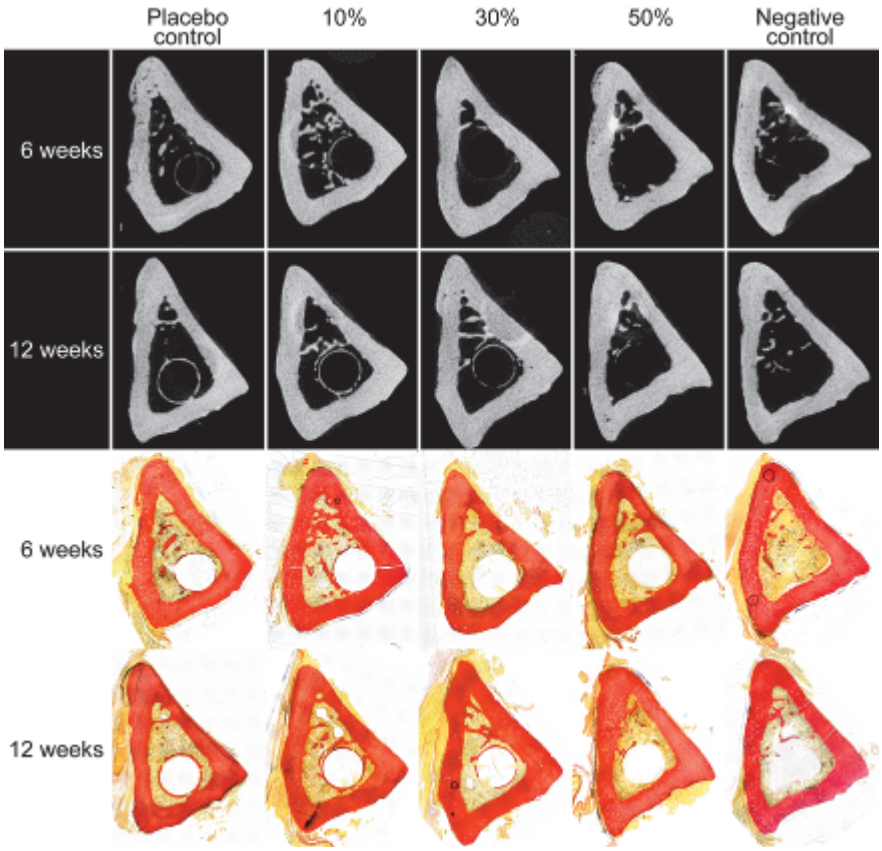

Figure 18. Cross-sectional µCT images and histological sections (van Gieson stain) of bone samples. (Adapted from Study V).

The results of histomorphometrical analysis of the whole medullary cavity are shown in Figure 19B. In 12 weeks time point, statistically significant differences in the area of newly formed bone were detected between group 10% and negative control. Spearman correlation analysis failed to show association between the amount of newly formed bone and the dose of ORM-11984. The area of newly formed bone was also evaluated in a peri-implant ring of 50 µm (Figure 20). In placebo control group and group 10%, numerous sites of direct contact between the implant and the newly formed bone were observed: there were no signs of connective tissue interlayer. In contrast, for implants in group 30% and group 50%, fibrous tissue was prevalent type of interfacial reaction at 6 weeks time point. At 12 weeks time point, peri-implant bone has formed in all groups. Statistically significant differences between the experimental groups were detected in both time points. Moreover, Spearman rank-order correlation analysis showed a negative correlation between the area of newly formed bone and the dose of SARM compound with r_s= -0.734 in 6 weeks time point and r_s= -0.930 in 12 weeks time point. BIC measurements were consistent with the measurements of the amount of newly formed in the peri-implant ring of 50 µm

(Figure 21). In 6 weeks time point, BIC in group 30% and group 50% was close to zero. In contrast, the mean value of BIC in placebo control group was around 40%. There were statistically significant differences between the groups. In 12 weeks time point, the amount of BIC has increased in group 30%. Consequently, group 10% was significantly different only from group 50% and group 30% became significantly different from group 50%. Spearman rank-order correlation analysis showed a negative correlation between BIC and dose of ORM-11984 with r_S= -0.704 in 6 weeks time point and r_S= -0.751 in 12 weeks time point.

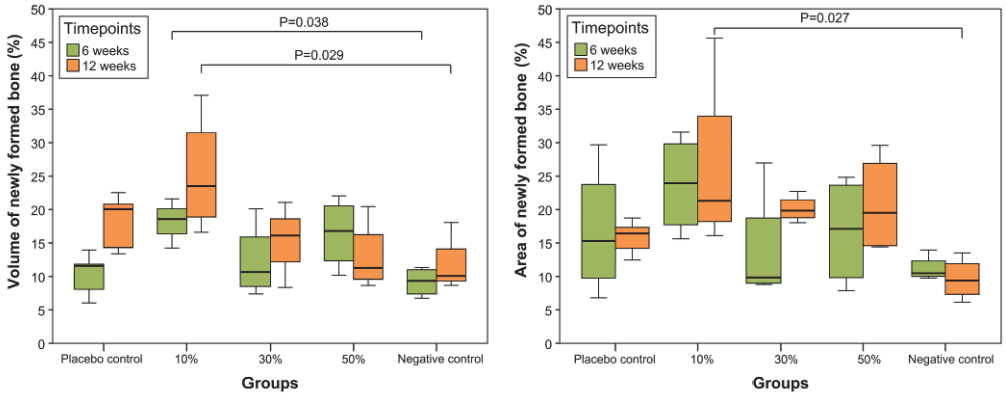

A B

Figure 19. Results of µCT analysis in 6 and 12 weeks time-points: bone formation in medullary cavity with implant volume deducted (A). Results of histomorphometrical analysis in 6 and 12 weeks time-points: bone formation in medullary cavity with implant volume deducted (B). Level of statistical significance P ≤ 0.05. (Adapted from Study V).

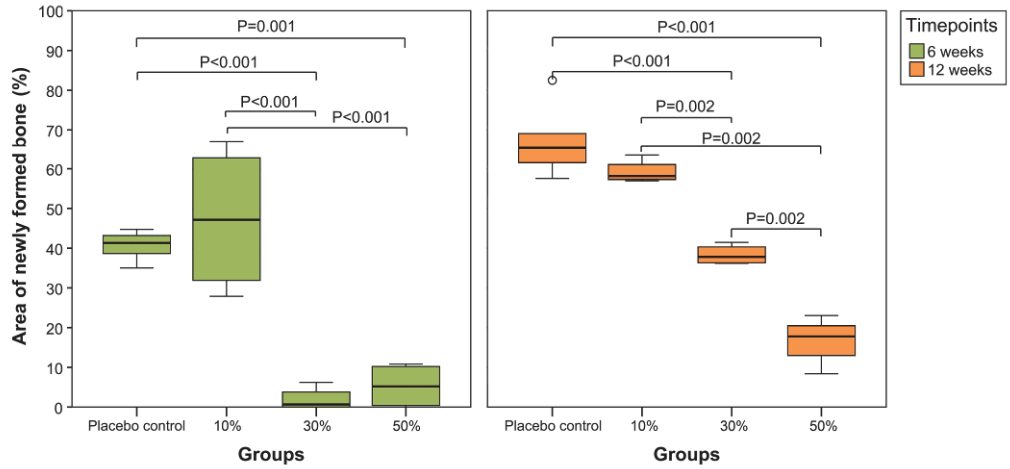

Figure 20. Results of histomorphometrical analysis in a peri-implant ring of 50 µm in 6 and 12 weeks time-points. Level of statistical significance P ≤ 0.05. (Adapted from Study V).

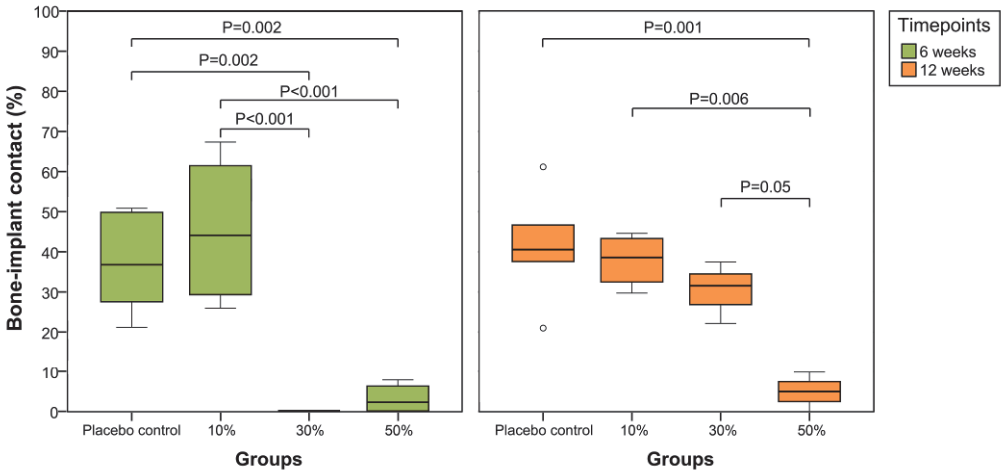

Figure 21. Results of BIC measurements. Level of statistical significance $P \leq 0.05$. (Adapted from Study V).

6 DISCUSSION

This thesis was focused on the research and development of a multifunctional implant model with enhanced osteoconductivity and low susceptibility to infection. In addition, the experimental models for assessment, diagnostics and prophylaxis of biomaterial-related infections were established.

Bioresorbable implants are used for short-term clinical applications to eliminate the need for the surgical removal of the implant [Middleton and Tipton 2000]. The rationale for the use of bioresorbable implants in orthopaedic surgery is based on the limitations associated with the metallic implants *e.g.* plate or screw migration, artifacts with diagnostic patient imaging (*e.g.* magnetic resonance imaging and computed tomography) and high rate of hardware-associated infections. Nevertheless, the clinical trials have shown that currently available bioresorbable implants have lower osteoconductivity compared with metallic implants, greater risk of breakage on insertion and slower healing of surgical access [Bergsma et al. 1995, Böstman and Pihlajamäki 2000, Andersson et al. 2009, Nho et al. 2009, Bourke et al. 2013]. These complications generate the need for further improvement of bioresorbable implant materials.

The most commonly used bioresorbable implant materials of the first generation are PGA, PLA and their copolymers [Athanasiou et al. 1998, Middleton and Tipton 2000]. However, fast degradation of these bioresorbable polymers resulting in increased local acidity, may compromise the osteogenic replacement [Barber and Dockery 2006, Meyer et al. 2012] and carry a risk of adverse tissue reactions [Böstman and Pihlajamäki 2000]. In addition, the mechanical properties and osteoconductivity of these pure polymers are low. The addition of ceramic particles e.g. β-TCP is supposed to overcome these limitations [Barber et al. 2011]. It was suggested that the weight fraction of β-TCP filler below 20% is an optimal balance between the strength and stiffness of PLGA/β-TCP composites [Damadzadeh et al. 2010]. The weight of β-TCP particulate content in **Study II** was based on this knowledge. However, our results have demonstrated that the addition of the ceramic particulate does not improve the mechanical properties, which is corroborated with previous reports [Kikuchi et al. 1997, Kunze et al. 2003, Damadzadeh et al. 2010]. On the contrary, the mechanical properties of the composites tend to decrease as a function of the particulate filler content [Verheyen et al. 1992, Kikuchi et al. 1997, Ignatius et al. 2001, Damadzadeh et al. 2010, Rakovsky et al. 2013]. In push-out testing, micro-CT analysis and histological examination, there were no significant differences in the biological response between the two PLGA/β-TCP composites. It has been shown previously in a rabbit model that in the long-term β-TCP composite showed better osteogenic properties than pure polymer [Daculsi et al. 2011]. These observations are in line with the clinical data [Barber et al. 2011]. In addition, the biological response to PLA/β-TCP composites was affected in a β-TCP content-dependent manner [Aunoble et al. 2006]. Consequently, the osteogenic response in **Study II** might have been challenged by suboptimal dose of β-TCP filler in the composites (16 wt-%).

At present, composites of bioresorbable polymers with bioactive additives such as HA or TCP, are prepared mainly by melt-compounding methods [Daculsi et al.

2011]. The size of the additive particles is often relatively high, < 50 μm [Verheyen et al. 1993, Daculsi et al. 2011]. Decreasing the size of these particles to sub-micron/nano scale would allow the manufacture of implants with superior properties. For example, improved mechanical properties would allow decreasing the size of the implant, while enhanced bioactivity would shorten the time needed for bone healing. However, melt-mixing of bioresorbable polymers with nano-sized bioceramic additives often results in two-phase composite which are immiscible, either due to the interfacial incompatibility of the components or due to lack of molecular adhesion between them [Kunze et al. 2003]. These problems can be avoided by application of novel manufacturing methods such as mechanical alloying. This new solid state mixing technology allows producing molecular level nanocomposites by compounding of immiscible components. The advantages of nano-structures have been extensively speculated in the literature [Tran and Webster 2009, Yang et al. 2011]. Some of these benefits were confirmed in *in vitro* studies [Zhou et al. 2012, Webster et al. 2000, Liu et al. 2008, Cui et al. 2009, Jayabalan et al. 2010, Kim et al. 2011]. In *in vivo* studies, various implant morphologies of experimental nano-structured composites have been compared with each other and with pure bioresorbable polymer matrix [Cui et al. 2009, Jayabalan et al. 2010, Kim et al. 2007, Zhang et al. 2009, Schneider et al. 2011]. Experimental micro-structured and nano-structured composites have also been compared *in vivo* [Chung et al. 2011]. While some advantages of nano-structures have been demonstrated, the question still remains, whether there is a clinically-relevant benefit of nano-structured composite implants. As an example, a literature-based comparison of the osseointegration of nano-structured electro-spun composite scaffolds with the clinically used materials did not reveal significant benefits of the nano-structured materials [Schneider et al. 2011]. In fact, to our knowledge, there is a lack of systematic *in vivo* studies designed to compare micro-sized and nano-structured composite implants. Contrary to our expectations, results of the characterization indicated that the high-energy ball milling route chosen **in Study II** to prepare nano-composite caused aggregation of the nano-sized particles and consequently the formation of nano-structured agglomerates. The agglomeration of the nano-sized β-TCP particles may be the primary reason to the lack of the expected enhancement of osseointegration. This issue highlights the importance of thorough characterization of nano-structured biomaterials and raises the bar for the evidence level for properties related to claimed nano-structures.

Regardless of the osteogenic properties of the implant materials, infection remains a substantial clinical issue. Orthopedic implant infections are frequently caused by coagulase-positive or-negative species, belonging to the *Staphylococcus* genus [Tsukayama et al. 2003, Montenaro et al. 2011]. Due to robust attachment to the implant surfaces, these infections are highly challenging for diagnostics by routine microbiologic techniques. Therefore, there is a strong clinical need for the development of new approaches for diagnosis of infection. An orthopaedic implant infection model is used to study bacterial behavior on biomaterial surface and is based on foreign body infection model [An and Friedman 1998]. Rat model is especially versatile [An et al. 2006]. In **Study III**, a well-known tibial animal model of chronic human post-traumatic osteomyelitis was adjusted for this study. This model

was based on rat tibial osteomyelitis model reported by Scheman and colleagues [Scheman et al. 1941] and later refined for rats by Zak [Zak et al. 1982]. Briefly, in comparison with the model previously reported by our group [Lankinen P et al. 2008], the cortical bone drilling was excluded; therefore, the surgical procedure was less invasive and less predisposed for further complications. In addition, medical catheter, which is one of the most common clinical reasons for hospital infections [Dohnt K et al. 2011, Shanks RM et al. 2006], was used for implantation. The surface of the catheter serves as a favorable substratum for bacterial colonization and subsequent biofilm formation.

In *S. aureus* group, 10^4 CFU inoculum was used in our previous rabbit study without the foreign body [Lankinen et al. 2012]. This bacterial dose is above the minimum level of 10^3 CFU reported to be sufficient for creation of implant-related infections [An and Friedman 1998]. However, the infection was detected only in 60% - 70% of the animals. Therefore, it might be assumed that the number of bacteria was insufficient to produce osteomyelitis in all experimental animals.

In *S. epidermidis* group, an inoculum of 10^7 CFU was used in this study. In experimental tibial animal models of osteomyelitis with *S epidermidis,* the bacterial dose was reported in range of $10^4 – 10^8$ CFU in rabbit [Lambe et al. 1989, Del Pozo et al. 2009, Lankinen et al. 2012, Sakaeda 1988, Croisier-Bertin et al. 2013]. Rat experimental tibial animal models of osteomyelitis with *S. epidermidis* are less common. However, Sakaeda reported that 10^5 CFU inoculum of *S epidermidis* was sufficient to produce implant-related osteomyelitis [Sakaeda 1988]. In this study, a 10^7 CFU inoculum was selected as an average value reported for the rabbit and rat models. Apparently, the optimal bacterial dose was not established in this study and the pilot study is missing. This may explain the unexpectedly severe osteomyelitis observed in the histological analysis. The rat model clearly needs refinement in the future studies.

Appropriate identification and localization of infectious/inflammatory foci are critical for adequate treatment of patients. Since the introduction in early 1960s, PET imaging evolved into an important clinical instrument. PET imaging of leukocyte trafficking using VAP-1 as a target molecule is a novel approach. VAP-1 is an inflammation inducible, endothelial sialoglycoprotein mediating interaction between leukocyte and endothelium [Salmi et al. 1992, Jaakkola et al. 2000]. VAP-1 is stored in intracellular granules within endothelial cells. However, upon inflammation it is rapidly translocated to the endothelial cell surface. Besides being an adhesion molecule, VAP-1 is also a semicarbazide-sensitive amine oxidase enzyme, which catalyzes oxidative deamination of primary amines resulting aldehyde formation and releasing of hydrogen peroxide [Salmi and Jalkanen 2001]. The end products are highly potent inflammatory mediators. Therefore, VAP-1 revealed as an optimal candidate for anti-inflammatory therapy and a target for imaging of inflammation. Previously, we have reported the feasibility of the VAP-1-targeting peptides for PET imaging of inflammation in different animal models [Lankinen et al. 2008, Ujula et al. 2009, Autio et al. 2010, Autio et al. 2011]. Initially, the most promising VAP-1-selective peptide was DOTA-conjugated, 68Ga-labeled and named as 68Ga-DOTAVAP-

P1 [Lankinen et al. 2008, Ujula et al. 2009, Autio et al. 2010]. The essential preclinical tests used to clarify its *in vivo* stability, tissue distribution and biokinetics revealed promising properties for an imaging agent. The ability to image inflammation was shown in rats with experimental bone inflammation caused by bacterial infection. These results represent a proof-of-concept that infection-induced VAP-1 can be targeted by ^{68}Ga-peptide. Thereafter, the applicability of ^{68}Ga-DOTAVAP-P1 for the assessment of uncomplicated bone healing and infection was studied in standardized animal models [Lankinen et al. 2008]. Siglec-9 is a leukocyte ligand of VAP-1 and a 68Ga-labeled Siglec-9 motif peptide can be used for PET imaging of inflammation and cancer [Aalto et al. 2011]. Siglecs are usually involved during inflammatory and immune responses [Crocker et al. 2012]. **Study III** was delineating the efficacy of ^{68}Ga-DOTA-Siglec-9 PET imaging in the diagnosis of *S. epidermidis* foreign-body infections. The comparison was made with foreign-body infection caused by *S. aureus*. Leukocyte migration is important step in several types of acute and chronic inflammation as well as autoimmune diseases. The results of this study have shown that ^{68}Ga-DOTASiglec-9 PET-CT is capable of detection *S. epidermidis* foreign-body bone infection, although the implantation of the foreign-body as such causes the significant uptake of the tracer. During the interpretation of the results of **Study III**, certain limitations became clear. Usually, the clinical infection caused by *S. epidermidis* is moderate. However, in this study the rate of infection caused by *S. epidermidis* in conjunction with aqueous sodium morrhuate was high suggesting the presence of severe acute bone infection. Therefore, the obtained data could not be directly extrapolated to a typical clinical situation. Hence, the applicability of PET-CT imaging using ^{68}Ga-DOTA-Siglec-9 tracer for the detection of low-grade *S. epidermidis* infection needs further investigation. In addition, *S. aureus*, which served as a positive control, induced infection only in 70% of the animals. This issue disturbed the statistical analysis of the data. Current experimental set-up included only one time point, two weeks. However, unspecific uptake of the tracer was detected which is difficult to relate to the inflammatory response or bone healing process. Despite these limitations, 68Ga-DOTA-Siglec-9 PET/CT seems to be a promising technique for imaging of the biomaterial-related infections. Future prospective includes the optimization of the current animal model.

The history of biomaterials can be traced to Incas of Peru, which used silver and gold to repair trephination defects over 3000 B.C. The last 300 years were denoted by the sporadic application of implant materials and infection was a common complication [Breibart and Ablaza 1997]. Systematic biomaterials research started in 1940s, when contemporary clinically used materials were introduced [Breibart and Ablaza 1997]. Today, the biomaterial field is focused on research and development of multifunctional implant. These smart devices are biologically active; do not provoke inflammatory reaction and bacterial colonization. In this thesis, **Study I**, **Study IV** and **Study V** were focused on improvement of antibacterial and osteoconductive properties of bioresorbable implant materials.

Biomaterials with enhanced antibacterial properties have evolved as potentially effective for the prevention of bacterial colonization and biofilm formation [Ho et al. 2004]. However, there are several drawbacks concerning the methodology for the *in*

vitro assessment of simultaneous surface reactions of the bioactive materials and biofilm formation and growth. **Study I** was designed to address this issue and represents a promising technique. Antibacterial properties of BAG are attributed to the local increase in pH level which is raised above the level tolerated by bacteria [Hu et al. 2009, Prabhakar and Kumar 2010]. However, when CaP has formed, the ions are no longer leaching into the surrounding solution; this averts the rise in pH [Stoor et al. 1996]. In addition, a rough surface of the CaP may in fact promote bacterial attachment [Stoor et al. 1996]. This implies that apatite-forming materials may not be suitable for some implant applications. Thus, biofilm formation on apatite-forming surfaces needs systematic investigation.

Silver is one of the most common antibacterial agents, which could be potentially used in coatings for bone implants [Darouiche 1999, Chen et al. 2006, Odekerken et al. 2013]. The antibacterial effect of silver ions is accomplished by disruption of various enzymatic activities of prokaryotes [Rai et al. 2001, Morones et al. 2005]. However, it should be noted that adverse effects of silver ions on eukaryotes are also well documented [Um et al. 1996, Zamzami et al. 1995, Lin and Beal 2006, Ott et al. 2007]. Therefore, further investigations are needed in order to develop a silver-based coating for implantable medical devices with diminished cytotoxicity.

Chitosan is widely described bioresorbable polymer of natural origin, which was approved by Food and Drug Administration as a food supplement and a wound dressing material [Illum 1998, Wedmore et al. 2006, Kean and Thanou 2010]. The broad range of *in vivo* studies has been performed in order to estimate the possible toxicity of chitosan. Subsequently, only negligible toxic effects were noted [Illum 1998, Kean and Thanou 2010]. However, it should be taken into consideration that modifications made to chitosan might increase the toxicity rate [Kean and Thanou 2010]. Chitosan has been extensively studied as a controlled release drug delivery system [Illum 1998]. The particular increased interest to certain applications is based on the unique chemical flexibility of this material [Illum 1998].

Chitlac is a modified polymer which is chemically composed of a chitosan bulk with lactitol moieties inserted via a reductive N-alkylation reaction with lactose. A range of toxicity tests performed on Chitlac revealed high biocompatibility of this material [D'Amelio et al. 2013]. Thus, Chitlac seems to be an attractive polymer which could be applied as an implant coating and serve as a controlled release drug delivery system. **Study IV** was performed to assess the efficacy and durability of antibacterial properties of Chitlac-nAg coating system *in vitro* conditions, which simulate the initial phase of implantation. In addition, the effect of Chitlac-nAg coating system on mesenchymal stem cells was investigated. Moreover, a minipig model was used to investigate the biological response to the Chitlac-nAg coated material.

The initial phase of implantation is characterized by rapid coating of foreign body, such as implant, with plasma proteins. This process gives microorganisms a privilege with regards to attachment and biofilm formation [Bos et al. 1999]. In addition, these plasma proteins may arrange in a stable protein-metal ion complexes, which are shielding the biological identity of the particulates and altering there *in vivo*

activity [Cedervall et al. 2007, Naveenraj et al. 2010, Li 2011]. Particularly, serum albumin, which is a key soluble protein in plasma with concentration range from 3.5% to 5%, is able to bind the metal ions and form stable metal ions-bovine serum albumin (BSA) complexes [Duff et al. 2009, Durgadas et al. 2011, Deng et al. 2010]. Moreover, recently it has been shown, that BSA is forming a stable complex with Ag^{+} [Zhao et al. 2011]. However, there is a lack of available data concerning the effect of plasma proteins on silver in the form of nanoparticles. With this respect, one of the primary goals of **Study IV** was to investigate the potential influence of serum proteins on antibacterial properties of silver nanoparticles. The results of this experiment clearly indicated that the antibacterial properties of silver nanoparticles were significantly challenged with the addition of serum proteins. Likewise, the overall antibacterial properties of Chitlac-nAg coating system were compromised by a protein conditioning film on the surface of the thermoset and inactivation of silver nanoparticles. Presumably, it could be speculated that protein conditioned film may affect the antibacterial properties of Chitlac-nAg coating system by changing the physical-chemical characteristics of the surface, and therefore the non-specific bacterial adhesion mechanisms [Bos et al. 1999, Lorite et al. 2011]. The release of silver content, and therefore duration of antibacterial properties of Chitlac-nAg coating system was investigated. The results obtained in this experiment were in-line with those described in the literature [Malcher et al. 2008, Babapour et al. 2011, Sileika et al. 2011]. The substantial metal release was observed during the first 7 days of the experiment and accounted for 90% of total silver content. The dissolution of the silver content is strongly dependent on the certain environmental factors *e.g.* pH and temperature of the aqueous solution, in addition to electrolyte type and concentration [Li et al. 2010, Stebounova et al. 2011, Yang et al. 2007, Zhang et al 2011]. In addition, the initial concentration and diffusion rate of the silver particulate on the surface is a crucial factor in a release rate [Kumar et al. 2005]. Unsurprisingly, the rapid reduction of the silver content was associated with a loss of antibacterial properties. In general, Chitlac-nAg coating system with high initial silver content can be considered as valuable, as it is able to address the need for rapid antibacterial effect and, therefore, predict the development of resistant bacterial strains [Bumgardner et al. 2011].

The effect of Chitlac-nAg coating system on mesenchymal stem cells was investigated in **Study IV**. The results revealed no cytotoxic effect on particular cell lineage. The precise explanation of cytotoxicity mechanism of silver nanoparticles remains unclear. However, there is evidence that the substantial uptake of silver nanoparticles by eukaryotes and subsequent cells lysis are associated with the lack of physiological barriers [Geiser et al. 2005]. Chitlac-nAg coating system induces the antibacterial effect by direct contact of silver nanoparticles with the thiol groups of bacterial membrane proteins [Clement and Jarrett 1994, Feng et al. 2000, Elechiguerra et al. 2005, Morones et al. 2005, Nel 2005]. While eukaryotes thiol group allocated inside the eukaryotic cells; thus, the possibility of strait silver nanoparticles-cell interaction is excluded [Kone et al. 1988, Oberdörster et al. 2002, Donaldson and Tran 2002, Donaldson et al. 2004, Braydich-Stolle et al. 2005. Hussain et al. 2005,

Hussain et al. 2006]. In addition, the silver nanoparticles are efficiently immobilized within the polysaccharide matrix. Hence, Chitlac-nAg coating system serves as a barrier system with the strong antibacterial properties.

The results of *in vivo* experiment in **Study IV** demonstrated no adverse bone tissue reaction. Moreover, the histomorphometrical and histological analysis revealed that Chitlac–nAg-coated material was interfaced with newly formed bone indicating good biocompatibility of this material. These results could be explained by previous observations presenting the evidence that Chitlac stimulates the aggregation of osteoblast-like MG63 cells [Travan et al. 2012]. The identification of exact mechanism of interaction between osteoblasts and Chitlac is still under investigation. However, one can speculate that this specific interaction occurs between the receptor for galactose on the side groups of the polymer and osteoblasts [Travan et al. 2012, Marcon et al. 2005].

Biomaterials used as drug delivery systems for *in situ* bone tissue regeneration are designed to release controlled rates of active compounds *e.g.* growth factors and drugs, which are able to activate cells [Hench et al. 2004]. SARMs are among novel treatment modalities with high tissue selectivity and partial agonist activity which allows overcoming the undesirable effects caused by steroidal androgens [Dalton et al. 1998, Negro-Vilar 1999, Yin et al. 2003]. **Study V** was focused on the evaluation of the local effect of ORM-11984 - PLCL drug delivery system in a rat bone healing model. The results of the *in vitro* experiment indicated the difference in release rate of ORM-11984 in three experimental groups; expectedly, the release rate of ORM-11984 from a single implant was higher in group 50% than in groups 30% and 10%. However, when the amount of ORM-11984 is kept constant, six implants in group 10%, two implants in group 30% and one implant in group 50%, the release of ORM-11984 from six implants in group 10% was higher than that from one implant in group 50%. These findings could be explained by poor dissolvability of the ORM-11984. When the content of ORM-11984 in the drug delivery system is high, e.g. 50%, it may re-crystallize within the chains of the polymer during the fabrication. Hence, the degradation of the polymer matrix could be faster than the dissolvability of the crystallized compound. In addition, the release rate might be influenced by the total surface area of the implants. The surface area of six implants in group 10% is larger compared with one implant in group 50%.

The *in vivo* experiment in **Study V** was designed to assess the effect of a novel ORM-11984 on intramedullary osteogenesis in a rat bone marrow ablation model. A rodent model for evaluation of androgenic and anabolic activity of SARM suggested by Hershberger is accomplished by castration of male rats. Consequently, changes in androgen-dependent tissues are validated [Hershberger et al. 1953, Mohler et al. 2012, Zhang et al. 2013]. This assay provides the knowledge about an osteoanabolic activity of the novel compound [Hanada et al. 2003, Gao et al. 2005, Kearbey et al. 2007, Kearbey et al. 2009]; however, there is a lack of enhanced understanding of bone response to local SARM administration. We have previously used bone marrow ablation models to study the osteogenic response to a variety of bioactive implant materials [Itälä et al. 2003]. In this study, we hypothesized that the ORM-11984 - PLCL

drug delivery system would promote enhanced new bone formation in the medullary cavity. We expected that the osteogenic response would be dependent on the dose of ORM-11984. The bone marrow ablation model in a conjunction with anabolic agents was suggested as a technique of choice for the investigation of site-directed bone growth in regions of high bone loss [Zhang et al. 2010]. After the bone marrow ablation, the initial blood clot is replaced by newly formed trabecular bone. In turn, within 2 weeks the resoption of the trabecular bone is complete by restoration of the bone marrow [Suva et al. 1993]. However, if the foreign body is inserted into the intramedullary cavity, the chemical composition and physical properties of the foregn body may influence this process and the half-life of the newly formed bone [Schwartz et al. 2008, Zhang et al. 2010]. Hence, the newly formed bone was quantitated after 6 weeks follow up, when the bone marrow is expected to be restored. The long-term effect of ORM-11984 was evaluated after 12 weeks follow up time.

The main outcome of the *in vivo* experiment was that the optimal dose of ORM-11984 was not established. However, multiparametric analysis of the micro-CT and histilogical data suggests that group 10% stands out from other groups. Enhanced bone formation was only associated with group 10%. Delayed bone formation in the medullary cavity was observed in group 30% and group 50% at 12 weeks time-point. Therefore, we believe that higher doses of of ORM-11984 had inhibitory effect on bone and were supra-physiological.

The main limitation of this screening study was the low number of experimental animals. Power analysis performed in retrospective indicated the need for ten experimental animals in each group to demonstrate statistical significances in the measured differences. To verify this suggestion, a statistical simulation was performed based on the data obtained in the measurements. For each group, the mean and standard deviation values were used to generate ten new data points. In the analysis of these data, the difference between placebo control and group 10% was significant.

In this study, the endosteal radius, periosteal radius, and the cortical thickness were measured. It has been shown previously, that the bone marrow ablation may lead to increase in thickness of cortical bone due to endosteal bone formation [Schwartz et al. 2008]. In the analysis of the data, no statistically significant differences in the endosteal radius measurements were obtained. Therefore, the endosteal bone formation did not occur. The cortical thickness has decreased in group 10%, followed by an increase in periosteal radius, although this difference narrowly failed ($P = 0.068$) the selected level of statistical significance due to the low number of animals. However, if the original data are compared using one-way ANOVA with Dunnett post-hoc test, i.e. comparing all groups with placebo control, a statistically significant difference with group 10% is observed ($P = 0.035$).

The increase in periosteal radius may be explained by the action of ORM-11984 and be considered from a physiological standpoint. SARMs form a complex with ARs, which are abundantly expressed in bone cells [Abu et al. 1997, Pederson et al. 1999]. AR signaling is a vital direct mediator of skeletal development and homeostasis [Wiren et al. 2002, Wiren 2005]. The enhanced androgen signaling in bone was

mimicked in two transgenic male mice lineages with overexpression of ARs [Wiren et al. 2004, Wiren et al. 2012]. In both models, the inhibition of bone formation at the endocortical envelope and reduced bone quality was observed. Furthermore, in one of the transgenic mice models there was an increased periosteal bone formation [Wiren et al. 2004, Wiren et al. 2012]. It was proposed as a physiological adaptive function in males associated with the maintenance of the total spatial amount of cortical bone [Wiren et al. 2012]. Hence, the trends for changes in cortical thickness and periosteal radius observed in this study may be related to this adaptation mechanism.

The delayed bone formation observed in group 30% and 50% could be explained by the results of the *in vitro* dissolution test. According to the *in vitro* release rate, after two weeks of dissolution, 25% of ORM-11984 was released from the polymer. The release was almost linear. Therefore, one could speculate that *in vivo* ORM-11984 may have been already excreted in 12 weeks.

There is a lack of information concerning the effect of supra-physiological doses of androgens on bone [Clarke and Khosla 2009]. Vanderschueren and colleagues recognized that there was no benefit in administration of supraphysiological doses of testosterone; however, there was a notable increase in endosteal perimeter [Vanderschueren et al. 2000], although, this was not confirmed by our results. This study was conducted from clinical point of view and therefore, we assume that the parallels with other treatment modalities are appropriate. For instance, it has been shown that the administration of suboptimal doses of rhBMP-2 is associated with prominent risk of post-operative ostelysis in transforaminal lumbar interbody fusion [Knox et al. 2011]. The direct comparison between rhBMP-2 and SARM cannot be drawn due to the difference in mechanisms of action; however, we expect that similar dose response could be observed in the case of SARM. Overall, the local administration of ORM-11984 did not result in enhanced osteogenesis in the ablated intramedullary cavity. Furthermore, an optimal concentration of ORM-11984 was not established in this study. The mechanism of the biological response to local administration of ORM-11984 remains unclear.

7 CONCLUSIONS

Study I

A new method for simultaneous evaluation of CaP and biofilm formation on bioactive surfaces was established.

Study II

The biological response of bone tissue to two PLA-PGA/β-tricalcium phosphate composites measured by the push-out test was similar. Contrary the Ti6Al4V was superior to two PLA-PGA/β-tricalcium phosphate composites, which in turn showed a better incorporation than pure PLGA implants.

Study III

Siglec-9 (VAP-1 ligand) tracer was feasible in the detection of inflammatory response due to S. epidermidis implant-related bone infections. Future prospective includes the modification of the current animal model to achieve a low-grade S. epidermidis infection and to compare the uptake of Siglec-9 (VAP-1 ligand) tracer in a model simulating aseptic loosening of joint prostheses.

Study IV

The antibacterial properties of the Chitlac-nAg coated material demonstrated in vitro antibacterial activity and cell biocompatibility. In addition, the Chitlac-nAg coated implants showed good biocompatibility in vivo in a minipig model.

Study V

The local administration of ORM-11984 did not show an expected positive dose-dependent osteogenic response. Implants with 10% ORM-11984 showed only a trend for a mild positive effect on local osteogenesis. Moreover, higher doses even inhibited new bone formation of peri-implant zone.

8 ACKNOWLEDGEMENTS

This study was started at the Institute of Dentistry and completed at the Department of Orthopaedic Surgery and Traumatology, University of Turku during the years of 2011-2015.

I wish to express my deepest gratitude to my supervisor, Professor Hannu Aro, who accepted me to be a part of his research group and has been utmost patient during all these years. In addition, I would like to thank Professor Hannu Aro for his skillful vision of scientific writing. The times were countless, when a question was replied with an answer, or with even a better question challenging me to think about the answer myself.

I would like to thank Professor Minna Kellomäki and Professor Juha Tuukkanen for acting as the official pre-examiners. Your constructive criticism and sharp-sighted comments were invaluable.

I am grateful to Professor Heimo Ylänen for accepting the invitation to be my dissertation opponent.

I would like to express my warmest gratitude to Professor Eija Könönen, Professor Timo Närhi and Associate Professor Ulvi Gürsoy who were my first teachers and encouraged me to start doing independent scientific work. I am truly grateful to Associate Professor Ulvi Gürsoy for teaching me the basics of scientific thinking and sharing with me his expertise in microbiology.

I am sincerely thankful to Professor Emeritus Allan Aho for his support. I admire his vast knowledge and encouraging attitude.

The endless support given to me and my family by Associate Professor Niko Moritz and Associate Professor Mervi Puska cannot be exaggerated. To be honest, I can never repay the guidance and support given to me by these people during my PhD. In fact, describing the enormous effort by Mervi and Niko under the modesty of title ‘acknowledgements’, is more of an offense than a justification. The achievements expressed in this thesis under my name would not have the status they now have, thanks to you both. I am indebted for the rest of my days for your understanding and time. You are my true friends in need and happiness.

I would like to acknowledge Professor Pekka Vallittu, the head of the TCBC and Dr. Lippo Lassila, the manager of the TCBC laboratory for providing the possibility to use the facilities and a convenient working place.

I am indebted to the group of prestigious scientists from University of Trieste for their collaboration in these studies. In particular, I am deeply grateful to my co-authors Professor Sergio Paoletti, Eleonora Marsich, Andrea Travan, Ivan Donati, Gianluca Turco, Matteo Crosera.

My sincere thanks go to my co-workers from PET center, Professor Anne Roivainen and Helena Ahtinen, for their help in imaging the pets. In addition, Professor Anne Roivainen, the member of my steering board, is especially acknowledged for her continuous enthusiasm and help in pushing the progress of this work. Your support and confidence were so important for me.

I owe special thanks to my co-authors from the Department of Medical Microbiology and Immunology, University of Turku and the National Institute for

Health and Welfare: Laura Lindholm, Erkki Eerola, Antti Hakanen. In addition, Minna Lamppu is acknowledged for performing the highly accurate microbiological analyses and for creating the friendly atmosphere around.

In addition, I want to thank all my co-authors, whom I never had a pleasure of meeting in person.

My special thanks go to all my colleagues at Orthopaedic Research Unit and TCBC. Satu Timlin is specially acknowledged for helping me to break through in many ways during my troubled PhD times. Petteri Lankinen is acknowledged for shearing the experience and mature knowledge of being a PhD student. Sara Nganga, Leila Perea Mosquera, Jasmina Bijelic, Jingwei He, Kohji Nagata, Onur Oral, Masahiko Kobayashi are acknowledged for their endless support and positive energy. I wish to owe exceptional appreciation to a very special friend of mine, Aous Abdulmajeed, for making atmosphere in TCBC palatable, fun and relaxing. Dear Aous, thanks you for your hilarious humor and optimism.

Eva Ahlfors, my friend, it has been privileged in my life to meet you and to have your brilliant company.

I am truly grateful to Timothy Wilson for correcting my English. Your comments and encouraging attitude were truly valuable.

I thank all the visiting researchers who have spent some time in TCBC scientific team.

I would like to thank the involved personnel of Institute of Dentistry and TCBC, namely Associate Professor Eva Söderling, Oona Hällfors, Katja Sampalahti, Hanna Mark, Minttu Vigren and Genevieve Alfont for their help with all sorts of matters.

Finally, I take this opportunity to express my special gratitude to my husband Ignat and daughter Nevelina who have always supported me. Without your understanding and unlimited belief in my success, this thesis would never have been completed.

This study was financially supported by Center for International Mobility (CIMO), Turun Yliopistosäätiö (Allan Aho rahasto), National Doctoral Programme of Musculoskeletal Disorders and Biomaterials (TBDP), University of Turku Joint Research Fund, Doctoral Programme of Clinical Investigation, Valtion tutkimusrahoitus (EVO), Finnish Cultural Foundation. Their support is gratefully acknowledged.

Turku, December 2014

Julia Kulkova

9 REFERENCES

Aalto K, Autio A, Kiss EA, Elima K, Nymalm Y, Veres TZ, Marttila-Ichihara F, Elovaara H, Saanijoki T, Crocker PR, Maksimow M, Bligt E, Salminen TA, Salmi M, Roivainen A Jalkanen S. Siglec-9 is a novel leukocyte ligand for vascular adhesion protein-1 and can be used in PET imaging of inflammation and cancer. Blood. 2011;118(13):3725-3733.

Abu EO, Horner A, Kusec V, Triffitt JT, Compston JE. The localization of androgen receptors in human bone. J Clin Endocrinol Metab. 1997; 82(10):3493-3497.

Ahmed S, Meghji S, Williams RJ, Henderson B, Brock JH, Nair SP. Staphylococcus aureus fibronectin binding proteins are essential for internalization by osteoblasts but do not account for differences in intracellular levels of bacteria. Infect Immun. 2001;69(5):2872-2877.

Akao M, Aoki H, Kato K. Mechanical properties of sintered hydroxyapatite for prosthetic applications. J Mater Sci Mater Med. 1981;16(3):809-812.

Al Laham N, Rohde H, Sander G, Fischer A, Hussain M, Heilmann C, Mack D, Proctor R, Peters G, Becker K, von Eiff C. Staphylococcus epidermidis mutant with the small-colony-variant phenotype. J Bacteriol. 2007;189(12): 4494-4501.

Albrektsson T, Johansson C. Osteoinduction, osteoconduction and osseointegration. Eur Spine J. 2001;10 Suppl 2:S96-101.

An YH, Stuart GW, McDowell SJ, McDaniel SE, Kang Q, Friedman RJ. Prevention of bacterial adherence to implant surfaces with a crosslinked albumin coating in vitro. J Orthop Res. 1996;14(5):846-849.

An YH, Friedman RJ. Animal models of orthopedic implant infection. J Invest Surg. 1998;11(2): 139-146.

An YH and Friedman RJ. Animal selections in orthopaedic research. In: An YH, Friedman RJ, editors. Animal Models in Orthopaedic Research: CRC Press LLC; 1999. pp 39-57.

An YH, Barfield WB and Draughn RA. Basic concepts of mechanical property measurement and bone biomechanics. In: An YH and Draughn RA, editors. Mechanical testing of bone and the bone-implant interface: CRC Press LLC; 2000. p. 23-40.

An YH. Mechanical properties of bone. In: An YH and Draughn RA, editors. Mechanical testing of bone and the bone-implant interface: CRC Press LLC; 2000. p. 41-64.

An YH, Kang QK, Arciola CR. Animal models of osteomyelitis. Int J Artif Organs. 2006;29(4): 407-420.

Andersson D, Samuelsson K, Karlsson J. Treatment of anterior cruciate ligament injuries with special reference to surgical technique and rehabilitation: an assessment of randomized controlled trials. Arthroscopy. 2009;25(6):653-685.

Angle SR, Sena K, Sumner DR, Virkus WW, Virdi AS. Healing of rat femoral segmental defect with bone morphogenetic protein-2: a dose response study. J Musculoskelet Neuronal Interact. 2012;12(1):28-37.

Arciola CR, Campoccia D, Speziale P, Montanaro L, Costerton JW. Biofilm formation in Staphylococcus implant infections. A review of molecular mechanisms and implications for biofilm-resistant materials. Biomaterials. 2012;33(26):5967-5982.

Arens S, Schlegel U, Printzen G, Ziegler WJ, Perren SM, Hansis M. Influence of materials for fixation implants on local infection. An experimental study of steel versus titanium DCP in rabbits. J Bone Joint Surg Br. 1996;78(4):647-651.

Arora S, Jain J, Rajwade JM, Paknikar KM. Cellular responses induced by silver nanoparticles: In vitro studies. Toxicol Lett. 2008;179(2):93-100.

AshaRani PV, Low Kah Mun G, Hande MP, Valiyaveettil S. Cytotoxicity and genotoxicity of silver nanoparticles in human cells. ACS Nano. 2009;3(2):279-290.

Athanasiou KA, Agrawal CM, Barber FA, Burkhart SS.Orthopaedic applications for PLA-PGA biodegradable polymers. Arthroscopy. 1998; 14(7):726-737.

Aunoble S, Clément D, Frayssinet P, Harmand MF, Le Huec JC. Biological performance of a new

beta-TCP/L PLA composite material for applications in spine surgery: in vitro and in vivo studies. J Biomed Mater Res A. 2006;78(2):416-422.

Autio A, Ujula T, Luoto P, Salomäki S, Jalkanen S, Roivainen A. PET imaging of inflammation and adenocarcinoma xenografts using vascular adhesion protein 1 targeting peptide 68Ga-DOTAVAP-P1: comparison with 18F-FDG. Eur J Nucl Med Mol Imaging. 2010;37(10):1918-1925.

Autio A, Henttinen T, Sipilä HJ, Jalkanen S, Roivainen A. Mini-PEG spacering of VAP-1-targeting 68Ga-DOTAVAP-P1 peptide improves PET imaging of inflammation. EJNMMI Res. 2011;1(1):10.

Babapour A, Yang B, Bahang S, Cao W. Low-temperature sol–gel-derived nanosilver-embedded silane coating as biofilm inhibitor. Nanotechnology. 2011;22(15):155602.

Baddour LM, Barker LP, Christensen GD, Parisi JT, Simpson WA. Phenotypic variation of Staphylococcus epidermidis in infection of transvenous endocardial pacemaker electrodes. J Clin Microbiol. 1990;28(4):676-679.

Baldassarri L, Bertuccini L, Ammendolia MG, Arciola CR, Montanaro L. Effect of iron limitation on slime production by Staphylococcus aureus. Eur J Clin Microbiol Infect Dis. 2001;20(5):343-345.

Barber FA, Dockery WD. Long-term absorption of poly-L-lactic Acid interference screws. Arthroscopy. 2006;22(8):820-826.

Barber FA, Dockery WD, Hrnack SA. Long-term degradation of a poly-lactide co-glycolide/β-tricalcium phosphate biocomposite interference screw. Arthroscopy. 2011;27(5): 637-643.

Barnes GL, Kostenuik PJ, Gerstenfeld LC, Einhorn TA. Growth factor regulation of fracture repair. J Bone Miner Res. 1999;14(11):1805-1815.

Beenken KE, Dunman PM, McAleese F, Macapagal D, Murphy E, Projan SJ, Blevins JS, Smeltzer MS. Global gene expression in Staphylococcus aureus biofilms. J Bacteriol. 2004;186(14):4665-4684.

Begun J, Gaiani JM, Rohde H, Mack D, Calderwood SB, Ausubel FM, Sifri CD. Staphylococcal biofilm exopolysaccharide protects against Caenorhabditis elegans immune defenses. PLoS Pathog. 2007;3(4):e57.

Bergsma JE, de Bruijn WC, Rozema FR, Bos RR, Boering G. Late degradation tissue response to poly(L-lactide] bone plates and screws. Biomaterials. 1995;16(1):25-31.

Bhasin S, Calof OM, Storer TW, Lee ML, Mazer NA, Jasuja R, Montori VM, Gao W, Dalton JT. Drug insight: Testosterone and selective androgen receptor modulators as anabolic therapies for chronic illness and aging. Nat Clin Pract Endocrinol Metab. 2006;2(3):146-159.

Blair JM, Zhou H, Seibel MJ, Dunstan CR. Mechanisms of disease: roles of OPG, RANKL and RANK in the pathophysiology of skeletal metastasis. Nat Clin Pract Oncol. 2006;3(1):41-49.

Blomgren G, Lundquist H, Nord CE, Lindgren U. Late anaerobic haematogenous infection of experimental total joint replacement. A study in the rabbit using Propionibacterium acnes. J Bone Joint Surg Br. 1981;63B(4):614-618.

Boles BR, Horswill AR. Staphylococcal biofilm disassembly. Trends Microbiol. 2011;19(9):449-455.

Bos R, Van der Mei HC, Busscher HJ. Physico-chemistry of initial microbial adhesive interactions--its mechanisms and methods for study. FEMS Microbiol Rev. 1999;23(2):179-230.

Bourke HE, Salmon LJ, Waller A, Winalski CS, Williams HA, Linklater JM, Vasanji A, Roe JP, Pinczewski LA. Randomized controlled trial of osteoconductive fixation screws for anterior cruciate ligament reconstruction: a comparison of the Calaxo and Milagro screws. Arthroscopy. 2013;29(1):74-82.

Bouxsein ML, Boyd SK, Christiansen BA, Guldberg RE, Jepsen KJ, Müller R. Guidelines for assessment of bone microstructure in rodents using micro-computed tomography. J Bone Miner Res. 2010;25(7):1468-1486.

Brandi ML, Cianferotti L, D'Asta F. A review on strontium ranelate long-term antifracture efficacy in the treatment of postmenopausal

osteoporosis. Ther Adv Musculoskel Dis. 2013;5(3):127-139.

Braydich-Stolle L, Hussain S, Schlager JJ, Hofmann MC. In vitro cytotoxicity of nanoparticles in mammalian germline stem cells. Toxicol Sci. 2005;88(2):412-419.

Breibart AS, Ablaza VJ. Implant materials. In: Aston SJ, Beasley RW, Thorne CHM, editors. Grabb and Smith's Plastic Surgery, 5th Ed: Lippincott-Raven; 1997. p. 58-65.

Buckwalter JA, Glimcher MJ, Cooper RR, Recker R. Bone biology. I: Structure, blood supply, cells, matrix, and mineralization. Instr Course Lect. 1996;45:371-386.

Buckwalter JA, Glimcher MJ, Cooper RR, Recker R.Bone biology. II: Formation, form, modeling, remodeling, and regulation of cell function. Instr Course Lect. 1996;45:387-399.

Bumgardner JD, Adatrow P, Haggard WO, Norowski PA. Emerging antibacterial biomaterial strategies for the prevention of peri-implant inflammatory diseases. Int J Oral Maxillofac Implant 2011;26(3):553-560.

Buret A, Ward KH, Olson ME, Costerton JW. An in vivo model to study the pathobiology of infectious biofilms on biomaterial surfaces. J Biomed Mater Res. 1991;25(7):865-874.

Busscher HJ, van der Mei HC, Subbiahdoss G, Jutte PC, van den Dungen JJ, Zaat SA, Schultz MJ, Grainger DW. Biomaterial-associated infection: locating the finish line in the race for the surface. Sci Transl Med. 2012;4(153): 153rv10.

Böstman O, Pihlajamäki H. Adverse tissue reactions to bioabsorbable fixation devices. Clin Orthop Relat Res. 2000;(371):216-227.

Cao W, Hench LL Bioactive materials, Ceram Intl. 1996;22:493-507.

Cedervall T, Lynch I, Lindman S, Berggard T, Thulin E, Nilsson H, et al. Understanding the nanoparticle–protein corona using methods to quantify exchange rates and affinities of proteins for nanoparticles. Proc Natl Acad Sci USA. 2007;104(7):2050-2055.

Chang CC, Merritt K. Infection at the site of implanted materials with and without preadhered bacteria. J Orthop Res. 1994; 12(4):526-531.

Chen J, Kim J, Dalton JT. Discovery and therapeutic promise of selective androgen receptor modulators. Mol Interv. 2005;5(3):173-188.

Chen W, Liu Y, Courtney HS, Bettenga M, Agrawal CM, Bumgardner JD, Ong JL. *In vitro* anti-bacterial and biological properties of magnetron co-sputtered silver-containing hydroxyapatite coating. Biomaterials. 2006; 27(32):5512-5517.

Choi K, Goldstein SA. A comparison of the fatigue behavior of human trabecular and cortical bone tissue. J Biomech. 1992;25(12):1371-1381.

Choi O, Deng KK, Kim NJ, Ross L Jr, Surampalli RY, Hu Z. The inhibitory effects of silver nanoparticles, silver ions, and silver chloride colloids on microbial growth. Water Res. 2008;42(12):3066-3074.

Christensen GD, Simpson WA, Younger JJ, Baddour LM, Barrett FF, Melton DM, Beachey EH. Adherence of coagulase-negative staphylococci to plastic tissue culture plates: a quantitative model for the adherence of staphylococci to medical devices. J Clin Microbiol. 1985;22(6):996-1006.

Christoffersen J, Christoffersen MR, Kjaergaard N. The kinetics of dissolution of calcium hydroxyapatite in water at constant pH. J. Crystal Growth. 1978;43(4):501-511.

Chung EJ, Kodali P, Laskin W, Koh JL, Ameer GA. Long-term in vivo response to citric acid-based nanocomposites for orthopaedic tissue engineering. J Mater Sci Mater Med. 2011;22(9):2131-2138.

Clarke B. Normal bone anatomy and physiology. Clin J Am Soc Nephrol. 2008;3 Suppl 3:S131-139.

Clarke BL, Khosla S. Androgens and bone. Steroids. 2009;74(3):296-305.

Clement JL, Jarrett PS. Antibacterial silver. Met Based Drugs. 1994;1(5-6):467-482.

Cook G, Costerton JW, Darouiche RO. Direct confocal microscopy studies of the bacterial colonization in vitro of a silver-coated heart

valve sewing cuff. Int J Antimicrob Agents. 2000;13(3):169-173.

Cosman F, Lindsay R. Selective estrogen receptor modulators: clinical spectrum. Endocr Rev. 1999;20(3):418-434.

Costerton JW, Cheng KJ, Geesey GG, Ladd TI, Nickel JC, Dasgupta M, Marrie TJ. Bacterial biofilms in nature and disease. Annu Rev Microbiol. 1987;41:435-464.

Cramton SE, Gerke C, Schnell NF, Nichols WW, Götz F. The intercellular adhesion (ica] locus is present in Staphylococcus aureus and is required for biofilm formation. Infect Immun. 1999;67(10):5427-5433.

Crocker PR, McMillan SJ, Richards HE. CD33-related siglecs as potential modulators of inflammatory responses. Ann N Y Acad Sci. 2012;1253:102-111.

Cue D, Lei MG, Lee CY. Genetic regulation of the intercellular adhesion locus in staphylococci. Front Cell Infect Microbiol. 2012;2:38.

Cui Y, Liu Y, Cui Y, Jing X, Zhang P, Chen X. The nanocomposite scaffold of poly(lactide-co-glycolide] and hydroxyapatite surface-grafted with L-lactic acid oligomer for bone repair. Acta Biomater. 2009;5(7):2680-2692.

Daculsi G, Goyenvalle E, Cognet R, Aguado E, Suokas EO. Osteoconductive properties of poly(96L/4D-lactide]/beta-tricalcium phosphate in long term animal model. Biomaterials 2011;32(12):3166-3177.

Dai KR, Xu XL, Tang TT, Zhu ZA, Yu CF, Lou JR, Zhang XL.Repairing of goat tibial bone defects with BMP-2 gene-modified tissue-engineered bone. Calcif Tissue Int. 2005;77(1):55-61.

Dalton JT, Mukherjee A, Zhu Z, Kirkovsky L, Miller DD. Discovery of nonsteroidal androgens. Biochem Biophys Res Commun. 1998 Mar 6;244(1):1-4.

Damadzadeh B, Jabari H, Skrifvars M, Airola K, Moritz N, Vallittu PK. Effect of ceramic filler content on the mechanical and thermal behaviour of poly-L-lactic acid and poly-L-lactic-co-glycolic acid composites for medical applications. J Mater Sci Mater Med. 2010;21:2523-2531.

D'Amelio N, Esteban C, Coslovi A, Feruglio L, Uggeri F, Villegas M, Benegas J, Paoletti S, Donati I. Insight into the molecular properties of Chitlac, a chitosan derivative for tissue engineering. J Phys Chem B. 2013;117(43): 13578-13587.

Damm C, Münstedt H. Kinetic aspects of the silver ion release from antimicrobial polyamide/silver nanocomposites. Appl Phys. 2008;A91;479-486.

Darouiche RO. Anti-infective efficacy of silver-coated medical prostheses. Clin Infect Dis. 1999;29(6):1371-1377.

De Smet E, Jaecques SV, Wevers M, Jansen JA, Jacobs R, Sloten JV, Naert IE. Effect of controlled early implant loading on bone healing and bone mass in guinea pigs, as assessed by micro-CT and histology. Eur J Oral Sci. 2006;114(3):232-242.

Deckers MM, van Bezooijen RL, van der Horst G, Hoogendam J, van Der Bent C, Papapoulos SE, Löwik CW. Bone morphogenetic proteins stimulate angiogenesis through osteoblast-derived vascular endothelial growth factor A. Endocrinology. 2002;143(4):1545-1553.

DeGrado TR, Turkington TG, Williams JJ, Stearns CW, Hoffman JM, Coleman RE. Performance characteristics of a whole-body PET scanner. J Nucl Med. 1994;35(8):1398-1406.

Del Pozo JL, Rouse MS, Euba G, Kang CI, Mandrekar JN, Steckelberg JM, Patel R. The electricidal effect is active in an experimental model of Staphylococcus epidermidis chronic foreign body osteomyelitis. Antimicrob Agents Chemother. 2009;53(10):4064-4068.

Den Boer FC, Patka P, Bakker FC, Wippermann BW, van Lingen A, Vink GQ, Boshuizen K, Haarman HJ. New segmental long bone defect model in sheep: quantitative analysis of healing with dual energy x-ray absorptiometry. J Orthop Res. 1999;17(5):654-660.

Deng B, Wang Y, Zhu P, Xu X, Ning X. Study of the binding equilibrium between zn(II) and HSA by capillary electrophoresis-inductively coupled plasma optical emission spectrometry. Anal Chim Acta. 2010;683(1):58-62.

De Winter F, Gemmel F, Van De Wiele C, Poffijn B, Uyttendaele D, Dierckx R. 18-Fluorine fluorodeoxyglucose positron emission

tomography for the diagnosis of infection in the postoperative spine. *Spine*. 2003;28(12): 1314–1319.

Dhawan A, Ghodadra N, Karas V, Salata MJ, Cole BJ. Complications of bioabsorbable suture anchors in the shoulder. Am J Sports Med. 2012;40(6):1424-1430.

Di Martino A, Sittinger M, Risbud V. Chitosan: a versible biopolymer for orthopaedic tissue-engineering. Biomaterials. 2005;26(30):5983-5990.

Dohnt K, Sauer M, Müller M, Atallah K, Weidemann M, Gronemeyer P, Rasch D, Tielen P, Krull R. An in vitro urinary tract catheter system to investigate biofilm development in catheter-associated urinary tract infections. J Microbiol Methods. 2011;87(3):302-308.

Donaldson K, Tran CL. Inflammation caused by particles and fibers. Inhal Toxicol. 2002;14(1):5-27.

Donaldson K, Stone V, Tran CL, Kreyling W, Borm PJ. Nanotoxicology. Occup Environ Med. 2004;61(9):727-728.

Donath K. Preparation of histologic sections by the cutting-grinding technique for hard tissue and other material not suitable to be sectioned by routine methods. EXaht-Kultzer-Oublication, Norderstedt 1995.

Donati I, Stredanska S, Silvestrini G, Vetere A, Marcon P, Marsich E, Mozetic P, Gamini A, Paoletti S, Vittur F. The aggregation of pig articular chondrocyte and synthesis of extracellular matrix by a lactose-modified chitosan. Biomaterials. 2005;26(9):987-998.

Dora C, Altwegg M, Gerber C, Böttger EC, Zbinden R. Evaluation of conventional microbiological procedures and molecular genetic techniques for diagnosis of infections in patients with implanted orthopedic devices. J Clin Microbiol. 2008;46(2):824-825.

Downey PA, Siegel MI. Bone biology and the clinical implications for osteoporosis. Phys Ther. 2006;86(1):77-91.

Ducheyne P, Qiu Q. Bioactive ceramics: the effect of surface reactivity on bone formation and bone cell function. Biomaterials. 1999;20(23-24):2287-2303.

Duff Jr MR, Kumar CV. The metallomics approach: use of Fe(II) and Cu(II) footprinting to examine metal binding sites on serum albumins. Metallomics. 2009;1(6):518-523.

Durgadas CV, Sharma CP, Sreenivasan K. Fluorescent gold clusters as nanosensors for copper ions in live cells. Analyst. 2011;136(5):933-940.

Edwards CJ, Williams E. The role of interleukin-6 in rheumatoid arthritis-associated osteoporosis. Osteoporos Int. 2010;21(8):1287-1293.

Ehrenfried LM, Patel MH, Cameron RE. The effect of tri-calcium phosphate (TCP] addition on the degradation of polylactide-co-glycolide (PLGA]. J Mater Sci Mater Med. 2008;19(1):459-466.

Elechiguerra JL, Burt JL, Morones JR, Camacho-Bragado A, Gao X, Lara HH, Yacaman MJ. Interaction of silver nanoparticles with HIV-1. J Nanobiotechnology. 2005;3(1):6.

Fan X, Biskobing DM, Fan D, Hofstetter W, Rubin J. Macrophage colony stimulating factor down-regulates MCSF-receptor expression and entry of progenitors into the osteoclast lineage. J Bone Miner Res. 1997;12(9):1387-1395.

Feldkamp LA, Goldstein SA, Parfitt AM, Jesion G, Kleerekoper M. The direct examination of three-dimensional bone architecture in vitro by computed tomography. J Bone Miner Res. 1989;4(1):3-11.

Feng QL, Wu J, Chen GQ, Cui FZ, Kim TN, Kim JO. A mechanistic study of the antibacterial effect of silver ions on Escherichia coli and Staphylococcus aureus. J Biomed Mater Res. 2000;52(4):662-668.

Fey PD and Olson ME. Current concepts in biofilm formation of Staphylococcus epidermidis Future Microbiol. 2010;5(6):917-933.

Fratzl P, Weinkamer R. Nature's hierarchical materials. Prog Mater Sci. 2007;52(8):1263–1334.

Fuchs S, Pane-Farre J, Kohler C, Hecker M, Engelmann S. Anaerobic gene expression in Staphylococcus aureus. J Bacteriol. 2007; 189(11):4275-4289.

Ganeshnarayan K, Shah SM, Libera MR, Santostefano A, Kaplan JB. Poly-N-acetylglucosamine matrix polysaccharide

impedes fluid convection and transport of the cationic surfactant cetylpyridinium chloride through bacterial biofilms. Appl Environ Microbiol. 2009;75:1308-1314.

Gao W, Reiser PJ, Coss CC, Phelps MA, Kearbey JD, Miller DD, Dalton JT. Selective androgen receptor modulator treatment improves muscle strength and body composition and prevents bone loss in orchidectomized rats. Endocrinology. 2005;146(11):4887-4897.

Gao W, Wu Z, Bohl CE, Yang J, Miller DD, Dalton JT. Characterization of the in vitro metabolism of selective androgen receptor modulator using human, rat, and dog liver enzyme preparations. Drug Metab Dispos. 2006;34(2):243-253.

Gao W, Dalton JT. Expanding the therapeutic use of androgens via selective androgen receptor modulators (SARMs). Drug Discov Today. 2007;12(5-6):241-248.

Geiser M, Rothen-Rutishauser B, Kapp N, Schürch S, Kreyling W, Schulz H, Semmler M, Im Hof V, Heyder J, Gehr P. Ultrafine particles cross cellular membranes by nonphagocytic mechanisms in lungs and in cultured cells. Environ Health Perspect. 2005;113(11):1555-1560.

Gerber T, Holzhüter G, Götz W, Bienengräber V, Henkel K-O, Rumpel E. Nanostructuring of biomaterials – A pathway to bone grafting substitute. Eur J Trauma. 2006;32(2):132-140.

Gerke C, Kraft A, Süssmuth R, Schweitzer O, Götz F. Characterization of the N-acetylglucosaminyltransferase activity involved in the biosynthesis of the Staphylococcus epidermidis polysaccharide intercellular adhesin. J Biol Chem. 1998;273(29):18586-18593.

Gerstenfeld LC, Cullinane DM, Barnes GL, Graves DT, Einhorn TA. Fracture healing as a post-natal developmental process: molecular, spatial, and temporal aspects of its regulation. J Cell Biochem. 2003;88(5):873-884.

Gitai Z. New fluorescence microscopy methods for microbiology: sharper, faster, and quantitative. Curr Opin Microbiol. 2009;12(3): 341-346.

Gratz S, Dörner J, Fischer U, Behr TM, Béhé M, Altenvoerde G, Meller J, Grabbe E, Becker W. 18F-FDG hybrid PET in patients with suspected spondylitis. *Eur J Nucl Med*. 2002;29(4):516–524.

Gristina AG, Costerton JW. Bacterial adherence to biomaterials and tissue. The significance of its role in clinical sepsis. J Bone Joint Surg Am. 1985;67(2):264-273.

Gristina AG. Biomaterial-centered infection: microbial adhesion versus tissue integration. Science. 1987;237(4822):1588-1595.

Hallab ND, Jacobs JJ, Katz JL. Orthopaedic Applications in B.D. Rutner et al, Editors; Biomaterials science:ab introduction to materials in medicine, Elsivier Academic Press 2004, pp 527-556.

Hanada K, Furuya K, Yamamoto N, Nejishima H, Ichikawa K, Nakamura T, Miyakawa M, Amano S, Sumita Y, Oguro N. Bone anabolic effects of S-40503, a novel nonsteroidal selective androgen receptor modulator (SARM), in rat models of osteoporosis. Biol Pharm Bull. 2003;26(11):1563-1569.

Hasegawa S, Ishii S, Tamura J, Furukawa T, Neo M, Matsusue Y, Shikinami Y, Okuno M, Nakamura T. A 5-7 year in vivo study of high-strength hydroxyapatite/poly(L-lactide] composite rods for the internal fixation of bone fractures. Biomaterials. 2006;27(8):1327-1332.

Hauck CR, Ohlsen K. Sticky connections: extracellular matrix protein recognition and integrin-mediated cellular invasion by Staphylococcus aureus. Curr Opin Microbiol. 2006;9(1):5-11.

Heilmann C, Schweitzer O, Gerke C, Vanittanakom N, Mack D, Götz F. Molecular basis of intercellular adhesion in the biofilm-forming Staphylococcus epidermidis. Mol Microbiol. 1996;20(5):1083-1091.

Heilmann C, Hussain M, Peters G, Götz F. Evidence for autolysin-mediated primary attachment of Staphylococcus epidermidis to a polystyrene surface. Mol Microbiol. 1997;24(5):1013-1024.

Heinlein CA, Chang C. The roles of androgen receptors and androgen-binding proteins in nongenomic androgen actions. Mol Endocrinol. 2002;16(10):2181-2187.

Hench LL, Splinter RJ, Allen WC, Greenlee TK. Bonding mechanisms at the interface of

ceramic prosthetic materials. J Biomed Mater Res Symposium. 1971;2:117-141.

Hench and Wilson . Introduction. In: Hench LL, Wilson J, editors. An introduction to bioceramics: World Scientific Publishing Co. Pte. Ltd.; 1993. p. 4.

Hench LL, Xynos ID, Polak JM. Bioactive glasses for in situ tissue regeneration. J Biomater Sci Polym Ed. 2004;15(4):543-562.

Hershberger LG, Shipley EG, Meyer RK. Myotrophic activity of 19-nortestosterone and other steroids determined by modified levator ani muscle method. Proc Soc Exp Biol Med. 1953;83(1):175-180.

Hickok NJ, Shapiro IM. Immobilized antibiotics to prevent orthopaedic implant infections. Adv Drug Deliv Rev. 2012;64(12):1165-1176.

Hlidek P, Biederman H, Choukourov A, Slavinska D. Behavior of polymeric matrices containing silver inclusions, 1 – review of adsorption and oxidation of hydrocarbons on silver surfaces/interfaces as witnessed by FT-IR spectroscopy. Plasma Processes Polym. 2008;5(9):807-824.

Ho CH, Tobis J, Sprich C, Thomann R, Tiller JC. Nanoseparated polymeric network with multiple antimicrobial properties. Adv Mater. 2004;16(12):957-961.

Horn J, Schlegel U, Krettek C, Ito K. Infection resistance of unreamed solid, hollow slotted and cannulated intramedullary nails: an in-vivo experimental comparison. J Orthop Res. 2005;23(4):810-815.

Hounsfield GN. Computerized transverse axial scanning (tomography): Part I. Description of system. Br J Radiol. 1973;46(552):1016-1022.

Hu S, Chang J, Liu M, Ning C. Study on antibacterial effect of 45S5 Bioglass. J Mater Sci Mater Med. 2009;20(1):281-286.

Huber DM, Bendixen AC, Pathrose P, Srivastava S, Dienger KM, Shevde NK, Pike JW. Androgens suppress osteoclast formation induced by RANKL and macrophage-colony stimulating factor. Endocrinology. 2001;142(9):3800-3808.

Hudson MC, Ramp WK, Nicholson NC, Williams AS, Nousiainen MT. Internalization of Staphylococcus aureus by cultured osteoblasts. Microb Pathog. 1995;19(6):409-419.

Huffer WE, Benedict JJ, Turner AS, Briest A, Rettenmaier R, Springer M, Walboomers XF. Repair of sheep long bone cortical defects filled with COLLOSS, COLLOSS E, OSSAPLAST, and fresh iliac crest autograft. J Biomed Mater Res B Appl Biomater. 2007;82(2):460-470.

Hussain SM, Hess KL, Gearhart JM, Geiss KT, Schlager JJ. In vitro toxicity of nanoparticles in BRL 3A rat liver cells. Toxicol In Vitro. 2005;19(7):975-983.

Hussain SM, Javorina AK, Schrand AM, Duhart HM, Ali SF, Schlager JJ. The interaction of manganese nanoparticles with PC-12 cells induces dopamine depletion. Toxicol Sci. 2006;92(2):456-463.

Huttunen M, Törmälä P, Godinho P, Kellomäki M. Fiber-reinforced bioactive and bioabsorbable hybrid composites. Biomed Mater. 2008;3(3): 034106.

Ignatius AA, Claes LE. In vitro biocompatibility of bioresorbable polymers: poly(L, DL-lactide] and poly(L-lactide-co-glycolide]. Biomaterials. 1996;17(8):831-839.

Ignatius AA, Augat P, Claes LE. Degradation behavior of composite pins made of tricalcium phosphate and poly(L,DL-lactide]. J Biomater Sci Polym Ed. 2001;12(2):185-194.

Illum L. Chitosan and its use as a pharmaceutical excipient. Pharm Res. 1998;15(9):1326-1331.

Itälä A, Välimäki VV, Kiviranta R, Ylänen HO, Hupa M, Vuorio E, Aro HT. Molecular biologic comparison of new bone formation and resorption on microrough and smooth bioactive glass microspheres. J Biomed Mater Res B Appl Biomater. 2003;65(1):163-170.

Itälä A, Koort J, Ylänen HO, Hupa M, Aro HT. Biologic significance of surface microroughing in bone incorporation of porous bioactive glass implants. J Biomed Mater Res A. 2003;67(2):496-503.

Jaakkola K, Nikula T, Holopainen R, Vähäsilta T, Matikainen MT, Laukkanen ML, Huupponen R, Halkola L, Nieminen L, Hiltunen J, Parviainen S, Clark MR, Knuuti J, Savunen T, Kääpä P, Voipio-Pulkki LM, Jalkanen S. In vivo detection of vascular adhesion protein-1 in experimental

inflammation. Am J Pathol. 2000;157(2):463-471.

Jansen JA, Dhert WJ, van der Waerden JP, von Recum AF. Semi-quantitative and qualitative histologic analysis method for the evaluation of implant biocompatibility. J Invest Surg. 1994;7(2):123-134.

Jayabalan M, Shalumon KT, Mitha MK, Ganesan K, Epple M. Effect of hydroxyapatite on the biodegradation and biomechanical stability of polyester nanocomposites for orthopaedic applications. Acta Biomater. 2010;6(3):763-775.

Jensen J. Biosynthesis of hematin compounds in a hemin requiring strain of Micrococcus pyogenes var. aureus. I. The significance of coenzyme A for the terminal synthesis of catalase. J Bacteriol. 1957;73(3):324-333.

Jiranek WA, Hanssen AD, Greenwald AS. Antibiotic-loaded bone cement for infection prophylaxis in total joint replacement. J Bone Joint Surg Am. 2006;88(11):2487-2500.

Jódar-Gimeno E. Full length parathyroid hormone (1-84) in the treatment of osteoporosis in postmenopausal women. Clin Interv Aging. 2007;2(1):163-174.

Johnson KD, August A, Sciadini MF, Smith C. Evaluation of ground cortical autograft as a bone graft material in a new canine bilateral segmental long bone defect model. J Orthop Trauma. 1996;10(1):28-36.

Jones JR, Atwood RC, Poologasundarampillai G, Yue S, Lee PD. Quantifying the 3D macrostructure of tissue scaffolds. J Mater Sci: Mater Med 2009;2:463-471.

Jones JR. Review of bioactive glass: From Hench to hybrids. Acta Biomater. 2013;9(1):4457-4486.

Jung W, Koo H, Kim K, Shin S, Kim S, Park Y. Antibacterial activity and mechanism of action of the silver ion *in Staphylococcus aureus* and *Escherichia coli*. Appl. Environ. Microbiol. 2008;74(7):2171-2178.

Kalfas IH. Principles of bone healing. Neurosurg Focus. 2001;10(4):E1.

Kaneko H, Arakawa T, Mano H, Kaneda T, Ogasawara A, Nakagawa M, Toyama Y, Yabe Y, Kumegawa M, Hakeda Y. Direct stimulation of osteoclastic bone resorption by bone morphogenetic protein (BMP]-2 and expression of BMP receptors in mature osteoclasts. Bone. 2000;27(4):479-486.

Kaur G, Pandey OP, Singh K, Homa D, Scott B, Pickrell G. 2014. A review of bioactive glasses: Their structure, properties, fabrication, and apatite formation. J Biomed Mater Res Part A. 2014:102A(1):254-274.

Kearbey JD, Gao W, Narayanan R, Fisher SJ, Wu D, Miller DD, Dalton JT. Selective Androgen Receptor Modulator (SARM) treatment prevents bone loss and reduces body fat in ovariectomized rats. Pharm Res. 2007; 24(2):328-335.

Kearbey JD, Gao W, Fisher SJ, Wu D, Miller DD, Dalton JT. Effects of selective androgen receptor modulator (SARM) treatment in osteopenic female rats. Pharm Res. 2009;26(11):2471-2477.

Keaveny TM, Morgan EF, Niebur GL, Yeh OC. Biomechanics of trabecular bone. Annu Rev Biomed Eng. 2001;3:307-333.

Kennel KA, Drake MT. Adverse effects of bisphosphonates: implications for osteoporosis management. Mayo Clin Proc. 2009;84(7):632-637.

Keränen P, Itälä A, Koort J, Kohonen I, Dalstra M, Kommonen B, Aro HT. Bioactive glass granules as extender of autogenous bone grafting in cementless intercalary implant of the canine femur. Scand J Surg. 2007;96(3):243-251.

Kikuchi M, Suetsugu Y, Tanaka J, Akao M. Preparation and mechanical properties of calcium phosphate/copoly-L-lactide composites. J Mater Sci Mater Med. 1997;8(6):361-364.

Kim K, Dean D, Lu A, Mikos AG, Fisher JP. Early osteogenic signal expression of rat bone marrow stromal cells is influenced by both hydroxyapatite nanoparticle content and initial cell seeding density in biodegradable nanocomposite scaffolds. Acta Biomater 2011;7(3):1249-1264.

Kim SS, Ahn KM, Park MS, Lee JH, Choi CY, Kim BS. A poly(lactide-co-glycolide)/hydroxyapatite composite scaffold with enhanced

osteoconductivity. J Biomed Mater Res A 2007;80:206-215.

Knobloch JK, Bartscht K, Sabottke A, Rohde H, Feucht HH, Mack D. Biofilm formation by Staphylococcus epidermidis depends on functional RsbU, an activator of the sigB operon: differential activation mechanisms due to ethanol and salt stress. J Bacteriol. 2001;183(8):2624-2633.

Knox JB, Dai JM 3rd, Orchowski J. Osteolysis in transforaminal lumbar interbody fusion with bone morphogenetic protein-2. Spine (Phila Pa 1976). 2011;36(8):672-676.

Kobayashi N, Fraser TG, Bauer TW, Joyce MJ, Hall GS, Tuohy MJ, Procop GW. The use of real-time polymerase chain reaction for rapid diagnosis of skeletal tuberculosis. Arch Pathol Lab Med. 2006;130(7):1053-1056.

Kohler C, von Eiff C, Liebeke M, McNamara PJ, Lalk M, Proctor RA, Hecker M, Engelmann S. A defect in menadione biosynthesis induces global changes in gene expression in Staphylococcus aureus. J Bacteriol. 2008; 190(19):6351-6364.

Kokubo T, Kushitani H, Sakka S, Kitsugi T, Yamamuro T. Solutions able to reproduce in vivo surface-structure changes in bioactive glass-ceramic A-W3. J Biomed Mater Res. 1990;24(6):721-731.

Kone BC, Kaleta M, Gullans SR. Silver ion (Ag+)-induced increases in cell membrane K+ and Na+ permeability in the renal proximal tubule: reversal by thiol reagents. J Membr Biol. 1988;102(1):11-19.

Kragstrup J, Richards A, Fejerskov O. Effects of fluoride on cortical bone remodeling in the growing domestic pig. Bone. 1989;10(6):421-424.

Kumar R, Howdle S, Munstedt H. Polyamide/silver antimicrobials: effect of filler types on the silver ion release. J Biomed Mater Res B Appl Biomater 2005;75(2):311-319.

Kumar R, Munstedt H. Silver ion release from antimicrobial polyamide/silver composites. Biomaterials 2005;26(14):2081-2088.

Kunze C, Freier T, Helwig E, Sandner B, Reif D, Wutzler A, Radusch HJ. Surface modification of tricalcium phosphate for improvement of the interfacial compatibility with biodegradable polymers. Biomaterials. 2003;24(6):967-974.

Kurtz SM, Devine JN. PEEK biomaterials in trauma, orthopedic, and spinal implants. Biomaterials. 2007;28(32):4845-4869.

Kälicke T, Schmitz A, Risse JH, Arens S, Keller E, Hansis M, Schmitt O, Biersack HJ, Grünwald F. Fluorine-18 fluorodeoxyglucose positron emission tomography in infectious bone diseases: Results of histologically confirmed cases. Eur J Nucl Med Mol Imaging. 2000;27(5):524–528.

Lambe DW Jr, Ferguson KP, Mayberry-Carson KJ, Tober-Meyer B, Costerton JW. Foreign-body-associated experimental osteomyelitis induced with Bacteroides fragilis and Staphylococcus epidermidis in rabbits. Clin Orthop Relat Res. 1991;(266):285-294.

Lamerigts NM, Buma P, Huiskes R, Schreurs W, Gardeniers J, Slooff TJ. Incorporation of morsellized bone graft under controlled loading conditions. A new animal model in the goat. Biomaterials. 2000;21(7):741-747.

Lankinen P, Mäkinen TJ, Pöyhönen TA, Virsu P, Salomäki S, Hakanen AJ, Jalkanen S, Aro HT, Roivainen A. (68)Ga-DOTAVAP-P1 PET imaging capable of demonstrating the phase of inflammation in healing bones and the progress of infection in osteomyelitic bones. Eur J Nucl Med Mol Imaging. 2008;35(2):352-364.

Lankinen P, Lehtimäki K, Hakanen AJ, Roivainen A, Aro HT. A comparative ^{18}F-FDG PET/CT imaging of experimental Staphylococcus aureus osteomyelitis and Staphylococcus epidermidis foreign-body-associated infection in the rabbit tibia. EJNMMI Res. 2012;2(1):41.

Lee SK, Lorenzo J. Cytokines regulating osteoclast formation and function. Curr Opin Rheumatol. 2006;18(4):411-418.

LeGeros RZ. Biodegradation and bioresorption of calcium phosphate ceramics. Clin Mater. 1993;14(1):65-88.

LeGeros RZ, Lin S, Rohanizadeh R, Mijares D, LeGeros JP. Biphasic calcium phosphate bioceramics: preparation, properties and applications. J Mater Sci Mater Med. 2003;14(3):201-209.

Lemos JA, Abranches J, Koo H, Marquis RE, Burne RA. Protocols to study the physiology of oral biofilms. Methods Mol Biol. 2010;666:87-102.

Leong KW, Langer R. Polymeric controlled drug delivery. Adv Drug Deliv Rev. 1987;1: 199-233.

Leppäranta O, Vaahtio M, Peltola T, Zhang D, Hupa L, Hupa M, Ylänen H, Salonen JI, Viljanen MK, Eerola E. Antibacterial effect of bioactive glasses on clinically important anaerobic bacteria in vitro. J Mater Sci Mater Med. 2008;19(2):547-551.

Lew DP, Waldvogel FA. Osteomyelitis. Lancet. 2004;364(9431):369-379.

Lewiecki EM. Denosumab: an investigational drug for the management of postmenopausal osteoporosis. Biologics. 2008;2(4):645-653.

Lewis K. Multidrug tolerance of biofilms and persister cells. Curr Top Microbiol Immunol 2008;322:107-131.

Li D, Zhu M, Xu C, Chen J, Ji B. The effect of Cu2+ or Fe3+ on the noncovalent binding of rutin with bovine serum albumin by spectroscopic analysis. Spectrochim Acta A Mol Biomol Spectrosc. 2011;78(1):74-79.

Li S. Hydrolytic degradation characteristics of aliphatic polyesters derived from lactic and glycolic acids. J Biomed Mater Res. 1999;48(3):342-353.

Li X, Lenhart JJ, Walker HW. Dissolution-accompanied aggregation kinetics of silver nanoparticles. Langmuir 2010;26(22):16690-16698.

Lin MT, Beal MF. Mitochondrial dysfunction and oxidative stress in neurodegenerative diseases. Nature. 2006;443(7113):787-795.

Lindsey RW, Gugala Z, Milne E, Sun M, Gannon FH, Latta LL. The efficacy of cylindrical titanium mesh cage for the reconstruction of a critical-size canine segmental femoral diaphyseal defect. J Orthop Res. 2006;24(7):1438-1453.

Lindsay R, Cosman F, Zhou H, Bostrom M, Shen V, Cruz J, Nieves JW, Dempster DW: A novel tetracycline labeling schedule for longitudinal evaluation of the short-term effects of anabolic therapy with a single iliac crest biopsy: Early actions of teriparatide. J Bone Miner Res. 2006;(21):366-373.

Lindfors NC, Hyvönen P, Nyyssönen M, Kirjavainen M, Kankare J, Gullichsen E, Salo J: Bioactive glass S53P4 as bone graft substitute in treatment of osteomyelitis. Bone. 2010;47(2):212-218.

Lissenberg-Thunnissen SN1, de Gorter DJ, Sier CF, Schipper IB.Use and efficacy of bone morphogenetic proteins in fracture healing. Int Orthop. 2011;35(9):1271-1280.

Liu H, Yazici H, Ergun C, Webster TJ, Bermek H. An in vitro evaluation of the Ca/P ratio for the cytocompatibility of nano-to-micron particulate calcium phosphates for bone regeneration. Acta Biomater. 2008;4(5):1472-1479.

Looney W J. Small-colony variants of Staphylococcus aureus. Br J Biomed Sci. 2000; 57(4): 317-322.

Lorite GS, Rodrigues CM, De Souza AA, Kranz C, Mizaikoff B, Cotta MA. The role of conditioning film formation and surface chemical changes on Xylella fastidiosa adhesion and biofilm evolution. J Colloid Interf Sci. 2011;359(1):289-295.

Love C, Tomas MB, Tronco GG, Palestro CJ. FDG PET of infection and inflammation. Radiographics. 2005;25(5):1357-1368.

Mack D, Fischer W, Krokotsch A, Leopold K, Hartmann R, Egge H, Laufs R. The intercellular adhesin involved in biofilm accumulation of Staphylococcus epidermidis is a linear beta-1,6-linked glucosaminoglycan: purification and structural analysis. J Bacteriol. 1996;178(1): 175-183.

Mahfouz T, Miceli MH, Saghafifar F, Stroud S, Jones-Jackson L, Walker R, Grazziutti ML, Purnell G, Fassas A, Tricot G, Barlogie B, Anaissie E. 18Ffluorodeoxyglucose positron emission tomography contributes to the diagnosis and management of infections in patients with multiple myeloma: a study of 165 infectious episodes. *J Clin Oncol*. 2005; 23(31):7857–7863.

Majola A, Vainionpää S, Rokkanen P, Mikkola HM, Törmälä P. Absorbable self-reinforced polylactide (SR-PLA) composite rods for fracture fixation: strength and strength retention in the bone and subcutaneous tissue of rabbits. J Mater Sci Mater Med. 1992;3(1):43-47.

Makadia HK, Siegel SJ. Poly Lactic-co-Glycolic Acid (PLGA] as Biodegradable Controlled Drug Delivery Carrier. Polymers. 2011;3(3):1377-1397.

Malcher M, Volodkin D, Heurtault B, André P, Schaaf P, Möhwald H, et al. Embedded silver ions-containing liposomes in polyelectrolyte multilayers: cargos films for antibacterial agents. Langmuir 2008;24(18):10209-10215.

Malin M, Hiljainen-Vaino M, Karjalainen T, Seppala J. Biodegradable lactone copolymers. II. Hydrolytic study of e-caprolactone and lactide copolymers. J Appl Polym Sci. 1996;59:1289-1298.

Manolagas SC, Kousteni S, Jilka RL. Sex steroids and bone. Recent Prog Horm Res. 2002;57:385-409.

Marambio-Jones C, Hoek EM. A review of the antibacterial effects of silver nanomaterials and potential implications for human health and environment. J Nanopart Res. 2010;12(5):1531-1551.

Marcon P, Marsich E, Vetere A, Mozetic P, Campa C, Donati I, Vittur F, Gamini A, Paoletti S. The role of Galectin-1 in the interaction between chondrocytes and a lactose-modified chitosan. Biomaterials. 2005;26(24):4975-4984.

Marsich E, Travan A, Donati I, Turco G, Kulkova J, Moritz N, Aro HT, Crosera M, Paoletti S. Biological responses of silver-coated thermosets: An in vitro and in vivo study. Acta Biomater. 2013;9(2):5088-5099.

McAndrew J, Efrimescu C, Sheehan E, Niall D: Through the looking glass; bioactive glass S53P4 (BonAlive®) in the treatment of chronic osteomyelitis. Ir J Med Sci. 2013; 182(3):509-511.

McDonald D J, Fitzgerald R H Jr, Ilstrup D M. Two-stage reconstruction of a total hip arthroplasty because of infection. J Bone Joint Surg Am. 1989; 71(6): 828-834.

McDowell A, Patrick S. Evaluation of nonculture methods for the detection of prosthetic hip biofilms. Clin Orthop Relat Res. 2005;(437):74-82.

Melcher GA, Claudi B, Schlegel U, Perren SM, Printzen G, Munzinger J. Influence of type of medullary nail on the development of local infection. An experimental study of solid and slotted nails in rabbits. J Bone Joint Surg Br. 1994;76(6):955-959.

Melcher GA, Metzdorf A, Schlegel U, Ziegler WJ, Perren SM, Printzen G. Influence of reaming versus nonreaming in intramedullary nailing on local infection rate: Experimental investigation in rabbits. J Trauma. 1995;39(6):1123-1128.

Merritt JH, Kadouri DE, O'Toole GA. Growing and analyzing static biofilms. Curr Protoc Microbiol. 2005;Chapter 1:Unit 1B.1.

Meyer F, Wardale J, Best S, Cameron R, Rushton N, Brooks R. Effects of lactic acid and glycolic acid on human osteoblasts: a way to understand PLGA involvement in PLGA/calcium phosphate composite failure. J Orthop Res. 2012;30(6):864–871.

Middleton JC, Tipton AJ. Synthetic biodegradable polymers as orthopaedic devices. Biomaterials. 2000;(21):2335-2346.

Mohler ML, Bohl CE, Jones A, Coss CC, Narayanan R, He Y, Hwang DJ, Dalton JT, Miller DD. Nonsteroidal selective androgen receptor modulators (SARMs): dissociating the anabolic and androgenic activities of the androgen receptor for therapeutic benefit. J Med Chem. 2009;52(12):3597-3617.

Mohler ML, Coss CC, Duke CB 3rd, Patil SA, Miller DD, Dalton JT. Androgen receptor antagonists: a patent review (2008-2011). Expert Opin Ther Pat. 2012; 22(5):541-565.

Mohn D, Ege D, Feldman K, Schneider OD, Imfeld T, Boccaccini AR, Stark WJ. Spherical calcium phosphate nanoparticle fillers allow polymer processing of bone fixation devices with high bioactivity. Polymer Eng Sci 2010;50(5):952-960.

Montanaro L, Speziale P, Campoccia D, Ravaioli S, Cangini I, Pietrocola G, Giannini S, Arciola CR. Scenery of Staphylococcus implant infections in orthopedics. Future Microbiol. 2011;6(11): 1329-1349.

Moritz N, Strandberg N, Zhao DS, Mattila R, Paracchini L, Vallittu PK, Aro HT. Mechanical properties and *in vivo* performance of load-bearing fiber-reinforced composite intramedullary nails with improved torsional strength. J Mech Behav Biomed Mater. 2014;40C:127-139.

Morones JR, Elechiguerra JL, Camacho A, Holt K, Kouri JB, Ramírez JT, Yacaman MJ. The bactericidal effect of silver nanoparticles. Nanotechnology. 2005;16(10):2346-53.

Mortazavi V, Nahrkhalaji MM, Fathi MH, Mousavi SB, Esfahani BN. Antibacterial effects of sol-gel-derived bioactive glass nanoparticle on aerobic bacteria. J Biomed Mater Res A. 2010; 94(1):160-168.

Muchmore DB. Raloxifene: A selective estrogen receptor modulator (SERM) with multiple target system effects. Oncologist. 2000;5(5):388-392.

Nair LS, Laurecin CT. Biopolymers as biomaterials for tissue engineering and controlled drug delivery. Adv Biochem Engin/Biotechnol. 2005;(102):47-90.

Narayanan R, Mohler ML, Bohl CE, Miller DD, Dalton JT. Selective androgen receptor modulators in preclinical and clinical development. Nucl Recept Signal. 2008;(6): e010.

Naveenraj S, Anandan S, Kathiravan A, Renganathan R, Ashokkumar M. The interaction of sonochemically synthesized gold nanoparticles with serum albumins. J Pharm Biomed Anal 2010;53(3):804-810.

Neer RM, Arnaud CD, Zanchetta JR, Prince R, Gaich GA, Reginster JY, Hodsman AB, Eriksen EF, Ish-Shalom S, Genant HK, Wang O, Mitlak BH. Effect of parathyroid hormone (1-34) on fractures and bone mineral density in postmenopausal women with osteoporosis. N Engl J Med. 2001;344(19):1434-1441.

Negro-Vilar A. Selective androgen receptor modulators (SARMs): a novel approach to androgen therapy for the new millennium. J Clin Endocrinol Metab. 1999;84(10):3459-3462.

Nel A. Atmosphere. Air pollution-related illness: effects of particles. Science. 2005;308(5723): 804-806.

Nel A, Xia T, Mädler L, Li N. Toxic potential of materials at the nanolevel. Science. 2006;311(5761):622-627.

Neut D, van de Belt H, Stokroos I, van Horn JR, van der Mei HC, Busscher HJ. Biomaterial-associated infection of gentamicin-loaded PMMA beads in orthopaedic revision surgery. J Antimicrob Chemother. 2001;47(6):885-891.

Neut D, van der Mei HC, Bulstra SK, Busscher HJ. The role of small-colony variants in failure to diagnose and treat biofilm infections in orthopedics. Acta Orthop. 2007;78(3):299-308.

Neyt JG, Buckwalter JA, Carroll NC. Use of animal models in musculoskeletal research. Iowa Orthop J. 1998;18:118-123.

Nho SJ, Provencher MT, Seroyer ST, Romeo AA. Bioabsorbable anchors in glenohumeral shoulder surgery. Arthroscopy. 2009;25(7):788-793.

Nielsen LE. Mechanical properties of polymers and composites. Marcel Dekker, Inc New York 1974.

Niemelä T. Effect of β-tricalcium phosphate addition on the in vitro degradation of self-reinforced poly-L, D-lactide. Polym Degrad Stabil. 2005;89:492–500.

Niemelä T, Niiranen H, Kellomäki M, Törmälä P. Self-reinforced composites of bioabsorbable polymer and bioactive glass with different bioactive glass contents. Part I: Initial mechanical properties and bioactivity. Acta Biomater. 2005;1(2):235-242.

Norden CW. Experimental osteomyelitis. I. A description of the model. J Infect Dis. 1970;122(5):410-418

Oberdörster G, Maynard A, Donaldson K, Castranova V, Fitzpatrick J, Ausman K, Carter J, Karn B, Kreyling W, Lai D, Olin S, Monteiro-Riviere N, Warheit D, Yang H; ILSI Research Foundation/Risk Science Institute Nanomaterial Toxicity Screening Working Group. Principles for characterizing the potential human health effects from exposure to nanomaterials: elements of a screening strategy. Part Fibre Toxicol. 2005;2(1):8.

Odekerken JCE, Welting TJM, Arts JJC, Walenkamp GHIM, Emans PJ. Modern orthopaedic implant coatings — their pro's, con's and evaluation. In: Aliofkhazraei M, editor. Methods, modern surface engineering treatments. InTech 2003. DOI: 10.5772/55976.

Ott M, Gogvadze V, Orrenius S, Zhivotovsky B. Mitochondria, oxidative stress and cell death. Apoptosis 2007;12(5):913-922.

Otto M. Staphylococcal biofilms. Curr Top Microbiol Immunol. 2008;322:207-228.

Panacek A, Kvítek L, Prucek R, Kolar M, Vecerova R, Pizúrova N, Sharma VK, Nevecna T, Zboril R. Silver colloid nanoparticles: synthesis, characterization, and their antibacterial activity. J Phys Chem B. 2006;110(33):16248-16253.

Park HB, Keyurapan E, Gill HS, Selhi HS, McFarland EG. Suture anchors and tacks for shoulder surgery, part II: the prevention and treatment of complications. Am J Sports Med. 2006;34(1):136-144.

Park TG, Lu W, Crotts G. Importance of in vitro experimental conditions on protein release kinetics, stability and polymer degradation in protein encapsulated poly(D,L-lactic acid-co-glycolic acid) microspheres. J Control Release. 1995;33:211-222.

Pearce AI, Richards RG, Milz S, Schneider E, Pearce SG. Animal models for implant biomaterial research in bone: a review. Eur Cell Mater. 2007;13:1-10.

Pederson L, Kremer M, Judd J, Pascoe D, Spelsberg TC, Riggs BL, Oursler MJ. Androgens regulate bone resorption activity of isolated osteoclasts in vitro. Proc Natl Acad Sci U S A. 1999;96(2):505-510.

Pei L, Flock JI. Functional study of antibodies against a fibrogenin-binding protein in Staphylococcus epidermidis adherence to polyethylene catheters. J Infect Dis. 2001;18(1)4:52-55.

Pei L, Flock JI. Lack of fbe, the gene for a fibrinogen-binding protein from Staphylococcus epidermidis, reduces its adherence to fibrinogen coated surfaces. Microb Pathog. 2001;31(4):185-193.

Peng H, Usas A, Olshanski A, Ho AM, Gearhart B, Cooper GM, Huard J. VEGF improves, whereas sFlt1 inhibits, BMP2-induced bone formation and bone healing through modulation of angiogenesis. J Bone Miner Res. 2005;20(11):2017-2027.

Petty W, Spanier S, Shuster JJ, Silverthorne C. The influence of skeletal implants on incidence of infection. Experiments in a canine model. J Bone Joint Surg Am. 1985;67(8):1236-1244.

Petty W, Spanier S, Shuster JJ. Prevention of infection after total joint replacement. Experiments with a canine model. J Bone Joint Surg Am. 1988;70(4):536-539.

Philipov JP, Pascalev MD, Aminkov BY, Grosev CD. Changes in serum carboxyterminal telopeptide of type I collagen in an experimental model of canine osteomyelitis. Calcif Tissue Int. 1995;57(2):152-154.

Piroth L, Que YA, Widmer E, Panchaud A, Piu S, Entenza JM, Moreillon P. The fibrinogen- and fibronectin-binding domains of Staphylococcus aureus fibronectin-binding protein A synergistically promote endothelial invasion and experimental endocarditis. Infect Immun. 2008;76(8):3824-3831.

Pittet D, Ducel G. Infectious risk factors related to operating rooms. Infect Control Hosp Epidemiol 1994;15(7):456-462.

Prabhakar AR and Kumar SC. Antibacterial effect of bioactive glass in combination with powdered enamel and dentin. Indian J Dent Res. 2010;21(1):30-34.

Prakasam G, Yeh JK, Chen MM, Castro-Magana M, Liang CT, Aloia JF. Effects of growth hormone and testosterone on cortical bone formation and bone density in aged orchiectomized rats. Bone. 1999;24(5):491-497.

Priester JH, Horst AM, Van de Werfhorst LC, Saleta JL, Mertes LA, Holden PA. Enhanced visualization of microbial biofilms by staining and environmental scanning electron microscopy. J Microbiol Methods. 2007;68(3): 577-587.

Proctor RA, Van Langevelde P, Kristjansson M, Maslow JN, Arbeit R D. Persistent and relapsing infections associated with small-colony variants of Staphylococcus aureus. Clin Infect Dis. 1995;20(1):95-102.

Proctor RA, Kahl B, von Eiff C, Vaudaux PE, Lew DP, Peters G. Staphylococcal small colony variants have novel mechanisms for antibiotic resistance. Clin Infect Dis. 1998;27 Suppl 1:S68-74.

Proctor RA, von Eiff C, Kahl BC, Becker K, McNamara P, Herrmann M, Peters G. Small colony variants: a pathogenic form of bacteria that facilitates persistent and recurrent

infections. Nat Rev Microbiol. 2006;4(4):295-305.

Quinn JM, Gillespie MT. Modulation of osteoclast formation. Biochem Biophys Res Commun. 2005;328(3):739-745.

Rai M, Yadav A, Gade A. Silver nanoparticles as a new generation of antimicrobials. Biotechnol Adv. 2001;27(1):76-83.

Rakovsky A, Gotman I, Rabkin E, Gutmanas EY. Strong bioresorbable Ca phosphate-PLA nanocomposites with uniform phase distribution by attrition milling and high pressure consolidation. J Mech Behav Biomed Mater. 2013;18:37-46.

Rani SA, Pitts B, Beyenal H, Veluchamy RA, Lewandowski Z, Davison WM, Buckingham-Meyer K, Stewart PS. Spatial patterns of DNA replication, protein synthesis, and oxygen concentration within bacterial biofilms reveal diverse physiological states. J Bacteriol. 2007;189(11):4223-4233.

Recker RR: Embryology, anatomy, and microstructure of bone, in Coe FL, Favus MJ (eds): Disorders of Bone and Mineral Metabolism. New York: Raven, 1992, pp 219–240.

Recker RR, Kimmel DB, Dempster D, Weinstein RS, Wronski TJ, Burr DB. Issues in modern bone histomorphometry. Bone. 2011;49(5):955-964.

Resch A, Rosenstein R, Nerz C, Gotz F. Differential gene expression profiling of Staphylococcus aureus cultivated under biofilm and planktonic conditions. Appl Environ Microbiol. 2005;71(5):2663-2676.

Rho JY, Kuhn-Spearing L, Zioupos P. Mechanical properties and the hierarchical structure of bone. Med Eng Phys. 1998;20(2):92-102.

Riggs BL, Parfitt AM. Drugs used to treat osteoporosis: the critical need for a uniform nomenclature based on their action on bone remodeling. J Bone Miner Res. 2005;20(2):177-184.

Rissing JP, Buxton TB, Weinstein RS, Shockley RK. Model of experimental chronic osteomyelitis in rats. Infect Immun. 1985;47(3):581-586.

Rizk A, Robertson J, Raber J. Behavioral performance of tfm mice supports the beneficial role of androgen receptors in spatial learning and memory. Brain Res. 2005; 1034(1-2):132-138.

Romanò CL, Logoluso N, Meani E, Romanò D, De Vecchi E, Vassena C, Drago L. A comparative study of the use of bioactive glass S53P4 and antibiotic-loaded calcium-based bone substitutes in the treatment of chronic osteomyelitis: a retrospective comparative study. Bone Joint J. 2014;96-B(6):845-850.

Roveri N, Iafisco M. Evolving application of biomimetic nanostructured hydroxyapatite. Nanotech Sci Appl. 2010;3:107-125.

Sakaeda H. Experimental polymicrobial osteomyelitis produced by both aerobic and anaerobic opportunistic pathogens. Nihon Seikeigeka Gakkai Zasshi. 1988;62(8):791-802.

Salmi M, Jalkanen S. A 90-kilodalton endothelial cell molecule mediating lymphocyte binding in humans. Science. 1992;257(5075):1407-1409.

Salmi M, Jalkanen S. VAP-1: an adhesin and an enzyme. Trends Immunol. 2001;22(4):211-216.

Salmi M, Yegutkin GG, Lehvonen R, Koskinen K, Salminen T, Jalkanen S. A cell surface amine oxidase directly controls lymphocyte migration. Immunity. 2001;14(3):265-276.

Schmitz A, Risse J, Grünwald F, Gassel F, Biersack H, Schmitt O. Fluorine-18 fluorodeoxyglucose positron emission tomography findings in spondylodiscitis: preliminary results. *Eur Spine J*. 2001;10 (10):534–539.

Schindeler A, McDonald MM, Bokko P, Little DG. Bone remodeling during fracture repair: The cellular picture. Semin Cell Dev Biol. 2008;19(5):459-466.

Schneider OD, Mohn D, Fuhrer R, Klein K, Kämpf K, Nuss KM, Sidler M, Zlinszky K, von Rechenberg B, Stark WJ. Biocompatibility and bone formation of flexible, cotton wool-like PLGA/Calcium phosphate nanocomposites in sheep. Open Orthop J. 2011;5:63-71.

Schouten C, Meijer GJ, van den Beucken JJ, Spauwen PH, Jansen JA. The quantitative assessment of peri-implant bone responses using histomorphometry and micro-computed tomography. Biomaterials. 2009;30(27):4539-4549.

Schwartz Z, Doukarsky-Marx T, Nasatzky E, Goultschin J, Ranly DM, Greenspan DC, Sela J, Boyan BD. Differential effects of bone graft substitutes on regeneration of bone marrow. Clin Oral Implants Res. 2008;19(12):1233-1245.

Seeman E, Delmas PD. Bone quality--the material and structural basis of bone strength and fragility. N Engl J Med. 2006;354(21):2250-2261.

Sellman BR, Timofeyeva Y, Nanra J, Scott A, Fulginiti JP, Matsuka YV, Baker SM. Expression of Staphylococcus epidermidis SdrG increases following exposure to an in vivo environment. Infect Immun 2008;76(7):2950-2957.

Sendi P, Rohrbach M, Graber P, Frei R, Ochsner P E, Zimmerli W. Staphylococcus aureus small colony variants in prosthetic joint infection. Clin Infect Dis. 2006;43(8):961-967.

Shanks RM, Sargent JL, Martinez RM, Graber ML, O'Toole GA. Catheter lock solutions influence staphylococcal biofilm formation on abiotic surfaces. Nephrol Dial Transplant. 2006;21(8): 2247-2255.

Sharma VK, Yngard RA, Lin Y. lver nanoparticles: Green synthesis and their antimicrobial activities. 2009; Adv Colloid Interface Sci. 2009; 145:83–96.

Sheehan E, McKenna J, Mulhall KJ, Marks P, McCormack D. Adhesion of Staphylococcus to orthopaedic metals, an in vivo study. J Orthop Res. 2004;22(1):39-43.

Shen C, Jiang SD, Jiang LS, Dai LY. Bioabsorbable versus metallic interference screw fixation in anterior cruciate ligament reconstruction: a meta-analysis of randomized controlled trials. Arthroscopy. 2010;26(5):705-713.

Shikinami Y, Okuno M. Bioresorbable devices made of forged composites of hydroxyapatite (HA) particles and poly-L-lactide (L PLA): Part I. Basic characteristics. Biomaterials. 1999;20(9): 859-877.

Shikinami Y, Okuno M. Bioresorbable devices made of forged composites of hydroxyapatite (HA) particles and poly L-lactide (L PLA). Part II: practical properties of miniscrews and miniplates. Biomaterials. 2001;22(23):3197-3211.

Shirtcliffe N, Nickel U, Schneider S. Reproducible preparation of silver sols with small particle size using borohydride reduction: for use as nuclei for preparation of larger particles. J Colloid Interface Sci. 1999;211(1):122-129.

Sileika TS, Kim HD, Maniak P, Messersmith PB. Antibacterial performance of polydopamine-modified polymer surfaces containing passive and active components. ACS Appl Mater Interf. 2011;3(12):4602-4610.

Siminoski K, Josse RG. Prevention and management of osteoporosis: consensus statements from the Scientific Advisory Board of the Osteoporosis Society of Canada. 9. Calcitonin in the treatment of osteoporosis. CMAJ. 1996;155(7):962-965.

Smeltzer MS, Nelson CL, Evans RP. Biofilms and aseptic loosening. In Shirtliff M and Leid J, editors. The role of biofilms in device related infections. Springer-Verlag Berlin Heidelberg; 2009. p. 57-74.

Southwood RT, Rice JL, McDonald PJ, Hakendorf PH, Rozenbilds MA. Infection in experimental hip arthroplasties. J Bone Joint Surg Br. 1985;67(2):229-231.

Stebounova L, Guio E, Grassian V. Silver nanoparticles in simulated biological media: a study of aggregation, sedimentation, and dissolution. J Nanopart Res. 2011;13(1):233-244.

Stewart PS, Franklin MJ. Physiological heterogeneity in biofilms. Nat Rev Microbiol 2008;6(3):199–210.

Stoodley P, Kathju S, Hu FZ, Erdos G, Levenson JE, Mehta N, Dice B, Johnson S, Hall-Stoodley L, Nistico L, Sotereanos N, Sewecke J, Post JC, Ehrlich GD. Molecular and imaging techniques for bacterial biofilms in joint arthroplasty infections. Clin Orthop Relat Res. 2005;(437):31-40.

Stoodley P, Nistico L, Johnson S, Lasko LA, Baratz M, Gahlot V, Ehrlich GD, Kathju S. Direct demonstration of viable Staphylococcus aureus biofilms in an infected total joint arthroplasty. A case report. J Bone Joint Surg Am. 2008;90(8):1751-1758.

Stoor P, Kirstilä V, Söderling E, Kangasniemi I, Herbst K, Yli-Urpo A. Interactions between bioactive glass and periodontal pathogens.

Microbial Ecology in Health and Disease. 1996;9(3):109-104.

Stoor P, Söderling E, Salonen JI. Antibacterial effects of a bioactive glass paste on oral microorganisms. Acta Odontol Scand. 1998;56(3):161-165.

Stoppie N, Wevers M, Naert I. Feasibility of detecting trabecular bone around percutaneous titanium implants in rabbits by in vivo microfocus computed tomography. J Microsc. 2007;228(Pt 1):55-61.

Suh JK, Matthew HW. Apllication of chitosan-based polysaccharide biomaterials in cartilage tissue engineering: a review. Biomaterials. 2000;21(24):2589-2598.

Sumner DR, Turner TM, Urban RM, Turek T, Seeherman H, Wozney JM. Locally delivered rhBMP-2 enhances bone ingrowth and gap healing in a canine model. J Orthop Res. 2004;22(1):58-65.

Surti S, Karp JS, Kinahan PE. PET instrumentation. Radiol Clin North Am. 2004;42(6):1003-16, vii.

Suva LJ, Seedor JG, Endo N, Quartuccio HA, Thompson DD, Bab I, Rodan GA. Pattern of gene expression following rat tibial marrow ablation. J Bone Miner Res. 1993;8(3):379-388.

Suzuki T, Matsuzaki T, Hagiwara H, Aoki T, Takata K. Recent advances in fluorescent labeling techniques for fluorescence microscopy. Acta Histochem Cytochem. 2007;40(5):131-137.

Takamatsu H, Miyazaki T, Ishida E, Ashizuka, Abe H. Mechanical properties of β-tricalcium phosphate/polylactic acid composites prepared through ball-milling. J Ceram Soc Jpn. 2006;114:332-335.

Tarkka T, Sipola A, Jämsä T, Soini Y, Ylä-Herttuala S, Tuukkanen J, Hautala T. Adenoviral VEGF-A gene transfer induces angiogenesis and promotes bone formation in healing osseous tissues. J Gene Med. 2003;5(7):560-566.

Tattevin P, Cremieux A C, Pottier P, Huten D, Carbon C. Prosthetic joint infection: when can prosthesis salvage be considered? Clin Infect Dis. 1999;29(2): 292-295.

Thevis M, Thomas A, Fusshöller G, Beuck S, Geyer H, Schänzer W. Mass spectrometric characterization of urinary metabolites of the selective androgen receptor modulator andarine (S-4) for routine doping control purposes. Rapid Commun Mass Spectrom. 2010;24(15):2245-2254.

Thorwarth M, Schultze-Mosgau S, Kessler P, Wiltfang J, Schlegel KA. Bone regeneration in osseous defects using a resorbable nanoparticular hydroxyapatite. J Oral Maxillofac Surg. 2005;63(11):1626-1633.

Tobias JH, Gallagher A, Chambers TJ. 5 alpha-Dihydrotestosterone partially restores cancellous bone volume in osteopenic ovariectomized rats. Am J Physiol. 1994;267(6 Pt 1):E853-859.

Toth JM, Boden SD, Burkus JK, Badura JM, Peckham SM, McKay WF. Short-term osteoclastic activity induced by locally high concentrations of recombinant human bone morphogenetic protein-2 in a cancellous bone environment. Spine (Phila Pa 1976). 2009;34(6):539-550.

Trampuz A, Zimmerli W. Prosthetic joint infections: update in diagnosis and treatment. Swiss Med Wkly. 2005;135(17-18):243-251.

Trampuz A, Piper KE, Jacobson MJ, Hanssen AD, Unni KK, Osmon DR, Mandrekar JN, Cockerill FR, Steckelberg JM, Greenleaf JF, Patel R. Sonication of removed hip and knee prostheses for diagnosis of infection. N Engl J Med. 2007;357(7):654-663.

Tran N, Webster TJ. Nanotechnology for bone materials. Wiley Interdiscip Rev Nanomed Nanobiotechnol. 2009;1(3):336-351.

Travan A, Pelillo C, Donati I, Marsich E, Benincasa M, Scarpa T, Semeraro S, Turco G, Gennaro R, Paoletti S. Non-cytotoxic silver nanoparticle-polysaccharide nanocomposites with antimicrobial activity.Biomacromolecules. 2009;10(6):1429-1435.

Travan A, Marsich E, Donati I, Foulc MP, Moritz N, Aro HT, Paoletti S. Polysaccharide-coated thermosets for orthopedic applications: from material characterization to in vivo tests. Biomacromolecules. 2012;13(5):1564-1572.

Tsai MJ, O'Malley BW. Molecular mechanisms of action of steroid/thyroid receptor superfamily members. Annu Rev Biochem. 1994;63:451-486.

Tsukayama DT, Goldberg VM, Kyle R. Diagnosis and management of infection after total knee arthroplasty. J Bone Joint Surg Am. 2003;85-A Suppl 1:S75-80.

Tunney MM, Patrick S, Curran MD, Ramage G, Hanna D, Nixon JR, Gorman SP, Davis RI, Anderson N. Detection of prosthetic hip infection at revision arthroplasty by immunofluorescence microscopy and PCR amplification of the bacterial 16S rRNA gene. J Clin Microbiol. 1999;37(10):3281-3290.

Törmälä P. Biodegradable self-reinforced composite materials; manufacturing structure and mechanical properties. Clin Mater. 1992;10(1-2):29-34.

Törmälä P. Ultra-high strength, self-reinforced absorbable polymeric composites for applications in different disciplines of surgery. Clin Mater. 1993;13(1-4):35-40.

Ubara Y, Fushimi T, Tagami T, Sawa N, Hoshino J, Yokota M, Kaitori H, Takemoto F, Hara S. Histomorphometric features of bone in patients with primary and secondary hyperparathyroidism. Kidney Int. 2003;63(5):1809-1816.

Ubara Y, Tagami T, Nakanishi S, Sawa N, Hoshino J, Suwabe T, Kaitori H, Takemoto F, Hara S, Takaichi K. Significance of minimodeling in dialysis patients with adynamic bone disease. Kidney Int. 2005;68(2):833-839.

Ueda H, Tabata Y. Polyhydroxyalkanonate derivatives in current clinical applications and trials. Adv Drug Deliv Rev. 2003;55(4):501-518.

Ujula T, Salomäki S, Virsu P, Lankinen P, Mäkinen TJ, Autio A, Yegutkin GG, Knuuti J, Jalkanen S, Roivainen A. Synthesis, ^{68}Ga labeling and preliminary evaluation of DOTA peptide binding vascular adhesion protein-1: a potential PET imaging agent for diagnosing osteomyelitis. Nucl Med Biol. 2009;36(6):631-641.

Um HD, Orenstein JM, Wahl SM. FAS mediates apoptosis in human monocytes by a reactive oxygen intermediate dependent pathway. J Immunol. 1996;156(9):3469-3477.

Vanderschueren D, Vandenput L, Boonen S, Van Herck E, Swinnen JV, Bouillon R. An aged rat model of partial androgen deficiency: prevention of both loss of bone and lean body mass by low-dose androgen replacement. Endocrinology. 2000;141(5):1642-1647.

Vaudaux P, Francois P, Bisognano C, Kelley WL, Lew DP, Schrenzel J, Proctor RA, McNamara PJ, Peters G, Von Eiff C. Increased expression of clumping factor and fibronectin-binding proteins by hemB mutants of Staphylococcus aureus expressing small colony variant phenotypes. Infect Immun. 2002;70(10):5428-5437.

Vaudaux P, Kelley W L, Lew D P. Staphylococcus aureus small colony variants: difficult to diagnose and difficult to treat. Clin Infect Dis. 2006;43(8):968-970.

Verheyen CC, de Wijn JR, van Blitterswijk CA, de Groot K. Evaluation of hydroxylapatite/poly(L-lactide] composites: mechanical behavior. J Biomed Mater Res. 1992;26(10):1277-1296.

Viguet-Carrin S, Garnero P, Delmas PD. The role of collagen in bone strength. Osteoporos Int. 2006;17(3):319-336.

Von Eiff C, Bettin D, Proctor RA, Rolauffs B, Lindner N, Winkelmann W, Peters G. Recovery of small colony variants of Staphylococcus aureus following gentamicin bead placement for osteomyelitis. Clin Infect Dis. 1997;25(5):1250-1251.

Von Eiff C, Proctor RA, Peters G. Staphylococcus aureus small colony variants: formation and clinical impact. Int J Clin Pract Suppl. 2000;(115):44-49.

Vos FJ, Bleeker-Rovers CP, Corstens FH, Kullberg BJ, Oyen WJ. FDG-PET for imaging of non-osseous infection and inflammation. Q J Nucl Med Mol Imaging. 2006;50(2):121-130.

Vuong C, Kocianova S, Voyich JM, Yao Y, Fischer ER, DeLeo FR, Otto M. A crucial role for exopolysaccharide modification in bacterial biofilm formation, immune evasion, and virulence. J Biol Chem 2004;279(52):54881-54886.

Vuong C, Voyich JM, Fischer ER, Braughton KR, Whitney AR, DeLeo FR, Otto M. Polysaccharide intercellular adhesin (PIA) protects Staphylococcus epidermidis against major components of the human innate immune system. Cell Microbiol. 2004;6(3):269-275.

Välimäki VV, Aro HT. Molecular basis for action of bioactive glasses as bone graft substitute. Scand J Surg. 2006;95(2):95-102.

Walker JT, Verran J, Boyd RD, Percival S. Microscopy methods to investigate structure of potable water biofilms. Methods Enzymol. 2001;337:243-255.

Wang M. Developing bioactive composite materials for tissue replacement. Biomaterials. 2003;24(13):2133-2151.

Webster TJ, Ergun C, Doremus RH, Siegel RW, Bizios R. Specific proteins mediate enhanced osteoblast adhesion on nanophase ceramics. J Biomed Mater Res. 2000;51(3):475-483.

Wedmore I, McManus J.G, Pusateri A.E, Holcomb J.B. A special report on the chitosan-based hemostatic dressing: experience in current combat operations J Trauma. 2006;60(3):655-658.

Weiler A, Hoffmann RGF, Stähelin AC, Helling H-J, Südkamp NP. Biodegradable implants in sports medicine: the biological base. Arthroscopy. 2000;16(3):305-321.

Weiner S, Wagner HD. The material bone: structure mechanical function relations. Ann Rev Mater Sci. 1998;28:271–298.

Widmer A F, Frei R, Rajacic Z, Zimmerli W. Correlation between in vivo and in vitro efficacy of antimicrobial agents against foreign body infections. J Infect Dis. 1990;162(1):96-102.

Williams DF. Biofunctionality and Biocompatibility. In Cahn RW, Haasen P, Kramer EJ, editors. Materials science and technology a comprehensive treatment, Volume 14: VCH Verlagsgesellschaft mbH; 1992. p. 1-28.

Williams DF. The Williams dictionary of biomaterials. Liverpool: Liverpool University Press. 1999.

Williams DF. On the nature of biomaterials. Biomaterials. 2009 ;30(30):5897-58909.

Wiren KM, Chapman Evans A, Zhang XW. Osteoblast differentiation influences androgen and estrogen receptor-alpha and -beta expression. J Endocrinol. 2002;175(3):683-694.

Wiren KM, Zhang XW, Toombs AR, Kasparcova V, Gentile MA, Harada S, Jepsen KJ. Targeted overexpression of androgen receptor in osteoblasts: unexpected complex bone phenotype in growing animals. Endocrinology. 2004;145(7):3507-3522.

Wiren KM. Androgens and bone growth: it's location, location, location. Curr Opin Pharmacol. 2005;5(6):626-632.

Wiren KM, Zhang XW, Olson DA, Turner RT, Iwaniec UT. Androgen prevents hypogonadal bone loss via inhibition of resorption mediated by mature osteoblasts/osteocytes. Bone 2012;51(5):835-846.

Wu D, Wu Z, Yang J, Nair VA, Miller DD, Dalton JT. Pharmacokinetics and metabolism of a selective androgen receptor modulator in rats: implication of molecular properties and intensive metabolic profile to investigate ideal pharmacokinetic characteristics of a propanamide in preclinical study. Drug Metab Dispos. 2006;34(3):483-494.

Wu D, Lin G, Gore AC. Age-related changes in hypothalamic androgen receptor and estrogen receptor alpha in male rats. J Comp Neurol. 2009;512(5):688-701.

Yamadi S, Kobayashi S. Effects of strain rate on the mechanical properties of tricalcium phosphate/poly(L: -lactide] composites. J Mater Sci Mater Med. 2009;20(1):67-74.

Yamamuro T, Shikata J, Kakutani Y, Yoshii S, Kitsugi T, Ono K. Novel methods for clinical applications of bioactive ceramics. Ann N Y Acad Sci. 1988;523:107-114.

Yang J, Zhang Q, Lee JY, Too HP. Dissolution–recrystallization mechanism for the conversion of silver nanospheres to triangular nanoplates. J Colloid Interf Sci 2007;308(1):157-161.

Yang L, Zhang L, Webster TJ. Nanobiomaterials: State of the Art and Future Trends. Adv Eng Mater. 2011;13(6):B197–B217.

Yang Z, Best SM, Cameron RE. The influence of α-tricalcium phosphate nanoparticles and microparticles on the degradation of poly(D,L-lactide-co-glycolide). Adv Mater. 2009;21(38-39):3900-3904.

Yao Y, Sturdevant DE, Otto M. Genomewide analysis of gene expression in Staphylococcus

epidermidis biofilms: insights into the pathophysiology of S. epidermidis biofilms and the role of phenol-soluble modulins in formation of biofilms. J Infect Dis. 2005;191(2):289-298.

Yeo M, Kang M. Effects of nanometer sized silver materials on biological toxicity during zebrafish embryogenesis. Bull Korean Chem Soc. 2008;29(6):1179-1184.

Yin D, Gao W, Kearbey JD, Xu H, Chung K, He Y, Marhefka CA, Veverka KA, Miller DD, Dalton JT. Pharmacodynamics of selective androgen receptor modulators. J Pharmacol Exp Ther. 2003;304(3):1334-1340.

Zak O, Zak F, Rich R, Tosch W, Kradolfer F, Sheld WM. Experimental staphylococcal osteomyelitis in rats: Therapy with rifampin and cloxacillin, alone or in combination. In: Periti P, Grassi GG, editors. Current chemotherapy and immunotherapy. Wasington DC: American Society for Microbiology; 1982. p. 973-974.

Zamzami N, Marchetti P, Castedo M, Decaudin D, Macho A, Hirsch T, et al. Sequential reduction of mitochondrial transmembrane potential and generation of reactive oxygen species in early programmed cell death. J Exp Med. 1995;182(2):367-377.

Zhang P, Hong Z, Yu T, Chen X, Jing X. In vivo mineralization and osteogenesis of nanocomposite scaffold of poly(lactide-co-glycolide) and hydroxyapatite surface-grafted with poly(L-lactide). Biomaterials. 2009;30(1): 58-70.

Zhang Q, Carlson J, Ke HZ, Li J, Kim M, Murphy K, Mehta N, Gilligan J, Vignery A. Dramatic increase in cortical thickness induced by femoral marrow ablation followed by a 3-month treatment with PTH in rats. J Bone Miner Res. 2010;25(6):1350-1359.

Zhang W, Yao Y, Li K, Huang Y, Chen Y. Influence of dissolved oxygen on aggregation kinetics of citrate-coated silver nanoparticles. Environ Pollut. 2011;159(12):3757-3762.

Zhang X, Sui Z. Deciphering the selective androgen receptor modulators paradigm. Expert Opin Drug Discov. 2013;8(2):191-218.

Zhao DS, Moritz N, Laurila P, Mattila R, Lassila LV, Strandberg N, Mäntylä T, Vallittu PK, Aro HT. Development of a multi-component fiber-reinforced composite implant for load-sharing conditions. Med Eng Phys. 2009;31(4):461-469.

Zhao X, Liu R, Teng Y, Liu X. The interaction between Ag+ and bovine serum albumin: a spectroscopic investigation. Sci Total Environ. 2011;409(5):892-897.

Zhou H, Lawrence JG, Bhaduri SB. Fabrication aspects of PLA-CaP/PLGA-CaP composites for orthopedic applications: a review. Acta Biomater 2012;8:1999-2016.

Zhu Y, Weiss EC, Otto M, Fey PD, Smeltzer MS, Somerville GA. Staphylococcus aureus biofilm metabolism and the influence of arginine on polysaccharide intercellular adhesin synthesis, biofilm formation, and pathogenesis. Infect Immun. 2007;75(9):4219-4226.

Zimmerli W, Trampuz A, Ochsner PE. Prosthetic-joint infections. N Engl J Med. 2004; 351(16):1645-1654.